THESIS ON NATURAL AND EXACT SCIENCES B107

Numerical Experiments on Matter Transport in the Baltic Sea

GERMO VÄLI

TUT PRESS

TALLINN UNIVERSITY OF TECHNOLOGY
Faculty of Science
Marine Systems Institute

Dissertation was accepted for the defence of the degree of Doctor of Philosophy in Natural Sciences on April 12, 2011

Supervisor: Prof. Victor Zhurbas, Marine Systems Institute at Tallinn University of Technology, Tallinn Estonia
P. P. Shirshov Institute of Oceanology, Russian Academy of Sciences, Moscow, Russia

Ph.D. Aleksander Toompuu, Marine Systems Institute at Tallinn University of Technology, Tallinn, Estonia

Opponents: Ph.D. Kai Myrberg, Finnish Environment Institute, Helsinki, Finland

Ph.D. Ülo Suursaar, Estonian Marine Institute, University of Tartu, Tallinn, Estonia

Defence of the thesis: June, 20, 2011

Declaration:
Hereby I declare that this thesis, my original investigation and achievement, submitted for the doctoral degree at Tallinn University of Technology, has not been submitted for any academic degree.

/GERMO VÄLI/

ISSN 1406–4723
ISBN 978–9949–23–100–3 (publication)
ISBN 978–9949–23–101–0 (PDF)

LOODUS- JA TÄPPISTEADUSED B107

Aine transpordi numbrilised eksperimendid Läänemeres

GERMO VÄLI

TTÜ KIRJASTUS

Contents

List of original publications

This thesis is based on the following papers, which will be referred to in the text by their Roman numerals.

I. Laanemets, J., Väli, G., Zhurbas, V., Elken, J., Lips, I., Lips, U. 2011. Simulation of mesoscale structures and nutrient transport during summer upwelling events in the Gulf of Finland in 2006. Boreal Environment Research, 16(A), 15–26

II. Väli, G., Zhurbas, V., Laanemets, J., Elken, J. 2011. Simulation of nutrient transport from different depths during an upwelling event in the Gulf of Finland. Oceanologia, 53(TI), 431–448

III. Zhurbas, V., Elken, J., Väli, G., Kuzmina, N., Paka, V. 2010. Pathways of suspended particles transport in the bottom layer of the southern Baltic Sea depending on wind forcing (numerical simulations). Oceanology, 50(6), 841–854

In Appendix A, copies of the papers are included.

Author's contribution

I. Germo Väli was responsible for setting up the hydrodynamic model with HIROMB thermohaline fields and HIRLAM atmospheric forcing. He had a major part in data analysis and helped with writing. Ph.D. Jaan Laanemets and Professor Victor Zhurbas supervised the work.

II. Germo Väli was responsible for the model setup and analysis of the results. He had a major part in writing. Professor Victor Zhurbas and Ph.D. Jaan Laanemets supervised the work.

III. Germo Väli assisted with the random walk model development, calculation of the particle pathways, writing the article and presenting the results at an international symposium. Professor Victor Zhurbas supervised the work.

Approbations of the results

The main results described in this thesis have been presented in the following international conferences, symposiums and workshops:

1. The 3rd US-EU-Baltic Symposium, Tallinn, Estonia, 27–29 May 2008: oral presentation — Pathways of Suspended Particles Released in the Bottom Boundary Layer of the Bornholm Deep, Baltic Sea (numerical simulations) (in cooperation with V. Zhurbas and J. Elken)

2. The 1st International Workshop on Modelling the Ocean: Dynamics, Syntheses, Prediction, Taipei, Taiwan, 23–26 February 2009: oral presentation — Simulation of Mesoscale Structure of an Anomalous Coastal Upwelling Event in the Southern Gulf of Finland, Baltic Sea (in cooperation with V. Zhurbas and J. Laanemets)

3. The 7th Baltic Sea Science Congress, Tallinn, Estonia, 17–21 August 2009: oral presentation — Simulation of mesoscale structure of a coastal upwelling event and related nutrient transport in the southern Gulf of Finland (in cooperation with J. Laanemets, V. Zhurbas, J. Elken, I. Lips and U. Lips)

4. The 6th Study Conference on BALTEX, Miedzyzdroje, Poland, 14–18 June 2010: oral presentation — Simulation of nutrient transport from different depths during an upwelling event in the Gulf of Finland (in cooperation with V. Zhurbas, J. Laanemets and J. Elken)

Acknowledgements

My deepest and eternal gratitude to my supervisors, Professor Victor Zhurbas and Ph.D. Aleksander Toompuu, for the opportunities, knowledge and interest in the marine science.

The most special thanks to Ph.D. Jaan Laanemets for his kindness, patience, support, belief and numerous instances of advice.

My gratitude to Professor Jüri Elken for his help, guidance and helpful discussions.

I thank our co-authors and colleagues Ph.D. Inga Lips and Professor Urmas Lips for the hardest work in setting up the measuring campaigns during summers 2006 up to now with the possibility to be onboard with this wonderful group.

I specially thank Ph.D Urmas Raudsepp for curiosity towards numerical modeling.

This work was financially supported by the Estonian Science Foundation (grant no. 7467) and the European Social Fund's Doctoral Studies and Internationalisation Programme DoRa.

I thank all the colleagues from Marine Systems Institute, who have turned these years into a wonderful experience.

I thank my family for supporting me over the years.

Finally and most importantly, I thank my wife Triin and her family for the endless and continuous support, kindness, encouragement and understanding during the hardest period of my studies.

1 Introduction

The Baltic Sea, comprising different sub-basins (HELCOM, 1996), is a semi-enclosed brackish water inner sea, with a limited water exchange to the North Sea (Atlantic Ocean) through the Danish straits. The strong stratification is the result of the large freshwater supply from rivers and net precipitation along with the reduced water exchange with the world ocean (Meier, 2007).

Some of the main problems in the Baltic are associated with eutrophication. Mostly, the Baltic Sea is nitrogen limited, except the northern parts, where nitrogen input from riverine loads exceeds the natural necessity and biological activity is phosphorus limited. The nutrient concentrations in the upper euphotic layer have an annual cyclic behavior. The dissolved inorganic nitrogen (DIN) in the nitrogen limited areas will become depleted in the upper layer after the spring bloom (usually April–May), while dissolved inorganic phosphorus (DIP) becomes depleted after the late summer bloom (July–August). The exchange of nutrients between different layers during summer periods is prevented by the existence of a strong thermocline. As a consequence, the nutrient concentrations in the upper layer are highest during the wintertime, when the thermocline has vanished and the water column is well mixed.

The nitrogen fixing cyanobacterial blooms in the Baltic are DIP limited. During the nutrient depleted summer period, one of the additional sources for phosphorus is the upwelling event, when deeper layers of the sea reach the surface and are mixed with the upper layer waters. Numerous modeling studies of upwellings in the Baltic Sea have been made (Myrberg and Andrejev, 2003; Kowalewski, 2005; Kowalewski and Ostrowski, 2005; Myrberg et al., 2010) with an extensive overview of recent development by Myrberg et al. (2008), but studies on the dynamics of nutrient transport during upwelling events have been lacking. Recently Zhurbas et al. (2008) and Laanemets et al. (2009) have started making high-resolution numerical experiments on nutrient transport for the Gulf of Finland (GoF).

Two approaches to the numerical simulation of matter transport in the marine environment can be taken. The first is to consider the matter as Lagrangian particles moving both continuously and randomly in a time-dependent velocity field (the Lagrangian approach), while the other is to consider the matter concentration as the solution of a continuous differential equation describing a scalar balance (the Eulerian approach). In the Lagrangian approach usually the trajectories of the particles in the Eulerian velocity field are calculated, while in the Eulerian approach the concentrations of matter under study are calculated. The Lagrangian approach, in principle, is more general and brings more detailed information on the process than the Eulerian approach, because the spatial distribution of the number of particles per unit volume can be easily re-calculated into matter concentration, while particle trajectories cannot be retrieved from the concentration field. However, numerical calculations of

concentration field using the Lagrangian approach are very time-consuming, which is disadvantageous. Both of these methods, either separately or in combination, are widely used for matter transport studies with different scopes including sedimentary material, tracing different water masses, oil spills, marine organisms, etc. Meier (2007) used the Eulerian approach to study the fresh- and saltwater ages in the Baltic Sea, while Döös et al. (2004) used the Lagrangian approach for studying residence times of Baltic water masses. Kuhrts et al. (2004) used the Eulerian approach for sedimentary material transport in the western Baltic, while Kling and Döös (2007) used the Lagrangian particles to study the possible transport of radio-nuclides in the sedimentary material in Swedish coastal regions. The Lagrangian approach applied to the calculation of dispersion near sea surface has been used for simulating oil spill spreading or drifter buoys propagation (Elken, 2001; Gästgifvars et al., 2006), while Lehmann and Javidpour (2010) used the same approach for determining the pathways of invasive species *Mnemiopsis leidyi* in the Baltic Sea. The assessment of differences between the results with both methods in the Baltic conditions is performed by Döös and Engqvist (2007).

In the present study both of the approaches were used. The pathways of suspended sedimentary material from a chemical warfare dumpsite in the Bornholm Deep were simulated under different wind conditions with the Lagrangian approach and the transport of nutrients in the GoF was simulated with the Eulerian approach by solving numerically the advection-dispersion equation similar for the temperature and salinity within the hydrodynamic model.

The primary objective of this thesis is to present the results of some matter transport simulations in the Baltic Sea. In addition, the numerical experiments on nutrient transport during upwelling events brought new interesting results concerting the mesoscale dynamics of the GoF, and these results are presented too.

This work consists of three chapters. Chapter I gives an overview of the methods applied as well as of the description of the hydrodynamic model and its validation. Also a short description of the GoF and the Baltic Proper is given. Chapter II describes the transport of nutrients in the GoF during an upwelling event. In the present study two different events were used for reference – the 1999 upwelling event along the northern coast of the GoF and the 2006 upwelling along the southern coast. Chapter III describes the results of experiments with a random walk model coupled to the hydrodynamic model on the transport of particulate suspended matter in the bottom layer of the southern Baltic.

2 Material and methods

2.1 Study area

The Baltic Proper (BP), consisting of the Arkona, the Bornholm, the Gotland basins and the Gdansk Bay, is a body of the Baltic Sea with a surface area of 211069 km^2 and a total volume of 13045 km^3 (with mean depth 62 m). Sub-basins with varying mean depth are separated through channels and sills with different lengths and depths. The deepest (115 m) is the Fårö sill, which connects the Eastern and Northern Gotland Basin, while the shallowest (40 m) Hoburg-Midsjö banks connects the Bornholm Basin and the Western Gotland Basin (Leppäranta and Myrberg, 2008) (see also Figure 1). The deepwater circulation in the BP is steered and restricted by these channels and sills.

The GoF is a shallow and elongated estuarine-like basin extending the Baltic Sea to the east (there is no sill separating the BP and GoF). The length of the Gulf is about 400 km, while the width varies from 48 to 135 km and the total volume is approximately to 1100 km^3, which is about 5% of the total volume of the Baltic Sea. The along-axis depth of the gulf decreases almost monotonically from 80–110 m at its entrance to 20–30 m in the eastern gulf. Also, the northern part of the GoF is shallower and the bottom slope is about 2 times lower at the northern side (Laanemets et al., 2009) but in general the real bathymetry of the Gulf is complicated, especially near coastal areas.

Most of its fresh water input enters the Gulf in the easternmost part of the basin, where the river Neva has a major impact on a large scale on the whole Baltic Sea river runoff with a mean value of 114 $km^3\ y^{-1}$, and locally on the water movement and salinity distribution of the estuary. The temperature possesses wide seasonal swings, but for salinity, these variations are low. During winter, the upper layer down to the halocline at a depth of 60 m is well-mixed. The heating of the water usually starts in early April and usually the strong thermocline, starting from 10–20 m, where temperature falls from 13–15°C to 2–4°C at the bottom, is formed by late July-early August. The thermocline vanishes by late October-early November. A comprehensive overview of the physical oceanography of the GoF was given by Alenius et al. (1998).

Similarly to the temperature, the surface layer and bottom layer nutrient concentrations differ, i.e., a seasonal nutricline exists. The nutricline is the layer, where the nutrient concentration increases just below the nutrient-depleted upper layer. Laanemets et al. (2004) found that there is a vertical spacing between the nitracline and the phosphacline, which usually varies within 3–5 m and 14 m in case of a deep nitracline. The separation is mainly caused by the difference in the vertical extent of the spring bloom and the depth of the seasonal thermocline.

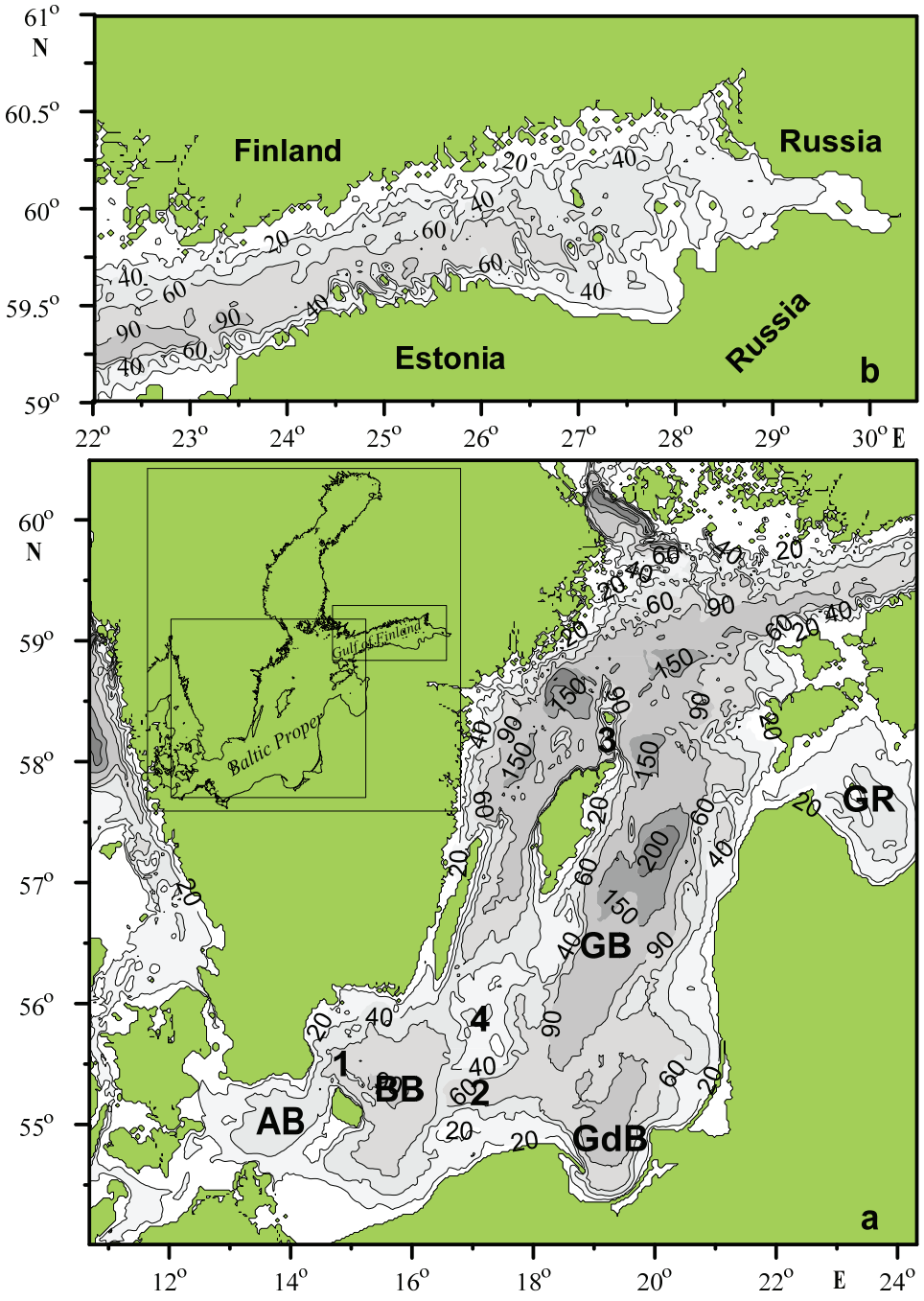

Figure 1: Bathymetric maps of the BP (a) and the GoF (b). The abbreviations on (a) mark the following sea basins: (AB) Arkona Basin; (BB) Bornholm Basin; (GdB) Gulf of Gdansk; (GB) Gotland Basin; (GR) Gulf of Riga. Digits on (a) mark 1 – Bornholm Channel, 2– Slupsk Furrow, 3 – Fårö channel, 4 – Hoburg-Midsjö Bank

2.2 Numerical model

2.2.1 Hydrodynamic model

The Princeton Ocean Model (POM) is a free surface, σ-coordinate, primitive equation hydrodynamic model with hydrostatic and Boussinesq approximations. The turbulence closure model from Mellor and Yamada (1982) is embedded. The equations govern the horizontal momentum equations for u and v, while the vertical velocity ω normal to the σ-surfaces is calculated from the continuity equation. Conservation equations for potential temperature T and salinity S are applied. All small-scale processes, which are not directly resolved by the model grid, are parameterized in terms of horizontal mixing processes (horizontal diffusive terms), which depend on the horizontal diffusivities (A_M, A_H) and are related to the scales of motions in the model as suggested by Smagorinsky (1963).

The vertical mixing coefficients K_M and K_H are obtained by appealing to a second and a half moment turbulence closure scheme, which characterizes the turbulence by equations for the turbulence kinetic energy $q^2/2$ and turbulence macroscale l. The length scale is a characteristic length of the turbulent motion at any point in space or time. The mixing coefficients are calculated from the q^2 and l with using the corresponding stability functions, which depend on the vertical gradients of the velocity fields, the buoyancy, the turbulent velocity q and the scale l.

The equations governing the dynamics of coastal circulation contain propagation of fast moving external gravity waves and slow moving internal gravity waves. For computational efficiency, the mode splitting technique is used. Vertically integrated shallow water motion equations are solved numerically with a smaller time-step within the external cycle that governs the vertical structure equations. The finite difference schemes in the model are the explicit central scheme for spatial differencing and an explicit leapfrog scheme for time-stepping. Implicit schemes are used for vertical diffusion terms, which otherwise require a small time-step to accommodate the small vertical spacing required to resolve the important surface and bottom boundary layers.

Boundary conditions for the differential equations are provided at the free surface, on the side walls and at the bottom of the basin. At the surface, the boundary conditions are described by the wind stress vector, the heat flux, and the evaporation–precipitation fresh water surface mass flux, while at the bottom the boundary conditions are set by the bottom frictional stress determined by matching velocities with the logarithmic law of the wall. In the present study, closed boundaries at the side walls were applied. A more detailed description of the model is given by Blumberg and Mellor (1983; 1987).

2.2.2 Particle transport model

The particle transport model consists of equations for calculating the coordinates after a small time increment Δt of particles moving in a three-dimensional velocity field:

$$x_{i+1} = x_i + u_i \Delta t + x_i'$$

$$y_{i+1} = y_i + v_i \Delta t + y_i'$$

$$z_{i+1} = z_i + (w_i - w_s)\Delta t + z_i',$$

where $(x_{i,}, y_i, z_i)$ and $(x_{i,+1}, y_{i+1}, z_{i+1})$ are the co-ordinates at times t_i and t_{i+1}, $(u_{i,}, v_i, w_i)$ are the velocity components, w_s is the settling velocity, and (x_i', y_i', z_i') are the components of a random displacement of the particle due to the turbulent velocity field.

The random displacements (x_i', y_i', z_i') are expressed through the eddy diffusivity and time increment by a "naive" random walk model for the horizontal and a "true" random walk model for the vertical direction:

$$(x_i', y_i') = (2 \cdot Kh_i \cdot \Delta t)^{1/2} \cdot A$$

$$z_i' = \frac{\partial Kv_i}{\partial z}\Big|_{z=z_i} \cdot \Delta t + \left\{ 2 \cdot Kv_i \left[z_i + 0.5 \frac{\partial Kv_i}{\partial z}\Big|_{z=z_i} \cdot \Delta t \right] \cdot \Delta t \right\}^{1/2} \cdot A,$$

where Kh_i and Kv_i are the horizontal and vertical eddy diffusivity at the space-time point $(x_{i,}, y_i, z_i, t_i)$ and A is a Gaussian random number with zero mean and unit variance. A "true" random walk model for the vertical direction was suggested by Hunter et al. (1993) and Visser (1997) to prevent an artificial accumulation of particles in layers with low eddy diffusivity. A "naive" random walk model in the horizontal direction could be used in the present study as the presence of stable horizontal gradients of lateral eddy diffusivity in the marine environment during model simulations was not expected.

2.3 Model setup

The model domain was either the whole Baltic Sea closed at sounds (papers I and II) or the BP within the limits of 10°40'–24°20'E and 54°00'–60°30'N (paper III). In order to model mesoscale variability, a high resolution in the horizontal plane was used, which in our case was either 0.5 nautical miles in the GoF and 2 nautical miles elsewhere (papers I and II) or 1 nautical mile

everywhere (paper III). In the vertical direction we used either 30 (papers I and III) or 45 (paper II) σ-layers, and the layer thickness was chosen based on the aim of the study – either high resolution in the bottom and surface boundary layers (papers I and III, accordingly) or equally separated layers over the entire water column (paper II). The bathymetry of the Baltic Sea was taken from Seifert et al. (2001). The model resolution of 0.5 nautical miles allowed resolving mesoscale phenomena, including upwelling filaments/squirts controlled by the internal baroclinic Rossby radius, which varies within 2–5 km in the GoF and 1.3–7 km in the BP (Fennel et al, 1991; Alenius et al, 2003).

The simulation periods were summer 2006, when an extensive upwelling event along the southern coast was observed (Suursaar and Aps, 2007; Lips et al. 2009; Kuvaldina et al. 2010), and summer 1999, when an upwelling event along the northern coast occurred (Vahtera et al., 2005) and for suspended particle transport in the BBL, fixed wind conditions over the BP were applied.

Atmospheric forcing (wind stress and surface heat flux components) for the simulation of upwelling in the GoF during summer 2006 was calculated from wind, solar radiation, air temperature, total cloudiness and relative humidity data and taken from the HIRLAM (High Resolution Limited Area Model) version of the Estonian Meteorological and Hydrological Institute (EMHI) with a spatial resolution of 11 km and forecast interval of 3 h ahead of 54 h, recalculated after every 6h (Männik and Merilain, 2007) (paper I). The overall simulation period could be divided into two parts: a relatively short westerly-component wind period (before 29 July) was followed by a long-lasting easterly-component wind period (after 31 July) (see also paper I, Fig. 2). There were four time intervals within the simulation period when the speed of the wind favourable for upwelling near the southern coast exceeded 10 m s^{-1}. Within the easterly wind period there was a 3-day interval of reverse, south-westerly wind which resulted in a temporary weakening of upwelling.

For the calculation of short-term nutrient transport from different depth intervals during an upwelling event in the GoF, the atmospheric forcing was calculated from the gridded dataset of the Swedish Meteorological and Hydrological Institute (SMHI) (paper II). The space and time resolutions for this data were 1° and 3 h, respectively. Winds at 10 m level were calculated following standard procedure from geostrophic wind vectors by turning the latter counterclockwise by 15° and multiplying by a factor 0.6 (Bumke and Hasse, 1989), and a posterior fine tuning of the modeled along-gulf wind stress for the simulation period to what was measured in the Kalbådagrund weather station was applied. Details are given by Zhurbas et al. (2008) and Laanemets et al. (2009). During the short simulation period, westerly winds prevailed (see paper II, fig. 2). The along-gulf wind stress component increased more or less steadily up to about 0.3 N m^{-2}, causing the development of an upwelling along the northern coast of the Gulf. From the peak onwards, the along-gulf wind stress decreased steadily. In order to model the upwelling along the southern

coast, the wind vectors were turned through 180° and a wind stress $\tau = \tau_0$ was applied.

For the simulations of suspended matter transport, prognostic runs of the POM model with a uniform wind stress (namely, for a 3 day period of 0.2 N/m^2 wind stress, which corresponds to about 11 m/s of wind speed at the 10 m level) and zero temperature and salinity flux were used. The wind direction was changed by 22.5° every run. As a result, 16 sets of flow velocity/eddy diffusivity fields typical for N, NNE, NE, ENE, E, ESE, SE, SSE, S, SSW, SW, WSW, W, WNW, NW and NNW winds were simulated (paper III).

Initial thermohaline fields were either taken from HIROMB (High Resolution Operational Model for the Baltic Sea) (Funkquist, 2001) (paper I), constructed using the Data Assimilation System (DAS) in combination with the Baltic Environmental Database (BED) (Sokolov et al. 1997; Wulff and Rahm 1991) (paper II) or created analytically from known characteristics of the seasonal thermocline and halocline in the region (Zhurbas et al. 2004) (paper III). The initial thermohaline fields taken from HIROMB, which is a *z*-level model with 1 nautical mile grid step as provided by SMHI, were interpolated to our model grid. The vertical grid step of the HIROMB was 4 m in the surface layer down to 12 m and increased towards greater depths, resulting in 16 layers at 230 m. The interpolated temperature and salinity fields were smoothed horizontally by using an averaging length of 10 nautical miles before their transformation from *z*-levels to σ-levels. The analytically created initial fields were used in the prognostic runs of the model to simulate velocity/eddy diffusivity fields as an input for sedimentary material transport (the random walk) model (paper III).

The hydrodynamic model runs in the experiments started from the motionless state and zero surface elevation. One justification for such an approach is that the Baltic Sea currents respond to changing wind in topographically controlled regions within approximately a day (Krauss and Brügge, 1991) and secondly due to the smoothed density field in the model setup the corresponding geostrophic currents are expected to be weak.

Initial nutrient fields for the GoF were based on measurements either during summer 1999 (paper II) or summer 2006 (paper I). The difference in the parameterizations was the use of isotherm depths of 7°C and 11°C for the characteristic points on the vertical profile of the nitrate and the phosphate concentrations in summer 2006 (see paper I, eq. 1), whereas for summer 1999 a vertical profile of nutrient concentrations (paper II, Fig. 3) measured in the GoF (Vahtera et al. 2005) was uniformly expanded to the whole model domain. In the vertical grid we had either nutrient concentration in all layers (paper I) or only one σ-layer (paper II).

2.4 Model validation

The model results were validated against in situ measurements in the GoF during summer 2006 (Lips et al. 2009; Kuvaldina et al. 2010) and satellite images. The nutrient dynamics and temporal course of the temperature in the upper layer

during an upwelling along the northern coast of the GoF in summer 1999 were successfully validated against measurements in fixed station by Laanemets et al. (2009) and sea surface temperature against satellite imagery by Zhurbas et al. (2008).

Modeled and measured sea surface temperature maps (Figure 2) during an upwelling in summer 2006 compared rather well to each other and coherent mesoscale structures were reasonably well reproduced. In addition, the differences of upwelling dynamics visible on remote sensing images due to differences in wind conditions (see paper I, Fig. 2) were also visible in the simulation results. More precisely, on 6 and 11 August, the most intensive upwelling along the southern coast is observed in the western part of the Gulf. On 25 August the intensive upwelling area had shifted to the eastern part of the Gulf. This was due to a spatial change in the wind field: the speed of E-SE winds on 25 August was larger at the eastern part of the Gulf, while for 6 and 11 August it was higher at the western part (paper I, Fig. 2). The intensity of the upwelling was weakened due to a transient SW wind on 18 August.

Comparison of measured and simulated NO_X and PO_4 concentrations along a transect between Tallinn and Helsinki on 8 August (Figure 3) showed that after nearly a month of calculation the model reproduced well the vertical distribution of nutrients in the upper 40-m layer. The simulated and measured PO_4 values were approximately the same (Figure 3, c and d) whereas NO_X concentrations (Figure 3a and b) differed more. Higher simulated NO_X and PO_4 values in the surface layer at the warmer side of the upwelling front can be explained by the lack of nutrient consumption in the model. Also, the observed nutrient distributions looked patchier than the modeled ones – this was due to parameterization of the initial nutrient fields, which implies a strong spatial averaging of the data available.

To ascertain that the random walk model is able to adequately describe the particle transport in the Baltic bottom boundary layer (BBL), numerical testing experiments were carried out using a vertically homogenous initial particle distribution in the layer with reflecting boundaries and vertical eddy diffusivity K_v taken from hydrodynamic model to represent identical diffusivity profiles to those of the Baltic BBL. Fick's diffusion equation (see paper III, Eq. 6) has a trivial solution $q(z,t)=q_0$=const under such initial and boundary conditions, and the results of testing the numerical model experiments have to be consistent with this solution. Numerical experiments with different time-steps revealed considerable particle migration from the strongly turbulent BBL into the upper layer with time-step 10 s (Figure 4a and b). The decrease of particle concentration was 74% from 1000 to 260 particles per meter as seen from the vertical profiles of the particle concentrations obtained from testing experiments. At a time-step of 1 s, the artificial particle migration fell to 23% and was insignificant (less than 4%) at 0.1 s. The time dependences of the mean particle concentration in the BBL reveal the inconsistency of the "naive" random walk model under the Baltic Sea BBL conditions: 95% of the particles artificially left

the BBL limits during two hours with time-step 1 s, while they remained in the BBL with the “true” random walk scheme. Time-steps less than 1 s prevent the migration of particles in the BBL.

To conclude, the hydrodynamic model used in the studies meets the requirements of our studies – the short-term simulation of nutrient transport during an upwelling event in the GoF and suspended matter transport under fixed wind conditions in the bottom boundary layer of the BP. The vertical turbulent transport of particles in the near-bottom layer with inhomogeneous diffusivity can be achieved through application of the “true” random walk scheme with time-steps less than or equal to 1 s.

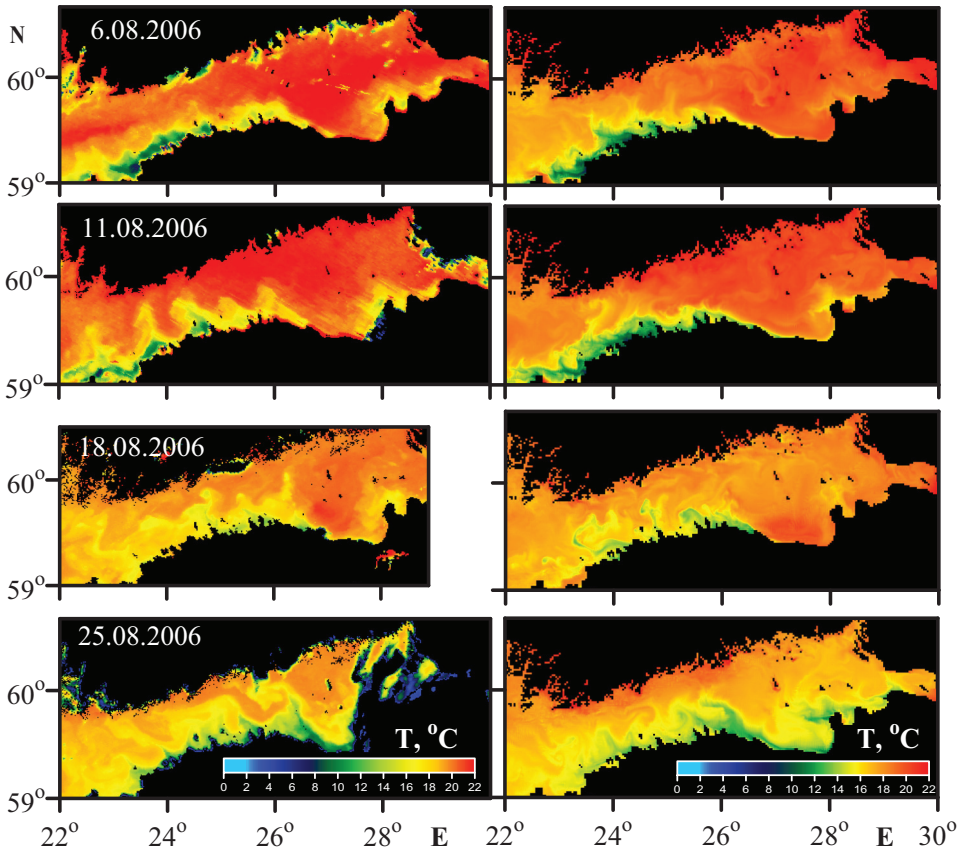

Figure 2: The comparison of simulated SST (right) with the one obtained from satellite imagery (left)

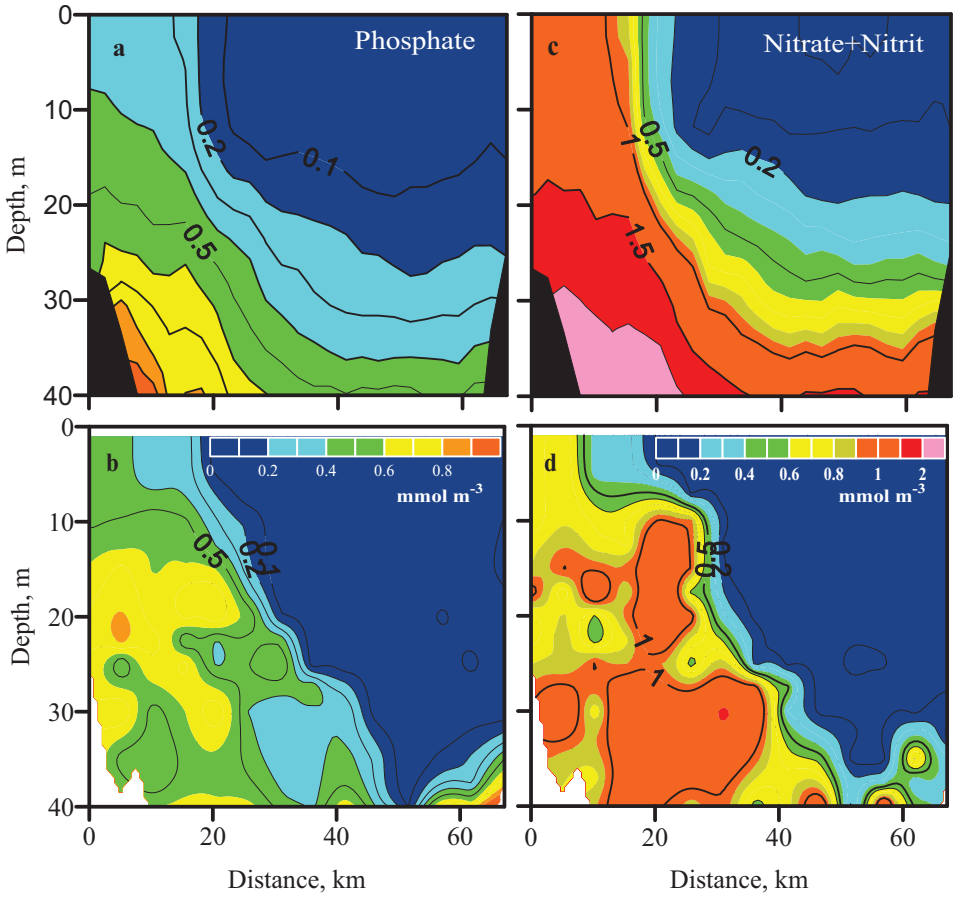

Figure 3: The comparison of (a, c) simulated and (b, d) measured NO_X and PO_4 concentrations along transect between Tallinn and Helsinki on 8 August. The values on the x-axis denote the distance from the southernmost sampling station. Separate colour scales for NO_X and PO_4 concentrations were used

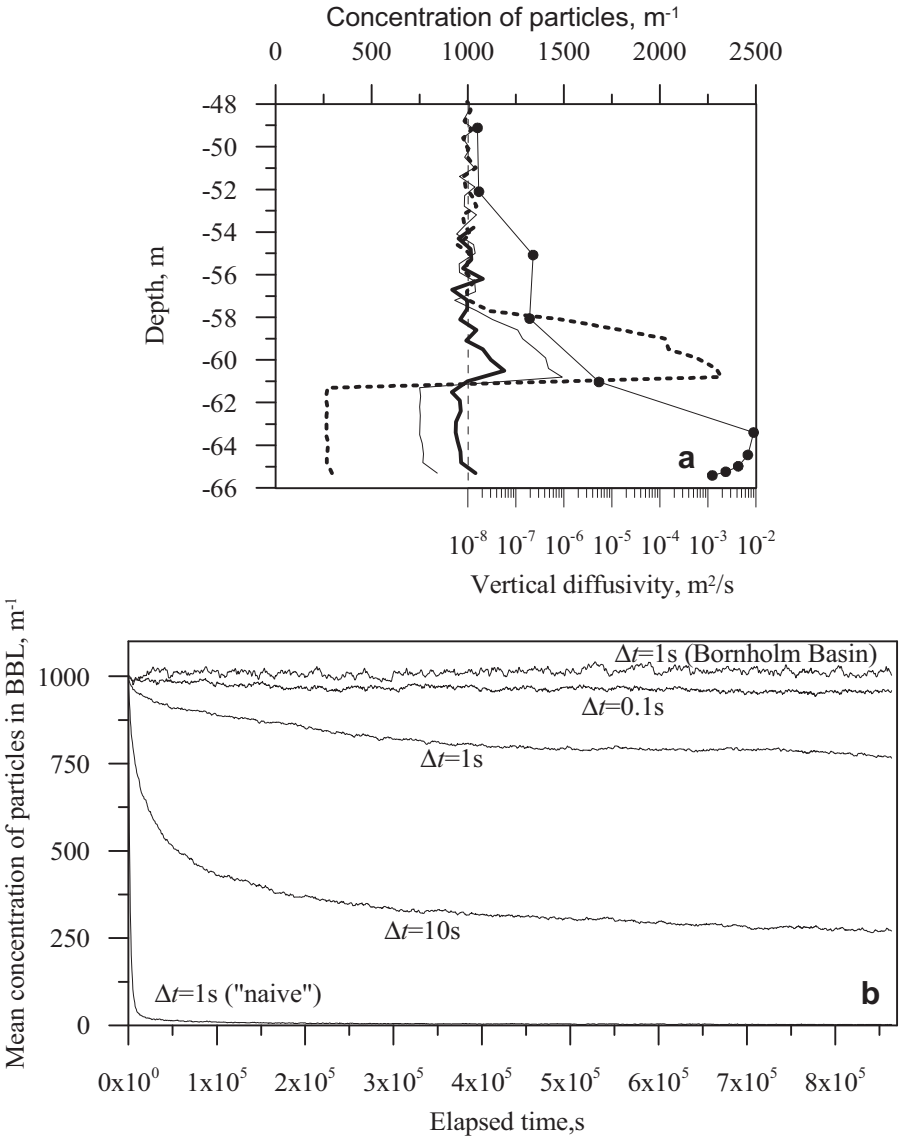

Figure 4: The theoretical validation of random walk model (a): The depth profiles of the particle concentration at the instant t=10 days obtained from the random walk model in the course of testing experiments with the vertically homogenous initial distribution of the particles at different values of time increment Δt. (b): The time dependence of the mean particle concentration in the BBL found from testing experiments at different Δt

3 Nutrient transport dynamics

Upwellings in the Baltic Sea are frequent (Gidhagen, 1987; Lehmann and Myrberg, 2008). In the east to west oriented GoF the upwellings along the northern coast are more frequent due to dominating southwesterly winds (Soomere and Keevallik, 2003). During the nutrient depleted summer period, these wind-driven upwellings transport waters with high nutrient concentration from deeper layers to the surface layer, as shown by field observations (Haapala, 1994; Kononen et al., 2003; Lips et al. 2009; Kuvaldina et al. 2010). According to field data, this transport into the surface layer is with clear excess of phosphorus in relation to the Redfield ratio. As a consequence, upwellings are considered as one external source of phosphorus for nitrogen fixing cyanobacterial blooms (Vahtera et al., 2005). The objectives of our study were the simulation of the mesoscale variability of temperature, velocity and nutrient fields with the characterization of the intensity of water motions with different natures and the estimation of the total inputs of nutrients caused by upwellings in the GoF. We also obtained the contributions of different layers to this transport by model simulations.

The current velocity components at 2 m can be considered as the sum of the mean velocity, eddy velocity and inertial oscillation velocity component (see paper I, Eq. 3). Hence, it was possible to calculate the mean kinetic energy of mesoscale motions (EKE) and mean inertial oscillation kinetic energy (IKE) (see paper I, Eq. 4). The largest EKE values (up to 0.03 $m^2\ s^{-2}$) were found in the coastal zone close to the southern and northern shores of the GoF where variable wind forcing produced alongshore baroclinic jet currents of alternating direction due to successive upwelling and downwelling events for the simulation period from 10 July to 31 August 2006 (Figure 5). The EKE was also higher in the narrow western and central part of the Gulf, where values varied from 0.01 to 0.02 $m^2 s^{-2}$. These values correspond to root mean square velocity fluctuations of 0.14–0.20 m s^{-1}. In those parts also intensive squirts and eddies were formed (paper I, Fig. 4).

The contemporaneous maps of the mean content of nitrogen and phosphorus in the upper mixed 10-m layer of the GoF were calculated (Figure 5). The largest areas of nutrient input by upwelling events in the GoF occurred in the upwelling zones along both coasts. In the eastern part of the open Gulf, the content of upwelled nutrients was low for at least two reasons. First, the simulation period was characterized by wind patterns favourable for upwelling events in the western and central parts of the Gulf in comparison to the eastern part. Uiboupin and Laanemets (2009) analysed the seven year (2000–2006) satellite SST data and found less extensive upwelling events in the eastern part of the GoF with filaments predominately stretching out from the upwelling front along the Finnish coast and in the western part of the Gulf. Secondly, the sea depth is lower and the bottom slope is less steep in the eastern part of the Gulf than in the

central and western part. The distance which a water particle carrying nutrients has to cover in order to reach the surface is inversely proportional to the bottom slope: a steeper slope gives a shorter distance (Laanemets et al., 2009). High values of content of nitrogen and phosphorus are found in the narrow western and central part of the Gulf. In those parts intensive transverse filaments/squirts and eddies were formed and the EKE was higher. This shows that in those areas the upwelled nutrients are more intensively transported from the coastal zone to the open Gulf area.

In order to evaluate the total nutrient input to the surface layer of the GoF produced by the series of upwelling event in July–August 2006, the simulated concentrations of phosphorus and nitrogen were integrated in the upper 10-m layer over the Gulf area. The longitude 22° E was taken as the western boundary of the Gulf, including the entrance area. The integration depth, 10 m, corresponded approximately to the depth of the euphotic zone in the relatively turbid GoF (Kononen et al., 2003). Previously Zhurbas et al. (2008) had showed that during an upwelling event in the GoF in summer 1999, the amount of phosphorus in the upper 10-m layer was greatest at 29 July with 536 tons, while for nitrogen the maximum was 135 tons, which reduced to values of 387 and 36 tons, respectively, after relaxation. Laanemets et al. (2009) showed that under similar conditions (identical value of wind impact) the transport of nutrients is higher during an upwelling along the southern coast. The amount of phosphorus transported to the upper 10-m layer during an upwelling along the southern coast was 887 tons and for nitrogen 611 tons reducing to 679 and 319 tons after relaxation. The simulation period for the summer 2006 covered several upwelling events along both coasts. During an upwelling event along the northern coast in July the amount of phosphorus transported to the upper 10-m layer was 450 tons and the amount of nitrogen was 400 tons (paper I, Fig. 8). In August, the westerly winds favourable for upwellings along the northern coast were replaced with easterly winds favourable for upwellings along the southern coast. By 16 August, the amount of phosphorus in the upper 10-m layer was 1000 tons and for nitrogen the amount was 1077 tons, which reduced to 734 and 707 tons, respectively, after the relaxation. In the end of August, one upwelling event along the southern coast still occurred and by the end of the simulation period the amounts of phosphorus and nitrogen increased to values close to 1046 and 1061 tons once again. In total, the upwelling events along the southern coast brought altogether about 700 tons of nitrogen and 650 tons of phosphorus into the surface layer. The higher transport of nitrogen during an upwelling along the northern coast in summer 2006 compared to that of summer 1999 can be explained by the more closely located phosphacline and nitracline and larger gradients in the thermocline layer in summer 2006. The nitrogen surplus during the upwelling along the southern coast is likely related to the changes in the vertical nutrient distributions attained by the beginning of the easterly wind period (see paper I, Fig. 9). The model simulation showed the dominance of westward flow in the upper 30 m along the southern coast in the period 18–30

July accompanied by a shallowing of both the phosphacline and the nitracline. The shallowing was likely caused by the westward flow's carrying nutrient-rich water from deeper layers along the eastward downsloping isopycnals. Taking into account that the vertical gradient of NO_x concentration had been initially larger than that of PO_4, the upper boundary of the nitracline (0.05 mmol m^{-3} contour on paper I, Fig. 9) being deeper initially had risen above that of the phosphacline due to a vertical turbulent diffusion explaining the slightly larger simulated transport of nitrogen into the surface layer by upwelling events along the southern coast of the Gulf in summer 2006 (paper I, Fig. 8).

A series of numerical experiments, where the initial tracer source was put at different depths for each experiment, was conducted to estimate the nutrient transport from different depths to the surface layer during upwelling events in the GoF (paper II). The results of the experiments were summarized as time and depth maps of cumulative nutrient mass transported to the upper layer from a layer of unit thickness at a certain depth in the GoF. The main source of phosphorus was between 17–41 m for the upwelling along both coasts of the GoF – it was slightly deeper along the southern coast (Figure 6). Transport was greatest from 17 m depth during the northern coast upwelling and from depths of 17–19 m during the southern coast upwelling (Figure 6a and c). The amount larger than 35 tons m^{-1} at these depths reduced to 2.5 tons m^{-1} at 45 m depth for the upwelling off the northern and 65 m depth off the southern coast. For nitrogen the largest amount was from depths of 40–65 m during the upwelling off the southern coast and 43–49 m off the northern coast. The regional upwelling response pattern differed more than 2.5 times – the amounts of nitrogen transported to the surface were higher than 10 tons m^{-1} for the southern coast within depth range of 45–55 m, while for the northern coast the amounts were higher than 4 tons m^{-1} within the depth range of 40–45 m. Amounts of nutrients transported to the upper 10-m layer were transformed into the cumulative volumes of water transported to the upper 10-m layer (Figure 7 and paper II, Fig. 8). The cumulative volumes of water transported to the upper 10-m layer decreased suddenly at depths greater than 40 m during the upwelling off the northern coast. The volume of upwelled water decreased more or less uniformly with depth in the case of the upwelling along the southern coast. The estimates of the Burger number, controlling the vertical position of the onshore flow (Lentz and Chapman, 2004), varied from 0.3–1.2 for the upwelling along the southern and 0.2–0.9 along the northern coast. This indicated the absence of any rigid restriction to the vertical position of the onshore flow in the GoF. As a result, a gradual decrease of cumulative volume transport was observed instead of the abrupt decrease at a certain depth (see paper II, Fig. 8).

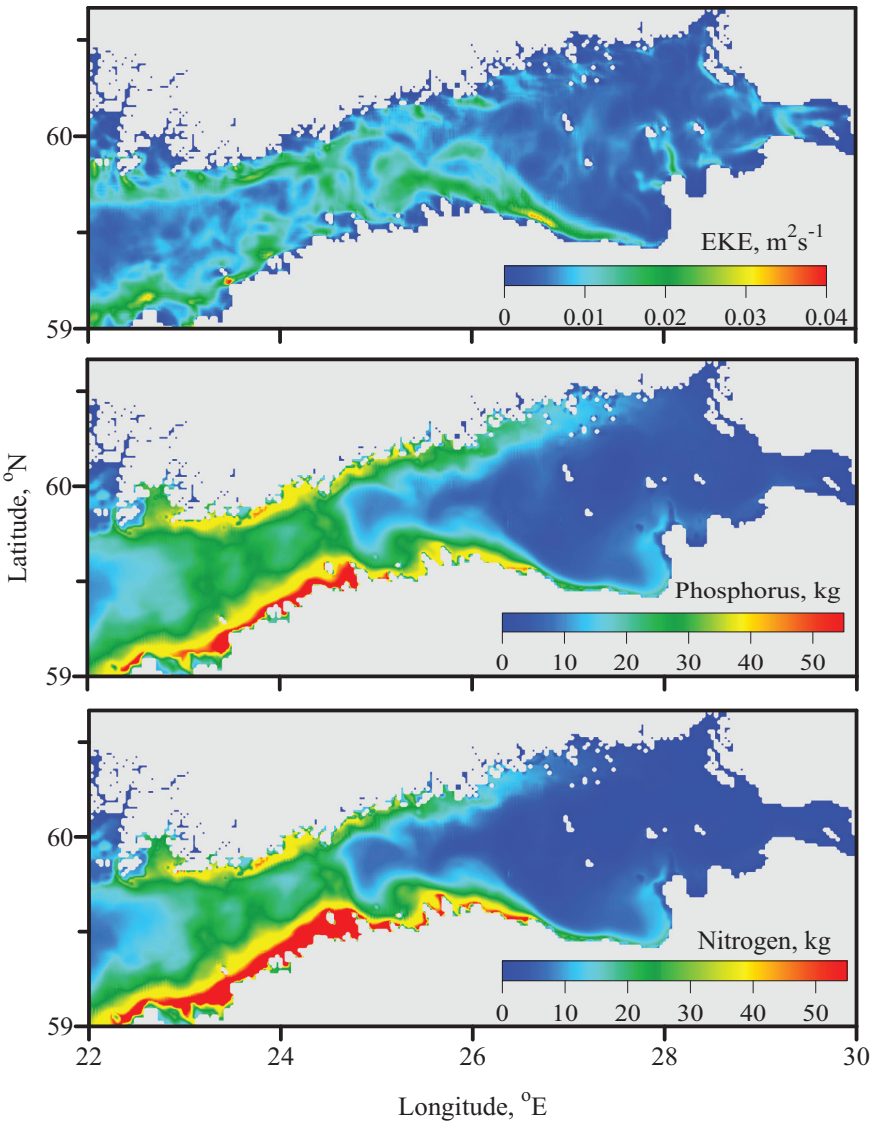

Figure 5: The map of mean kinetic energy in the surface layer of the GoF during the simulation period with the maps of mean phosphorus and nitrogen contents in the upper 10-m water column with the cross section area of 0.5×0.5 nautical miles

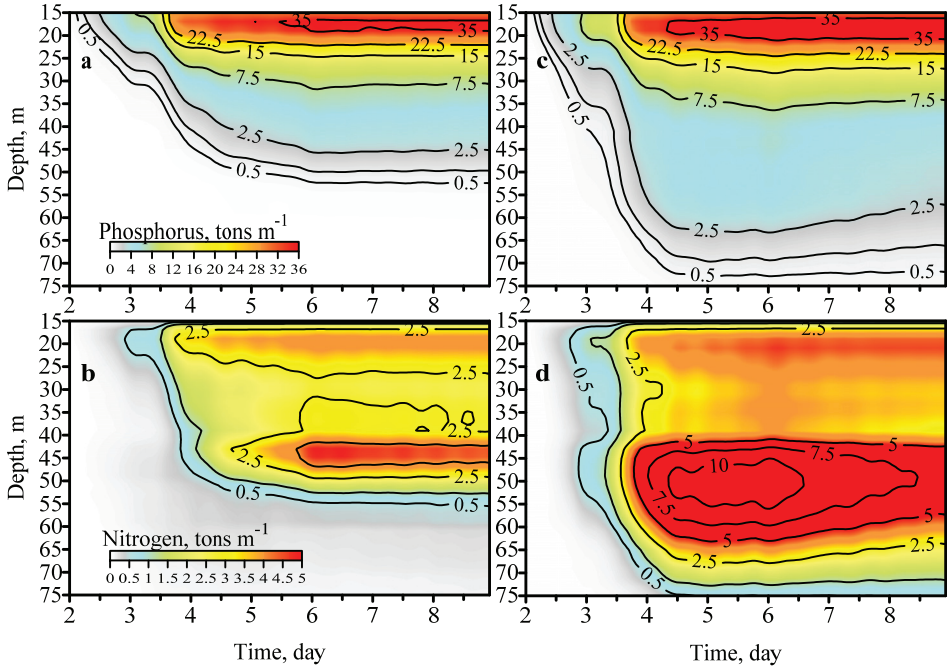

Figure 6: The plots of differential nutrient transport to the upper 10-m layer of the GoF (in tons m^{-1}) versus the depth and time obtained from the simulations. The time is from 20 July 1999 onwards and the depth is the one where the nutrients were located in a layer with unit thickness as the initial source and from where they were brought to the surface layer. The results for the upwelling along the northern coast are on the left hand side, those for the upwelling along the southern coast are on the right hand side

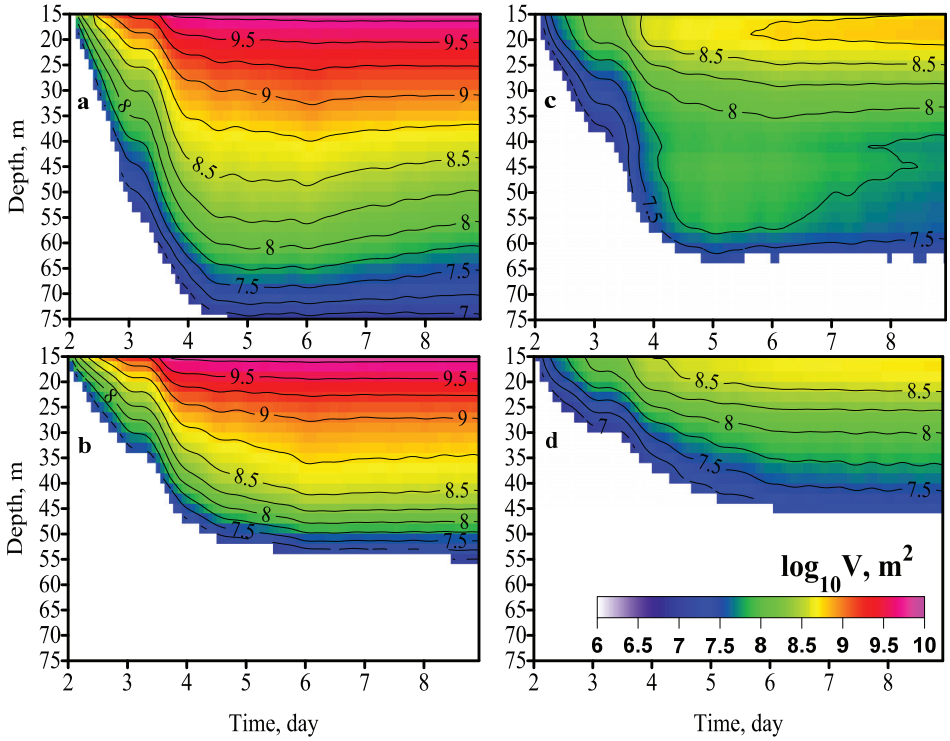

Figure 7: The cumulative volume transports per unit layer thickness to the upper 10-m layer from different depths during the upwelling along the southern (a,c) and northern (b,d) coast. Cumulative volume transports were calculated for wind stress $\tau = \tau_0$ (a,b) and $\tau = 0.5\,\tau_0$ (c,d). The scale is logarithmic

4 Sedimentary material transport

The deep-water sediments in the Baltic are not motionless, as is shown by analysis of the sediment samples (Christiansen et al. 2002). The understanding of the patterns of sediment redistribution in the deeper layers of the basin is important for forecasting pollutant dispersion. A large amount of chemical weapons (CW) were buried in the Bornholm Basin after World War II (HELCOM, 1994) and simulation of the suspended particle transport in the BBL can help to reveal the migration pathways of the CW components and their decay products from their initial burial place. On the other hand, Lagrangian particles could be used for tracing the deep circulation of the Baltic Sea depending on different wind conditions. The purpose of the study was the simulation of the idealized pathways of transport of the sediment material in the deep-water parts of the southern Baltic Sea basins as a function of the wind direction.

Particles were released from a fixed point in either one of three locations in the Baltic Proper – the Bornholm Strait, the Bornholm Deep or the Slupsk Furrow (paper III, Fig. 1) and their pathways during 90–180 days, travelling dependent on the settling velocity, which varied from 0.5 to 4.0 m/day, were analysed. The predicted pathways of the particles will differ from those produced by "real" alternating wind, since the fields of the velocity and diffusion coefficients are specified as changeless ("frozen") during the whole random walk period, but it is exactly the particle pathways computed from the "frozen" fields of the velocity and diffusion coefficients that are consistent with the goal of the present work aimed at the examination of the dependence of the pathways of the particle transport in the BBL upon the wind direction.

The pathway of suspended particles released in the bottom boundary layer of the Bornholm Strait under easterly and northerly wind conditions underwent a bifurcation – some of the particles moving westward along the Swedish coast entering the Arkona Basin and others eastward to enter the Bornholm Basin (Figure 8). The forking of the particle transport pathways occurred due to the oppositely directed currents in the deep layer of the strait. The westward transport takes place at the northern slope of the strait close to the Swedish coast, while the eastward one occurs at the southern slope of the strait near Bornholm Basin. Further pathways of particles entering the Bornholm Basin underwent bifurcation once again – some of the particles followed the northern (clockwise) detour of the Bornholm Deep and were absorbed into the Slupsk Furrow, while the others chose the southern (counter-clockwise) detour and became trapped in the Bornholm Basin maintaining a cyclonic rotation. The current pattern separating the pathways coincides with the pattern suggested by Emelyanov et al. (2004) based on the horizontal distribution of bottom sediments with the only difference being that, according to latter, both branches of the bottom current should enter the Slupsk Furrow.

Wind conditions changing from northerly to easterly made the southern detour more preferable – more particles entering the Bornholm Basin through the Bornholm Strait turn to the south due to Ekman dynamics: the easterly wind forces a northward Ekman transport in the surface layers, which is compensated by a southward flow in the deeper layers. For the same reason, particles that passed the Slupsk Furrow from the west to east turn either to north or south moving towards Gotland Deep or Gulf of Gdansk under northerly or easterly wind conditions.

The particles released in the Bornholm Deep, with settling velocity w_s = 2m/day, displayed an ability to leave the Basin at SE, ESE, E, ENE, NE, NNE, N and NNW winds. For the rest of the wind directions the particles remained trapped within the basin. Under westerly and southerly wind conditions particles moved to the northeast about 20 km, got involved in a cyclonic rotation and remained trapped within an area of 30 km in diameter (paper III, Fig. 9). These particles were unable to leave the cyclonic rotation, which implies the convergence of the Ekman transport in the bottom boundary layer and in view of continuity, the upwelling. Therefore, these particles remained trapped only if the settling velocity was high enough to overcome the upwelling (paper III, Fig. 9).

Depending on the wind direction, particles released in the Slupsk Furrow move either to the east to enter the East Gotland/Gdansk Basin (under NNW, N, NNE, NE, ENE and E wind condition) or to the west to enter the Bornholm Basin (under SE, SSE, S, SSW, SW, WSW, W and WNW wind condition). The pathway of particles entering the Bornholm Basin from either the Slupsk Furrow (paper III, Fig. 10) or the Bornholm Strait (paper III, Fig. 6) underwent a bifurcation characterized by the southern and northern detours. In contrast, there were no bifurcations of the pathway of suspended particles entering the East Gotland/Gdansk Basin under any fixed wind conditions. Instead of bifurcations, the pathways changed markedly with the wind direction, which suggests that the process controlling the further pathways of suspended particles either to the Gdansk Basin or to the eastern Gotland Basin at the outlet of the Slupsk Furrow is the wind forcing.

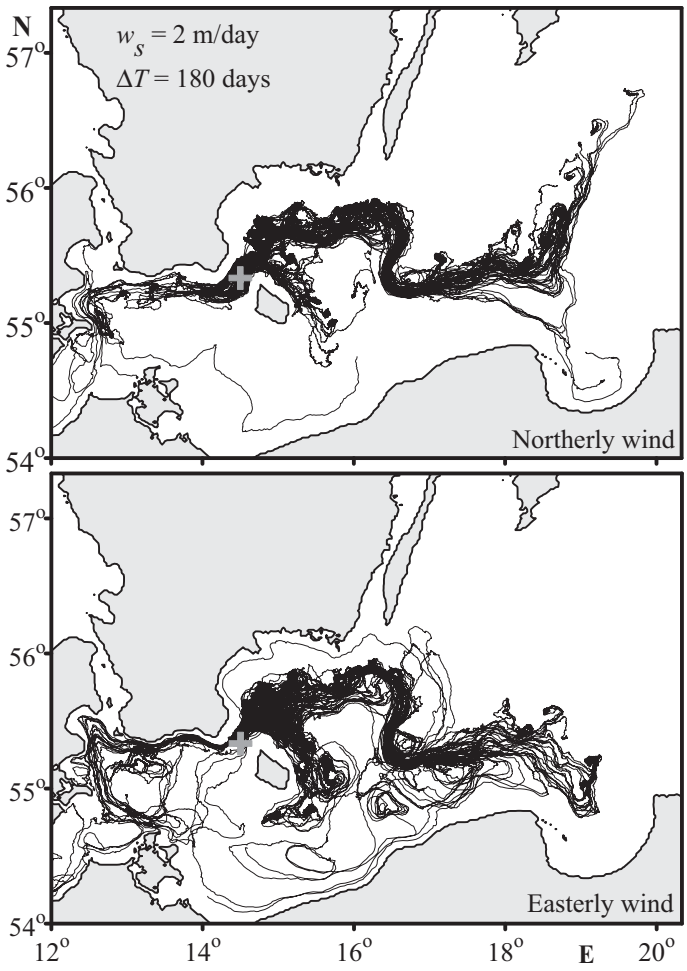

Figure 8: The pathways of particles with the settling velocity w_s = 2 m/day released in the BBL of the Bornholm Strait at northerly and easterly winds

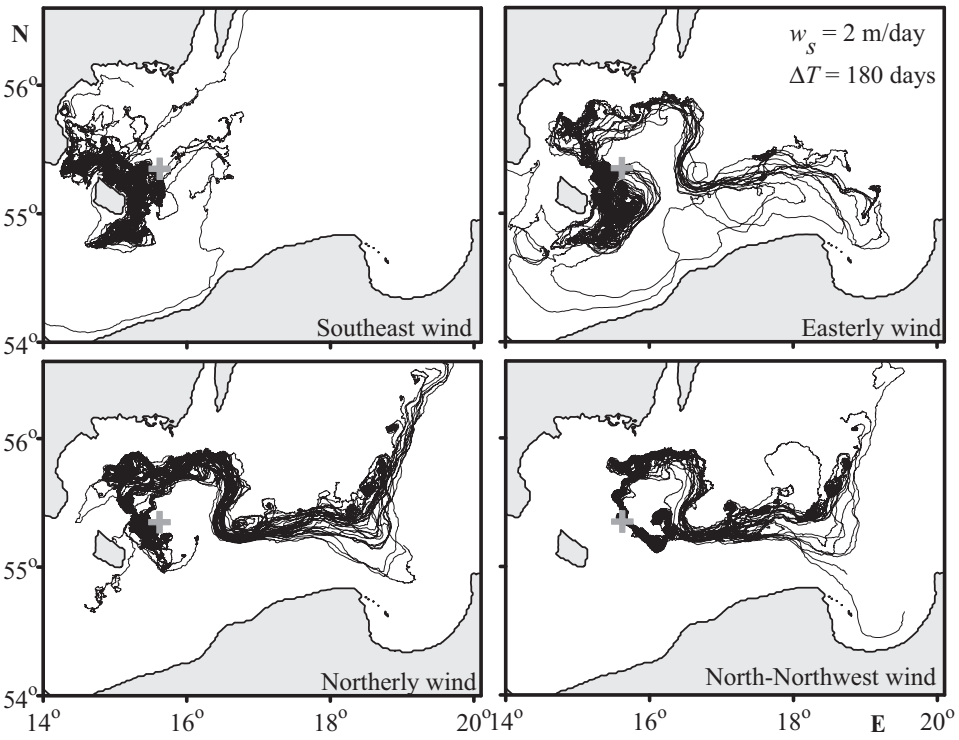

Figure 9: The pathways of suspended particles released in the bottom layer of the Bornholm Basin under southeasterly, easterly, northerly and north-northwesterly winds

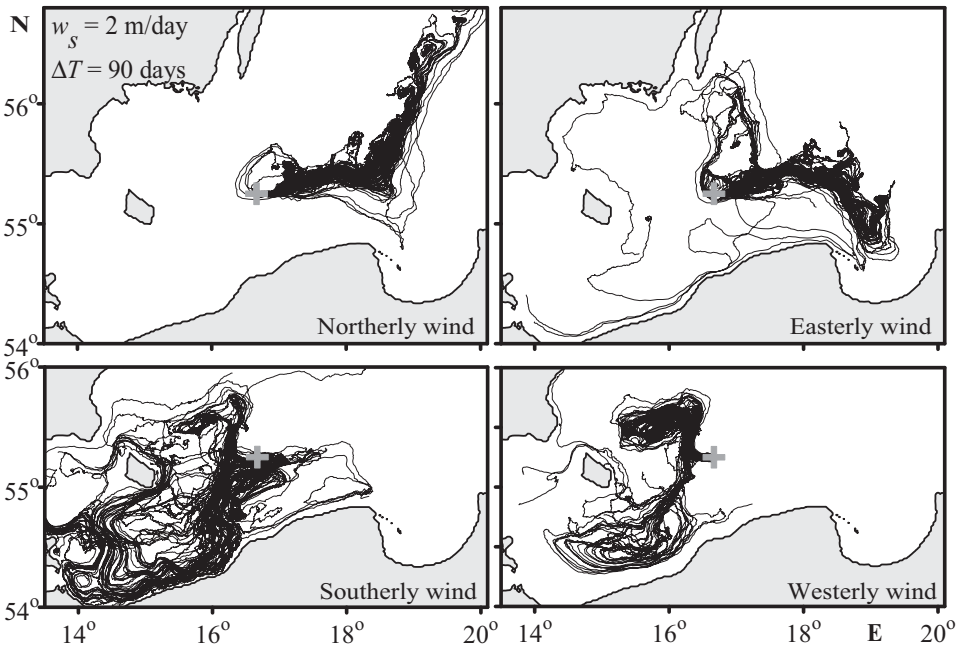

Figure 10: The pathways of suspended particles released in the bottom layer of the Slupsk Furrow under winds of different conditions

Conclusions

Wind-driven upwellings, which are common in the Baltic region, have a major impact on the nutrient dynamics during the nutrient depleted summer period. Numerical experiments in the GoF, the easternmost part of the Baltic Sea, with 3D hydrodynamic model reveal that:

- the total inputs of phosphorus and nitrogen along the northern and southern coasts during upwelling events were characterized by a clear excess of phosphorus;
- mesoscale processes have a large impact on coastal offshore exchange of nutrients – the mean nutrient amount was largest at regions with high mean eddy kinetic energy during the simulation period;
- the highest phosphorus transport to the upper 10-m layer was from depths shallower than 35 m for both the upwellings off the northern and southern coast;
- the largest amounts of nitrogen were transported to the surface layer from depths of 40–50 m off the northern and 40–60 m off the southern coast;
- the volume of water transported to the upper 10-m layer from the deeper layers is greater during the upwelling along the southern coast – there is a clear decrease in the water volume reaching the surface layer from depths greater than 50 m during the upwelling along the northern coast;

Simulations of matter transport as Lagrangian particles released in the bottom boundary layer of Baltic Proper under different wind conditions show that:

- the pathways of the suspended particles that enter the Bornholm Basin from Bornholm Strait in the west bifurcate into north and south branches. The particles involved in the northern detour are sucked into the Slupsk Furrow, while most of those in the southern pathway avoid the Slupsk Furrow and are trapped in the Bornholm Basin;
- "heavier" particles with settling w_s = 2 m/day from Bornholm Strait move closer to the bottom and are more easily trapped by the bottom Ekman transport, which makes the northern detour of the Bornholm Deep more preferable than the southern one;
- under westerly and southerly wind conditions "heavy" particles with settling velocity $w_s \geq 2$ m/day released in the central Bornholm Basin remain trapped, keeping a cyclonic rotation. The phenomenon of trapping can be explained by the combined effects of the upwelling and convergence of the Ekman transport in the BBL;
- the trapping effect vanishes with a decrease in w_s because the vertical velocity in the BBL exceeds the particle settling velocity under upwelling conditions;
- the transport pathways of the suspended particles are controlled by the wind direction as they enter the eastern Baltic Sea from the Slupsk Furrow – under northerly wind conditions the particles move to the north towards the

Gotland Deep, while under easterly wind conditions the particles turn to the south towards Gdansk Bay. There are no bifurcations in the particle pathways as in the case of release in the Bornholm Strait, suggesting strict dependence on wind conditions.

Abstract

In the present thesis some results of the numerical simulation of matter transport in the Baltic Sea are presented. The transported matter in the experiments was either the suspended particles in the bottom boundary layer (BBL) or the nutrient concentrations (nitrogen, phosphorus) in the water column.

In order to model the nutrient concentrations, two equations, the same as with the temperature and salinity, were added to the 3-dimensional hydrodynamic model with only difference being the boundary conditions. Unlike the temperature and salinity the nutrients are treated as a passive tracer.

For the simulation of particulate suspended particle transport, a coupled model system was used. The first component was used to calculate the current velocity fields with the horizontal and vertical eddy diffusivity fields under fixed wind conditions with 16 different wind directions. The second component was used to calculate the idealized pathways of moving Lagrangian particles in the BBL under wind-driven circulation and turbulent diffusion.

We found that the mesoscale processes (eddies, filaments) have a major impact on the nutrient offshore exchange during the upwelling events – the mean total amounts of nutrients in the upper 10-m layer were larger in regions with higher mean eddy kinetic energy during the simulation period. Additionally, we found that the phosphorus transport to the upper 10-m layer along both the northern and southern coasts of the GoF was larger compared to that of nitrogen in terms of the Redfield ratio. The total amount of nitrogen transported to the upper 10-m layer was larger along the southern coast, where the contribution of deeper layers to the transport is larger. The cumulative volumes of water, which are transported to the upper 10-m layer in the GoF during an upwelling event, were also obtained.

The idealized pathways of suspended particles show that in the Bornholm Basin particles with settling velocity above 2 m/day were being “trapped” under dominant south-westerly wind conditions for the Baltic Sea. The pathways of particles released in the Slupsk Furrow are directly influenced by the wind direction, which suggests that the saline water inflow to the Gdansk Basin and the East Bornholm Basin depend strictly on the wind impulse. On the other hand, the pathways of suspended particles released in the BBL of the Bornholm Strait display bifurcations, when the particles moved to the Bornholm Basin and chose either the northern or the southern detour.

Kokkuvõte

Vaadeldavas väitekirjas esitatakse mõningad tulemused ainelevi numbriliste eksperimentidega Läänemeres. Transporditavaks aineks on põhjalähedases kihis asuvad osakesed või toitainetete kontsentratsioonid veesambas.

Toitainete transpordi modelleerimiseks lisati kolmemõõtmelisse hüdrodünaamika mudelisse kaks võrrandit, mis on samad temperatuuri ja soolsuse jaoks ning ainsaks erinevuseks on rajatingimused. Erinevalt temperatuurist ja soolsusest on toitained mudelis passiivse ainena.

Osakeste transpordi modelleerimisel kasutati kahekomponendilist mudelsüsteemi, kus kolmemõõtmelise hüdrodünaamika mudeliga arvutatakse hoovuse kiiruse komponendid ja horisontaalse ning vertikaalse turbulentsi koefitsiendid fikseeritud tuuletingimustes 16 erineva tuulesuuna korral. Mudelsüsteemi teise komponendiga arvutati põhjalähedases kihis liikuvate Lagrange'i osakeste trajektoorid.

Antud töö tulemustena leidsime, et apvellingutega seotud toitainete transpordis rannalähedastelt aladelt avamere aladele on tähtis roll mesomastaapsetel protsessidel (keerised, filamendid) – keskmine toitainete hulk ülemises 10-m veekihis on suurem aladel, kus mesomastaapsete protsesside keskmine kineetiline energia on kõrgem. Lisaks leidsime, et ülemisse 10-m veesambasse domineerib fosfori transport Soome lahes nii põhja- kui lõunarannikul Redfieldi suhte seisukohalt, samas on apvellingu käigus transporditud kogu lämmastiku hulk suurem suurem lõunarannikul, kus sügavamal paiknevad kihid panustavad transporti rohkem. Leitud on ka kumulatiivsed veehulgad, mis apvellingu käigus Soome lahes erinevatest sügavustest 10-m veekihti transporditakse.

Osakeste idealiseeritud trajektooride analüüs näitab, et Bornholmi Basseini tsirkulatsioon Läänemerel domineerivate edelatuulte tingimustes hoiab osakesed settimiskiirusega suurem kui 2 m/päevas lõksus. Slupski kanalis lahti päästetud osakeste trajektoorid on otseselt tuule mõjustatud, mistõttu soolase vee sissevool Gdanski Lahte ja Gotlandi basseini idaossa sõltub otseselt tuuleimpulsist – idatuulte tingimustes liiguvad osakesed Gdanski basseini, põhjatuule korral Gotlandi basseini. Seevastu Bornholmi kanali põhjalähedases kihis lahti päästetud osakeste trajektoorides esinevad bifurkatsioonid nii ida- kui ka põhjatuulte tingimustes, kus üks osa osakesi sisenedes Bornholmi basseini liiguvad põhjasuunda ja teine osa lõunasuunda.

References

Alenius P., Myrberg K., Nekrasov A., 1998, The physical oceanography of the Gulf of Finland: A review, *Boreal Env. Res., 3,* 97–125

Alenius P., Nekrasov A., Myrberg K., 2003, Variability of the baroclinic Rossby radius in the Gulf of Finland, *Cont. Shelf Res., 23,* 563–573

Blumberg A. F., Mellor G.L., 1983, Diagnostic and prognostic numerical calculation studies of the South Atlantic Bight, *J. Geophys. Res., 88,* 4579–4592

Blumberg A.F., Mellor G.L., 1987, A description of the three-dimensional coastal ocean circulation model, in: *Three-dimensional Coastal Ocean Models*, Heaps N.S. (ed.), Am. Geophys. Union, Washington, DC, 1–16

Bumke K., Hasse L., 1989, An analysis scheme for determination of true surface winds at sea from ship synoptic wind and pressure observations, *Bound.-Lay. Meteorol., 47,* 295–308

Christiansen C., Kunzendorf H., Emeis K.-C., et al., 2002, Temporal and spatial sedimentation rate variabilities in the eastern Gotland Basin, the Baltic Sea, *Boreas, 31,* 65–74

Döös K., Meier H. E. M., Döscher R., 2004, The Baltic haline conveyor belt or the overturning circulation and mixing in the Baltic, *Ambio, 33,* 258–262

Döös K., Engqvist A., 2007, Assessment of water exchange between a discharge region and the open sea – a comparison of different methodological concepts, *Est. Coastal and Shelf Science, 74,* 709–721

Elken J., 2001, Modelling of coastal circulation and oil drift at possible deep harbor sites, north-western Saaremaa island, *Proc. Estonian Acad. Sci. Eng., 7,* 141–156

Emelyanov M. E., Gritsenko A. V., Egorikhin D. V., 2004, Near-bottom circulation in the Gdansk Deep of the Baltic Sea: Bottom sediments and dynamics of Inflows of the North Sea waters, *Oceanology, 44,* 262–274

Fennel W., Seifert T., Kayser B.,1991, Rossby radii and phase speeds in the Baltic Sea, *Cont. Shelf Res., 11,* 23–36

Funkquist L., 2001, HIROMB, an operational eddy-resolving model for the Baltic Sea, *Bulletin of the Maritime Institute in Gdansk, 28,* 7–16

Gidhagen L., 1987, Coastal upwelling in the Baltic Sea –- Satellite and in situ measurements of sea-surface temperatures indicating coastal upwelling, *Estuarine Coastal Shelf Sci., 24,* 449–462

Gästgifvars M., Lauri H., Sarkanen A., Myrberg K., Andrejev O., Ambjörn C., 2006, Modelling surface drifting of buoys during a rapidly-moving weather front in the Gulf of Finland, Baltic Sea, *Est. Coastal and Shelf Science, 70,* 567–576

Haapala J., 1994, Upwelling and its influence on nutrient concentration in the coastal area of Hanko peninsula, entrance to the Gulf of Finland, *Estuarine Coastal Shelf Sci., 38,* 507–521

HELCOM, 1994, *Report on chemical munitions dumped in the Baltic. Report to the 15th meeting of the Helsinki Commission from the ad-hoc working group on dumped*

chemical munition (HELCOM CHEMU), Danish Environmental Protection Agency, 39 pp.

HELCOM, 1996, *Third periodic assessment of the state of the marine environment of the Baltic Sea, 1989–93; Background document*, *Baltic Sea Environ. Proceedings,* 64B, 252 pp.

Hunter R. J., Craig D. P., Phillips E. H., 1993, On the use of random walk models with spatially variable diffusivity, *J. Comput. Phys., 106,* 366–376

Kling H., Döös K., 2007, *Radio-nuclide particle transport, sedimentation and resuspension in the Forsmark and Laxemar coastal regions*, SKB R-07-43, 27 pp.

Kononen K., Huttunen M., Hällfors S., Gentien P., Lunven M., Pavelson J., Stips A., 2003, Development of a deep chlorophyll maximum of Heterocapsa triquetra Ehrenb. at the entrance to the Gulf of Finland, *Limnol. Oceanogr., 48,* 594–607

Kowalewski M., 2005, The influence of the Hel upwelling (in the Baltic Sea) on nutrient concentration and primary production – the results of an ecohydrodynamic model, *Oceanologia, 47,* 567–590

Kowalewski M., Ostrowski M., 2005, Coastal up- and downwelling in the southern Baltic, *Oceanologia, 47,* 453–475

Krauss W., Brügge B., 1991 Wind-produced water exchange between the deep basins of the Baltic Sea, *J. Phys. Oceanogr., 21,* 373–394

Kuhrts C., Fennel W., Seifert T., 2004, Model studies of transport of sedimentary material in the Western Baltic, *J. Mar. Sys., 52,* 167–190

Kuvaldina N., Lips I., Lips U., Liblik T., 2010, The influence of a coastal upwelling event on chlorophyll a and nutrient dynamics in the surface layer of the Gulf of Finland, Baltic Sea, *Hydrobiologia, 639,* 221–230

Laanemets J., Kononen K., Pavelson J., Poutanen E.-L., 2004, Vertical location of seasonal nutriclines in the western Gulf of Finland, *J. Mar. Sys., 52,* 1–13

Laanemets J., Zhurbas V., Elken J., Vahtera E., 2009, Dependence of upwelling mediated nutrient transport on wind forcing, bottom topography and stratification in the Gulf of Finland: model experiments, *Boreal Env. Res., 14,* 213–225

Lehmann A., Myrberg K., 2008, Upwelling in the Baltic Sea – a review, *J. Mar. Sys., 74*, S3–S12

Lehmann A., Javidpour J., 2010, Potential pathways of invasion and dispersal of *Mnemiopsis leidyi A. Agassiz 1865* in the Baltic Sea, *Hydrobiologia, 649,* 107–114

Lentz S. J., Chapman D. C., 2004, The importance of nonlinear cross-shelf momentum flux during wind-driven coastal upwelling, *J. Phys. Oceanogr., 34,* 2444–2457

Leppäranta M., Myrberg K., 2009, *Physical Oceanography of the Baltic Sea*, Springer Praxis Books, 378 pp.

Lips I., Lips U., Liblik T., 2009, Consequences of coastal upwelling events on physical and chemical patterns in the central Gulf of Finland (Baltic Sea), *Cont. Shelf Res., 29,* 1836–1837

Meier H. E. M. 2007, Modeling the pathways and ages of inflowing salt- and freshwater in the Baltic Sea, *Estuar. Coast. Shelf Sci., 74,* 610–627

Mellor G. L., Yamada T., 1982, Development of a turbulence closure model for geophysical fluid problems, *Rev. Geophys., 20,* 851–875

Myrberg K., Andrejev, O., 2003, Main upwelling regions in the Baltic Sea – a statistical analysis based on three-dimensional modeling, *Boreal Env. Res., 8,* 97–112

Myrberg K., Lehmann A., Raudsepp U., Szymelfenig M., Lips I., Lips U., Matciak M., Kowalewski M., Krężel A., Burska D., Szymanek L., Ameryk A., Bielecka L., Bradtke K., Gałkowska A., Gromisz S., Jędrasik J., Kalużny M., Kozłowski L., Krajewska-Sołtys A., Ołdakowski B., Ostrowski M., Zalewski M., Andrejev O., Suomi I., Zhurbas V., Kauppinen O.-K., Soosaar E., Laanemets J., Uiboupin R., Talpsepp L., Golenko M., Golenko N., Vahtera E., 2008, Upwelling events, coastal offshore exchange, links to biogeochemical processes, in *Highlights from the Baltic Sea Science Conference, March 19–22, 2007 at Rostock University*. *Oceanologia, 50*(1), 95–113

Myrberg K., Andrejev O., Lehmann A., 2010, Dynamic features of successive upwelling events in the Baltic Sea – a numerical case study, *Oceanologia, 52*(1), 77–99

Männik A., Merilain M., 2007, Verification of different precipitation forecasts during extended winter-season in Estonia, *HIRLAM Newsletter, 52,* 65–70

Seifert T., Tauber F., Kayser B., 2001, A high resolution spherical grid topography of the Baltic Sea – revised edition. *Baltic Sea Science Congress 2001: Past, Present and Future – A Joint Venture. Abstract Volume.* Stockholm Marine Research Centre, Stockholm University, 298

Smagorinsky J., 1963, General circulation experiment with the primitive equations. I. The basic experiment, *Mon. Weather Rev., 91,* 99–164

Sokolov A., Andrejev O., Wulff F., Rodriguez Medina M., 1997, The data assimilation system for data analysis in the Baltic Sea, *System Ecology Contributions 3,* Stockholm University, Sweden, 66 pp.

Soomere T., Keevallik, S., 2003, Directional and extreme wind properties in the Gulf of Finland, *Proc. Estonian Acad. Sci. Eng., 9,* 73–90

Suursaar Ü., Aps R., 2007, Spatio-temporal variations in hydrophysical and chemical parameters during a major upwelling event off the southern coast of the Gulf of Finland in summer 2006, *Oceanologia, 49,* 209–229

Uiboupin R., Laanemets J., 2009, Upwelling characteristics derived from satellite sea surface temperature data in the Gulf of Finland, Baltic Sea, *Boreal Env. Res., 14,* 297–304

Vahtera E., Laanemets J., Pavelson J., Huttonen M., Kononen K., 2005, Effect of upwelling on the pelagic environment and bloom-forming cyanobacteria in the Western Gulf of Finland, Baltic Sea, *J. Mar. Sys.*, 58, 67–82

Visser W. A., 1997, Using random walk models to simulate the vertical distribution of particles in a turbulent water column, *Mar. Ecol.: Proc. Ser., 158,* 275–281

Wulff F., Rahm L., 1991, A database and its tools. Wulff F. (ed), *Large-scale environmental effects and ecological processes in the Baltic Sea. Reasearch programme for the period 1990–95 and background documents. SNV Report 3856,* 217–225

Zhurbas V., Stipa T., Mälkki P., Paka V., Golenko N., Hense I., Sklyarov V., 2004, Generation of subsurface cyclonic eddies in the Southeast Baltic Sea: Observations and numerical experiments, *J. Geophys. Res., 109*, doi: 10.1029/2003JC002074

Zhurbas V., Laanemets J., Vahtera E., 2008, Modeling of the mesoscale structure of coupled upwelling/downwelling events and the related input of nutrients to the upper mixed layer in the Gulf of Finland, Baltic Sea, *J. Geophys. Res., 113*, C05004, doi:10.1029/2007JC004280

APPENDIX A: PAPERS

Paper I

Laanemets, J., **Väli, G.**, Zhurbas, V., Elken, J., Lips, I., Lips, U. 2011. Simulation of mesoscale structures and nutrient transport during summer upwelling events in the Gulf of Finland in 2006. Boreal Environment Research, 16(A), 15–26

BOREAL ENVIRONMENT RESEARCH 16 (suppl. A): 15–26
ISSN 1239-6095 (print) ISSN 1797-2469 (online)

Helsinki 31 March 2011

Simulation of mesoscale structures and nutrient transport during summer upwelling events in the Gulf of Finland in 2006

Jaan Laanemets[1)], Germo Väli[1)], Victor Zhurbas[1)2)], Jüri Elken[1)], Inga Lips[1)] and Urmas Lips[1)]

[1)] *Marine Systems Institute, Tallinn University of Technology, Akadeemia tee 21, Tallinn 12618, Estonia*
[2)] *Shirshov Institute of Oceanology, 36 Nakhimovsky Prospect, Moscow 117851, Russia*

Received 30 Oct. 2009, accepted 15 Apr. 2010 (Editor in charge of this article: Kai Myrberg)

Laanemets, J., Väli, G., Zhurbas, V., Elken, J., Lips, I. & Lips, U. 2011: Simulation of mesoscale structures and nutrient transport during summer upwelling events in the Gulf of Finland in 2006. *Boreal Env. Res.* 16 (suppl. A): 15–26.

A high resolution numerical study was carried out to simulate a series of upwelling events and related nutrient transport in the Gulf of Finland. In order to characterize the intensity of water motions of different nature in the surface layer, simulated velocity components were decomposed into mesoscale fluctuations, inertial oscillations and mean currents. Mean currents contained 14%, inertial oscillations 20% and mesoscale fluctuations 66% of the total kinetic energy. High values of kinetic energy of mesoscale fluctuations were in the coastal zones (up to 0.03 m^2 s^{-2}) due to along-shore baroclinic upwelling/downwelling jets and in the narrowest western-central part (0.01–0.02 m^2 s^{-2}) of the Gulf, where intensive squirts and eddies were formed. In this region also the most intensive coastal offshore exchange of upwelled nutrients occurred. The total content of phosphorus and nitrogen in the upper 10-m layer introduced by the upwelling events was estimated at 1100 tonnes, with a clear excess of phosphorus.

Introduction

Upwelling is a typical phenomenon in the Baltic Sea, redistributing both the heat and salt in coastal regions and replenishing the surface layer with nutrients, especially in summer when the surface layer is depleted of nutrients. Model simulations have shown that the annual-averaged frequency of strong upwelling may be as high as 30% in some parts of the Baltic Sea (Kowalewski and Ostrowski 2005). Owing to the prevailing south-westerly winds (e.g. Soomere and Keevallik 2003) the northern part of the Gulf of Finland is an active upwelling area as shown by satellite sea surface temperature data (e.g. Kahru *et al*. 1995, Uiboupin and Laanemets 2009) and model simulations (Myrberg and Andrejev 2003). According to field data, summer upwelling events usually transport nutrients with the excess of phosphorus in relation to the Redfield ratio into the surface layer in the Gulf of Finland (Haapala 1994, Kononen *et al*. 2003, Vahtera *et al*. 2005, Lips *et al*. 2009). The excess phosphorus input is most likely a result of low nitrogen to phosphorus ratio in the deeper layers of the Gulf (Lehtoranta 2003) and the higher depth of phosphacline than nitracline in the range of thermocline (Laanemets *et al*. 2004). Model experiments by Laanemets *et al*. (2009) showed that a different ability of upwelling along the

northern and southern coast to transport nutrients to the surface layer is caused by the features of bottom topography. A steeper bottom slope and greater sea depths along the southern coast caused larger nutrient inputs under the same magnitude of wind forcing. An important aspect related to the nutrient enrichment of the whole Gulf surface layer by upwelling is an enhanced coastal offshore exchange during the relaxation phase. Model simulations by Zhurbas *et al*. (2008) showed that the instability of along-shore baroclinic jets and related thermohaline fronts caused by coupled upwelling and downwelling events lead to the development of filaments/squirts remarkably increasing the lateral eddy diffusivity.

A comprehensive review of the Baltic Sea upwelling, its dynamics and reflections to ecosystem is presented by Lehmann and Myrberg (2008) and Myrberg *et al*. (2008).

Summer 2006 was characterized by quite a rare meteorological situation — easterly winds that are favourable for the upwelling along the southern coast of the Gulf prevailed during a relatively long period (whole August). As a result, a very intensive upwelling was observed along the southern coast (Lips *et al*. 2009). During 2000–2006, it was the largest upwelling by area on the southern coast [20% of the total Gulf area; Uiboupin and Laanemets (2009)]. The cross-shore extent of the upwelling zone amounted to 25 km (about 1/3 of the Gulf's width) and the along-shore extent up to 360 km (Suursaar and Aps 2007). Water temperature along the southern coast was as low as 5–8 °C for about two weeks (based on the unpublished data of operational measurements from the TUT Marine Systems Institute and the Estonian Meteorological and Hydrological Institute) while the offshore temperature was in a range 18–22 °C (Lips *et al*. 2008).

The present paper is aimed to investigate a sequence of upwelling events including intensive upwelling along the southern coast of the Gulf in July–August 2006, combining the results of model simulations with these of the field measurements and satellite imagery. The objectives are (1) to simulate mesoscale variability of temperature, velocity and nutrients fields, (2) to characterize the intensity of water motions of different nature (mesoscale fluctuations, inertial oscillations, and mean currents) in the surface layer, (3) to estimate total inputs and averaged spatial distributions of nutrients caused by a sequence of upwelling events.

Model setup

We applied the Princeton Ocean Model (POM) (Blumberg and Mellor 1983) in the Baltic Sea. The POM is a primitive equation, sigma coordinate, free surface, hydrostatic model with a second moment turbulent closure sub-model embedded. The horizontal step of the model grid is 0.5 nautical miles in the Gulf (Fig. 1) and reaches 2 nautical miles in the rest of the Baltic Sea; there are 30 σ-levels in the vertical direction. The digital topography of the sea bottom is taken from Seifert and Kayser (1995). The refinement of the bottom topography in the Gulf was done by means of bilinear interpolation of the original 1.0 nautical-mile grid. A model resolution of 0.5 nautical miles allows resolving mesoscale phenomena, including upwelling filaments/squirts (Zhurbas *et al*. 2008) controlled by the internal baroclinic Rossby radius the value of which varies within 2–5 km in the Gulf (Alenius *et al*. 2003).

Model simulations were carried out from 10 July to 31 August 2006 covering several upwelling events along both the northern and the southern coasts of the Gulf, including a very intense upwelling event along the southern coast during the first half of August. Atmospheric forcing (wind stress and surface heat flux components) was calculated from wind, solar radiation, air temperature, total cloudiness and relative humidity data taken from HIRLAM (High Resolution Limited Area Model) version of the Estonian Meteorological and Hydrological Institute with the spatial resolution of 11 km and forecast interval of 1 h ahead of 54 h, recalculated after every 6 h (Männik and Merilain 2007). Wind velocity components at the 10-m level along with the other HIRLAM meteorological parameters were interpolated to the model grid. The model domain is closed at the Danish straits by an artificial shore since during the simulation period the spatially mean Baltic Sea

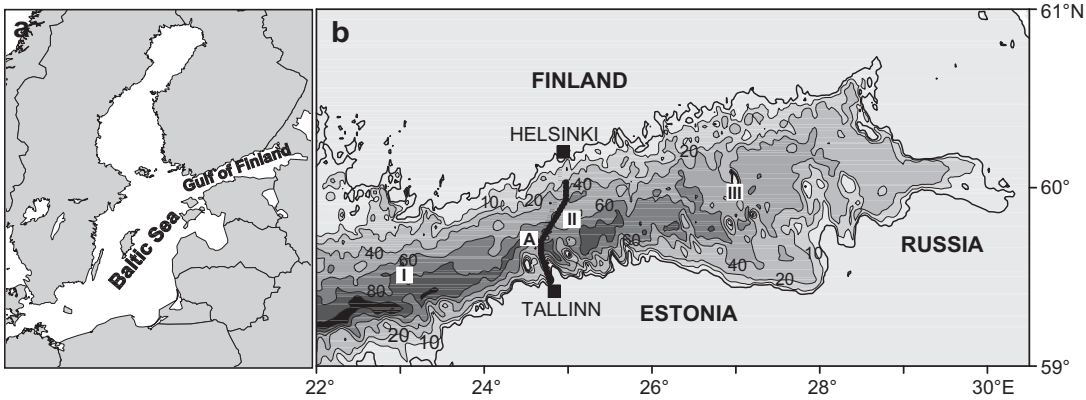

Fig. 1. (**a**) A map of the Baltic Sea, and (**b**) a close-up of the Gulf of Finland, where the model grid is refined to 0.5 nautical miles. Location of the transect (thick line) of nutrient sampling stations between Tallinn and Helsinki; the time series of HIRLAM wind data in the (I) western, (II) central and (III) eastern Gulf; and (A) a temporal snapshot of a simulated vertical distribution of the *u* component of velocity, phosphate and NO_x concentrations are shown. The depths are given in meters.

level was very stable: by our estimates from the open boundary model, the variations were less than 0.05 m, while the long-term variations of the mean sea level of the Baltic may exceed 1 m (Lehmann *et al*. 2004). Freshwater supply, although of secondary importance for the upwelling dynamics, was applied as the Neva river inflow with the volume rate of 77.6 km^3 yr^{-1} (Bergström *et al*. 2001).

Initial thermohaline fields were taken from HIROMB (High Resolution Operational Model of the Baltic Sea), a *z*-level model, from the 1 nautical mile grid step version as provided by SMHI (Funkquist 2001). The vertical grid step is 4 m in the surface layer down to 12 m and increases towards greater depths, resulting in 16 layers at 230 m. Thermohaline fields of HIROMB were first interpolated to our horizontal model grid and before the transformation from *z*-levels to σ-levels were smoothed horizontally with averaging length of 10 nautical miles in the Gulf. The latter procedure was necessary to suppress the dynamical imbalances of mesoscale motions that may occur during the grid conversion. In upwelling-dominated situations, POM is able to reproduce mesoscale variability of upwelling in the Gulf, including filaments/squirts and eddies, starting from quite smooth initial thermohaline conditions (Zhurbas *et al*. 2008).

Two equations describing passive tracer balance were introduced to POM to simulate nutrient (phosphate, and nitrate + nitrite henceforth called NO_x) transport. In order to estimate the amount of nutrients transported from deep layers to the upper mixed layer due to upwelling and further lateral transport by filaments and eddies, nutrients were considered as conservative passive tracers. This approach does not include the effects of biogeochemical processes the contribution of which to the time rate of the change of nutrients is small during intensive upwelling (Tilstone *et al*. 2000). The equations were solved numerically within the POM code in the same way as those for temperature and salinity. In order to describe the initial fields of nutrients, we used the data collected along a repeated transect of 14 stations on the line Tallinn–Helsinki on 11 and 25 July 2006 (Fig. 1); the distance between sampling stations was 5.2 km; the samples were collected mainly from the 0–40-m layer (Lips *et al*. 2009). Vertical resolution in the thermocline layer was 2.5–5 m and one sample was taken from the near-bottom layer. In the upper mixed layer, nutrient concentrations were below or close to the detection level and in the model, the initial fields were therefore set to zero in this layer. According to the measurements the nutriclines were tightly coupled with the thermocline and slightly separated, the phosphacline situated at shallower depths (*see* Lips *et al*. 2009). We, therefore, introduced linear profiles for PO_4 and NO_x concentrations between the depth of a certain isothermal surface in the thermocline and

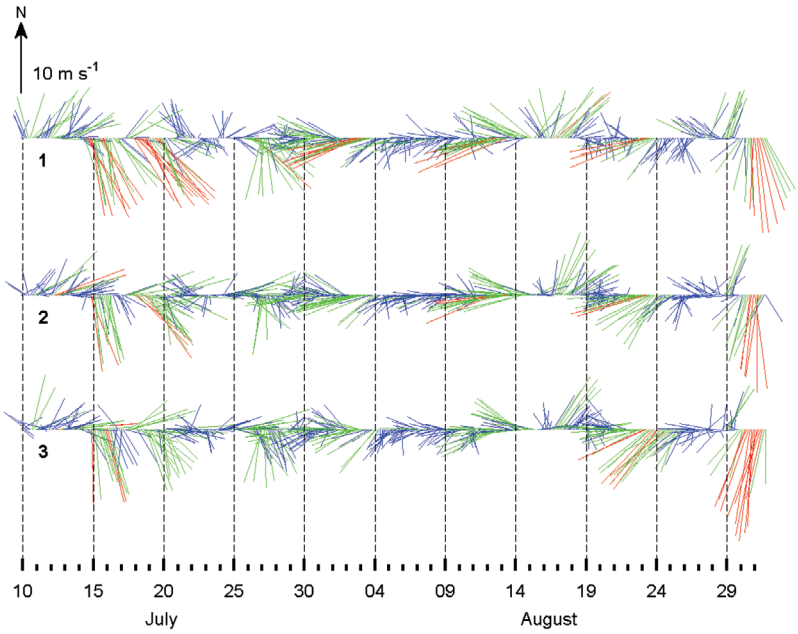

Fig. 2. Time series of the 10-m level HIRLAM wind vector in the (1) western, (2) central and (3) eastern parts of the Gulf of Finland for the period 10 July–31 August, 2006. Colours: blue = wind speed < 6 m s^{-1}, green = 6 ≤ wind speed ≤ 10 m s^{-1}, red = wind speed > 10 m s^{-1}.

the 40-m depth. The best fit was obtained when isothermal surfaces of 7 and 11 °C as upper locations of nitracline and phosphacline, and PO_4 and NO_x concentrations at the 40-m depth of 0.6 and 1.7 mmol m^{-3} were used, respectively. We extended nutrient profiles to a greater depth using the data from other sources (Zhurbas *et al*. 2008). The assembled vertical distributions of nutrient concentrations are

$$PO_4 = \begin{cases} 0, & 0 \le z \le h_{11°C} \\ 0.6\left(z - h_{11°C}\right) \Big/ \left(40 - h_{11°C}\right), & h_{11°C} < z \le 40 \text{ m} \\ 0.013\left(z - 40\right) + 0.6, & z > 40 \text{ m} \end{cases}$$

$$NO_x = \begin{cases} 0, & 0 \le z \le h_{7°C} \\ 1.7\left(z - h_{7°C}\right) \Big/ \left(40 - h_{7°C}\right), & h_{7°C} < z \le 40 \text{ m} \\ 0.066\left(z - 40\right) + 1.7, & z > 40 \text{ m} \end{cases} \quad (1)$$

where z is the depth in meters, $h_{11°C}$ and $h_{7°C}$ are the depths of 11 °C and 7 °C isothermal surfaces in the model initial data, respectively. The vertical profiles of nutrients described above were extended to the whole Baltic Sea. This procedure excludes the effects of horizontal nutrient fluxes, which do exist due to the horizontal gradients of nutrient concentrations (in summer below the euphotic zone). There are large horizontal gradients of nutrients in the Gulf of Finland (e.g. Kuuppo *et al*. 2006: fig. 5). However, the approach we used allows us better to single out the effects of vertical nutrient fluxes.

The model runs from the motionless state and zero surface elevation starting at 00:00 of 10 July 2006.

Results and discussion

Modelled upwelling dynamics

Depending on the ability to drive upwelling, the overall simulation period can be divided into two parts: a relatively short westerly-component wind period (before 29 July) followed by a long-lasting easterly-component wind period (after 31 July) (Fig. 2). The easterly (westerly) component winds are favourable for upwelling along the southern (northern) coast of the Gulf. There were four time intervals when the speed of the wind favourable for upwelling near the southern coast exceeded 10 m s^{-1} (on 3, 13, 23, and 30 August). Within this easterly wind period there was a 3-day interval of reverse, south-westerly wind (from 16 to 18 August) which would result in a temporary weakening of upwelling (i.e., the decrease of cold water temperature contrast) along the southern coast or would even produce upwelling along the opposite, northern coast.

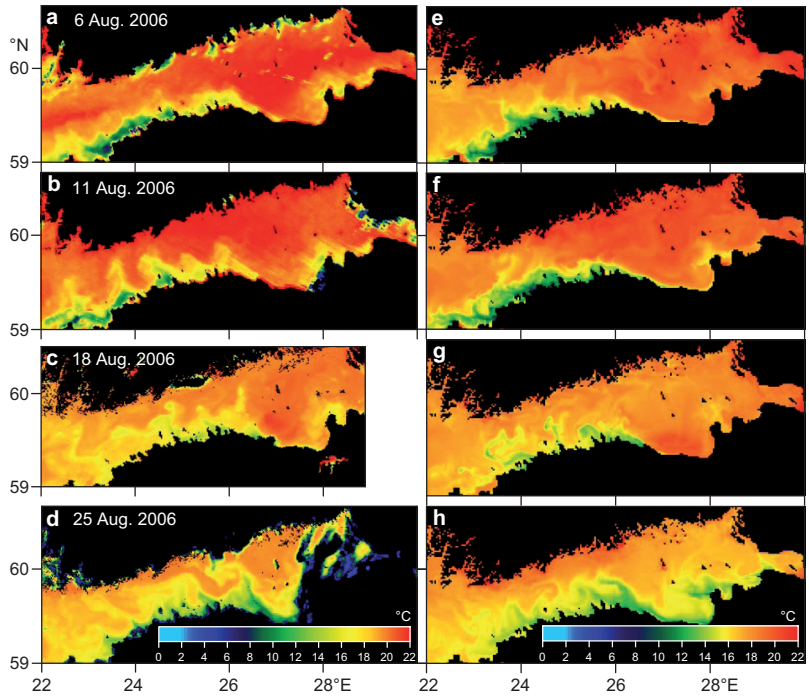

Fig. 3. SST maps of the Gulf of Finland in August 2006: (**a**–**d**) satellite imagery and (**e**–**h**) simulations.

The real effect of the reverse wind will be discussed later in this section.

A comparison of SST maps obtained from satellite imagery within the period of upwelling along the southern coast of the Gulf with that of simulations (Fig. 3) indicates that:

1. on 6 and 11 August, the most intensive upwelling along the southern coast is observed in the western part of the Gulf,
2. on 25 August the intensive upwelling area shifted to the eastern part of the Gulf. The displacement of the upwelling area occurred due to spatial changes in the wind field: the speed of E–SE winds on 25 August (6 and 11 August) was higher in the eastern (western) part of the Gulf (*see* Fig. 2),
3. on 18 August the intensity of upwelling was weakened due to transient SW winds (*see* Fig. 2),
4. the characteristic features of mesoscale coherent structures (i.e. filaments/squirts) observed in the satellite SST maps were reasonably well reproduced by simulations. Of course it does not mean the identity of individual mesoscale structures.

A simulated mesoscale variability of the surface layer currents in the course of upwelling/downwelling events is illustrated in Fig. 4. In order to eliminate inertial oscillations, which are able to mask 'pure' mesoscale motions, the former were filtered out using a simple procedure:

$$\tilde{\boldsymbol{v}}(\boldsymbol{x},t) = 0.5\boldsymbol{v}(\boldsymbol{x},t) + 0.25\left[\boldsymbol{v}\left(\boldsymbol{x},t-\frac{T_\mathrm{i}}{2}\right)+\boldsymbol{v}\left(\boldsymbol{x},t+\frac{T_\mathrm{i}}{2}\right)\right], \quad (2)$$

where $\boldsymbol{v}(\boldsymbol{x},t)$ and $\tilde{\boldsymbol{v}}(\boldsymbol{x},t)$ are the velocity vectors at the 2-m depth before and after the filtration, respectively, $T_\mathrm{i} \equiv 2\pi/f = 0.58$ day is the inertia oscillation period, f is the Coriolis parameter. Upwelling along the north coast of the Gulf (Fig. 4a) is characterized by transverse cold water filaments and related to transverse jet-like currents or squirts with southward velocities up to 0.3 m s^{-1}. Some of the squirts penetrate almost the whole width of the Gulf.

The culmination of upwelling along the southern coast of the Gulf is shown in Fig. 4b. The pattern of cold water transverse filaments and squirts developed from the upwelling along

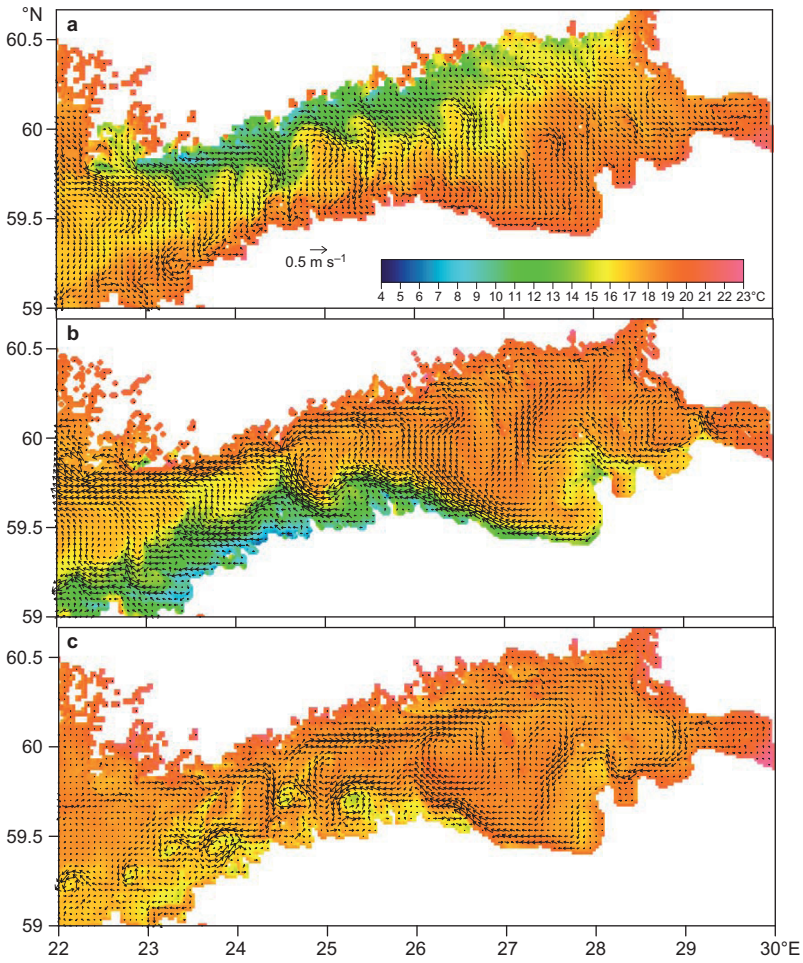

Fig, 4. Simulated surface layer currents (vectors) and SST in the Gulf in the course of upwelling/downwelling events on (**a**) 26 July (01:00 UTC), (**b**) 13 August (17:00 UTC), and (**c**) 19 August (18:15 UTC). The vectors of current are depicted in every fourth grid nodes.

the southern coast to some extent looks like a mirror image of the upwelling along the northern coast (cf. Fig. 4a and b). The most intensive cold water filament and squirt with northward velocity up to 0.4 m s^{-1} was observed at the narrowest part of the Gulf between Tallinn and Helsinki. Note that the along-shore distribution of transverse filaments and squirts related to the upwelling along the southern coast is less uniform than that of the northern coast likely because the southern coast of the Gulf is curved while the northern coast is relatively straight.

Due to the transient reverse of wind direction from east to west, the upwelling along the southern coast weakened (Fig. 4c). A striking feature here is the formation of several mesoscale cyclonic eddies in the southwestern part of the Gulf of Finland: one can discern at least six cyclonic eddies with the diameter of 12–24 km and rotation velocity of 0.2 m s^{-1}. This is just in accordance with Zhurbas *et al.* (2006), who showed that the instability of an upwelling (downwelling) baroclinic jet results in a selective formation of mostly cyclonic (anticyclonic) eddies.

Kinetic energy during upwelling

In order to characterize the intensity of water motions of different nature in the surface layer of the Gulf, the simulated velocity components at the 2-m depth, (u,v) were decomposed into mesoscale (eddy) fluctuations (u'_E, v'_E), inertial oscillations (u'_I, v'_I) and mean currents $(\overline{u}, \overline{v})$

$$u = u'_E + u'_I + \overline{u}, \quad v = v'_E + v'_I + \overline{v}, \qquad (3)$$

where overbar means the time averaging over the whole simulation period. Inertial oscillations were separated using Eq. 2. Then the mean kinetic energy per unit volume was calculated for each type of motions

$$\begin{aligned} \mathrm{EKE} &= \left(\overline{u_{\mathrm{E}}'^2} + \overline{v_{\mathrm{E}}'^2}\right)\Big/2 \\ \mathrm{IKE} &= \left(\overline{u_{\mathrm{I}}'^2} + \overline{v_{\mathrm{I}}'^2}\right)\Big/2 \cdot \\ \mathrm{MKE} &= \left(\overline{u}^2 + \overline{v}^2\right)\Big/2 \end{aligned} \qquad (4)$$

The MKE data are of minor interest because the averaging period (53 days) does not allow MKE interpretation as seasonal or annual means. At the same time, the simulation period of 53 days is long enough to obtain some statistics of mesoscale fluctuations (eddies, squirts) and inertial oscillations and, therefore, to analyze EKE and IKE maps (Fig. 5). The EKE level is the highest (up to 0.03 m^2 s^{-2}) in the coastal zone close to the southern and northern shores of the Gulf where variable wind forcing produces alongshore baroclinic jet currents of alternating direction due to successive upwelling and downwelling events (Fig. 5a). Again, high enough values of EKE (0.01–0.02 m^2 s^{-2} which corresponds to r.m.s. velocity fluctuations of 0.14–0.20 m s^{-1}) are found in the narrow western and central parts of the Gulf, where intensive transverse squirts and eddies are formed (cf. Figs. 4 and 5a).

In contrast to EKE, the energy of inertial oscillations is relatively uniformly distributed within open waters (IKE ≈ 0.004 m^2 s^{-2}) and decreases below 0.002 m^2 s^{-2} in coastal and shallow zones (as close as 1–2 nautical miles to the shore and as shallow as 20 m of the sea depth) (Fig. 5b).

The average levels of EKE, IKE and MKE in the surface layer of the Gulf were estimated as <EKE>/<IKE>/<MKE> = 0.0072/0.0021/0.0015 m^2 s^{-2}. In other words, EKE, IKE, and MKE contain 66%, 20% and 14% of the total kinetic energy, respectively.

A cold water filament and a related transverse squirt on the beam of Tallinn Bay being initially wide (*see* Fig. 4b) narrowed and created a bottleneck in the middle to connect with a cyclonically rotating cold water pool in the north (Fig. 6a).

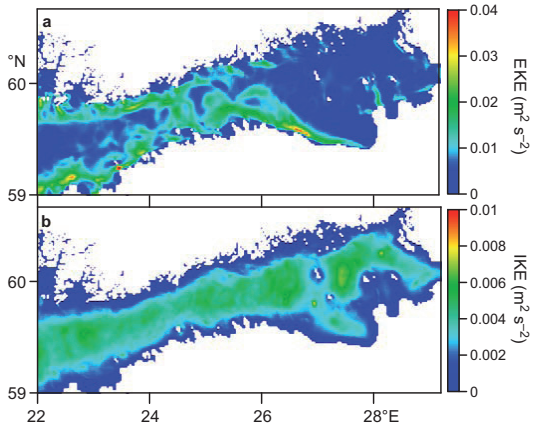

Fig. 5. Maps of simulated (**a**) eddy kinetic energy and (**b**) inertial oscillation kinetic energy in the surface layer of the Gulf.

The bottleneck was expected to vanish in a while, which would mark the accomplishment of cyclonic eddy formation. This cyclonic eddy was clearly identified for more than two days (Fig. 4c). The currents related to the bottleneck and it is likely that also the cyclonic eddy could occupy the upper sea layer that is 20–30 m thick (Fig. 6c).

Nutrient dynamics

The ability of the model to reproduce nutrient transport into the surface layer in the course of upwelling events is demonstrated by comparing the simulated nutrient distribution with a corresponding distribution sampled on a transect between Tallinn and Helsinki (Fig. 7). The model reproduced both the PO_4 and NO_x distributions reasonably well even after about one-month simulation period covering several upwelling events along the northern coast and a strong upwelling event along the southern coast (Fig. 7). The simulated and measured PO_4 concentration values in the upwelling zone (Fig. 7c and d) were approximately the same whereas NO_x concentrations (Fig. 7a and b) differed more. This and the higher simulated NO_x and PO_4 concentrations in the surface layer at the warmer side of the upwelling front can be explained by the lack of nutrient consumption in the model. Also, it is worth mentioning that the observed nutrient

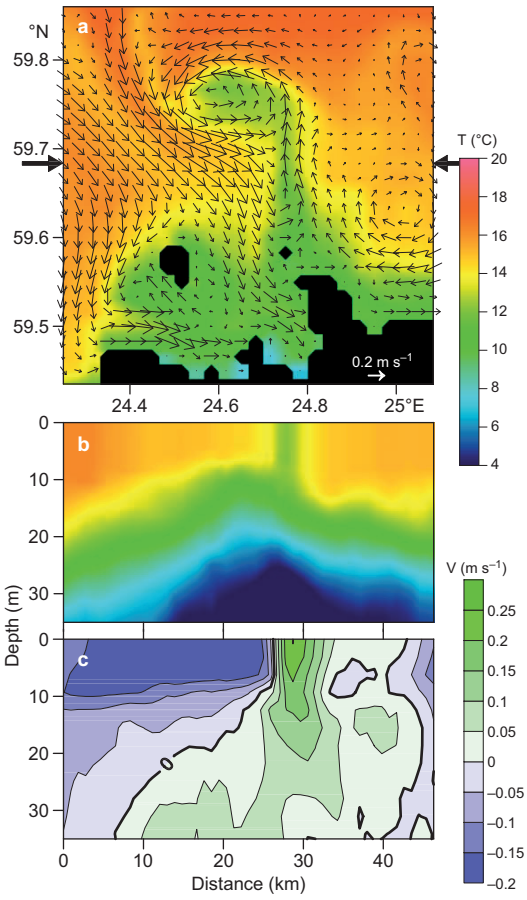

Fig. 6. Snapshot of a simulated cold-water filament and related transverse squirt transforming into a cyclonic eddy. (**a**) SST and surface layer currents off Tallinn Bay on 17 August, 06:45 UTC, (**b**) temperature, and (**c**) *v* component of velocity *vs.* distance and depth on a zonal transect marked by thick arrows. Velocity vectors are depicted in every second grid nodes.

distributions look more patchy than the modelled ones. This is not surprising because the above-described parameterisation of initial nutrient distributions implies strong spatial averaging of data available.

Upwelling along the northern coast of the Gulf is accompanied by downwelling along the southern coast and vice versa. When the wind forcing weakens, the instability of two alongshore baroclinic jets and related fronts of a coupled upwelling/downwelling event produce cold/warm filaments (Fig. 4). The important role of filaments and eddies in the offshore transport and lateral mixing of upwelled nutrients in the Gulf was shown by Zhurbas *et al*. (2008) and Laanemets *et al*. (2009).

In order to evaluate the total nutrient input to the surface layer of the Gulf produced by a series of upwelling events in July–August 2006, the simulated concentrations of phosphorus and nitrogen were integrated in the upper 10-m layer over the whole Gulf area. The longitude 22°E was taken as the western boundary of the Gulf, including the entrance area. The integration depth of 10 m corresponds approximately to the depth of the euphotic zone in the relatively turbid Gulf of Finland (e.g. Kononen *et al*. 2003). Temporal courses of the total content of phosphorus and nitrogen in the surface layer of the Gulf are depicted in Fig. 8.

During the period from 10 July by the end of July a relatively weak westerly wind dominated (Fig. 2) and upwelling did develop along the northern coast of the Gulf. Total phosphorus and nitrogen transport into the surface layer (before upwelling events along the southern coast) was with the surplus of phosphorus as compared with the Redfield ratio of 7.2, about 450 and 400 tonnes correspondingly. The transport of surplus phosphorus is in accordance with our previous model simulations (Zhurbas *et al*. 2008) and field observations (Vahtera *et al*. 2005) in 1999. However, the relatively larger transport of nitrogen needs some explanation. Such an explanation can be based on the fact that stratification of the water column in the Gulf became stronger and, therefore, the phosphacline and the nitracline were located closer to each other and gradients were larger in the thermocline layer in the summer of 2006 than in 1999.

Easterly wind events — wind speed more than 10 m s^{-1} on 3, 13, 23 and 30 August (Fig. 2) — caused intensive upwelling events along the southern coast of the Gulf and brought altogether about 700 tonnes of nitrogen and 650 tonnes of phosphorus into the surface layer, i.e. a slight surplus of nitrogen. The nitrogen surplus is likely related to the changes in vertical nutrient distributions attained by the beginning of the period of upwelling events along the southern coast (*see* Fig. 9). The model simulation showed the dominance of westward flow in the upper 30-m layer along the southern coast in the period 18–30 July accompanied by a shallowing of

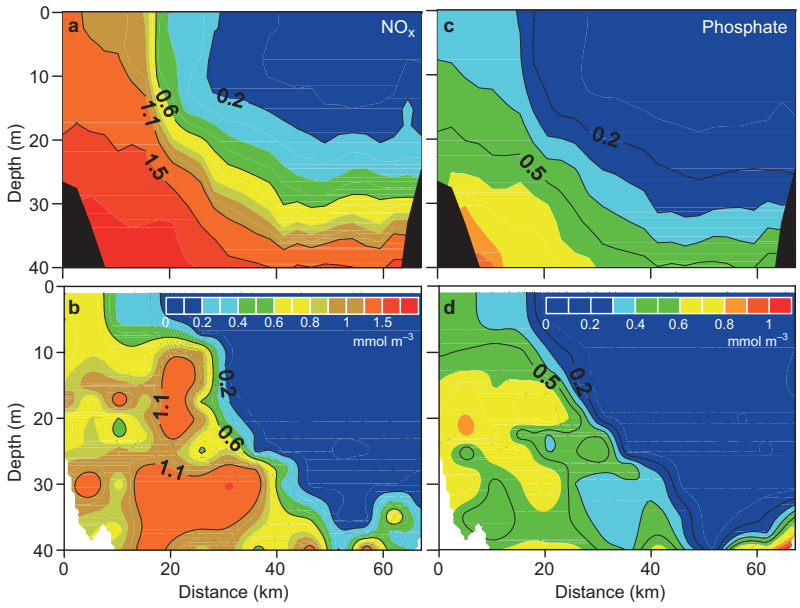

Fig. 7. Comparison of (**a**, **c**) simulated and (**b**, **d**) measured NO_x and PO_4 concentrations along the transect between Tallinn and Helsinki on 8 August. The values on the *x*-axis denote the distance from the southernmost sampling station. Separate colour scales for NO_x and PO_4 concentrations were used.

both the phosphacline and the nitracline. The shallowing was likely caused by the westward flow that would carry nutrient-rich water from deeper layers along the eastward sloping-down isopycnals. Again, taking into account that vertical gradient of NO_x concentration had been initially larger than that of PO_4, the upper boundary of the nitracline (i.e. 0.05 mmol m^{-3} contour) being deeper initially has risen above that of the phosphacline due to a vertical turbulent diffusion which is clearly seen in Fig. 9. This explains a slightly larger simulated transport of nitrogen than of phosphorus into the surface layer by upwelling events along the southern coast of the Gulf in 2006 (Fig. 8). Lips *et al*. (2009) also estimated from field measurements that about equal amounts of nitrogen and phosphorus were transported by upwelling into the surface layer.

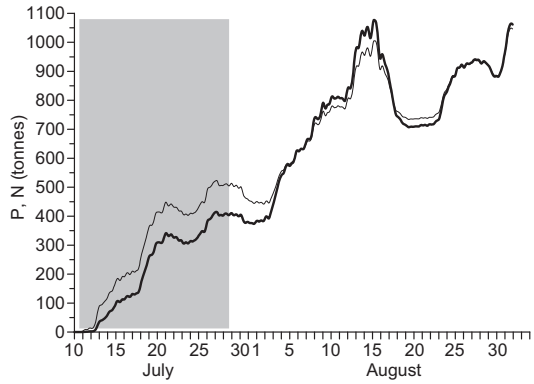

Fig. 8. Temporal course of total content of phosphorus (thin line) and nitrogen (bold line) introduced to the upper 10-m layer due to upwelling events along the northern (shaded area) and southern coasts during the simulation period in the Gulf of Finland.

In order to evaluate how much the lack of nutrient consumption in the model had influenced the above results we compared the changes of nutrient concentrations in the upper layer (0–25 m) for the period of 11–25 July estimated from the model with the measurements along the transect Tallinn–Helsinki. The changes in average concentrations were overestimated by the model only by < 0.02 mmol m^{-3} for PO_4 and < 0.12 mmol m^{-3} for NO_x, which is an order of magnitude less than the observed and calculated increase of nutrient concentrations in the upper layer during the upwelling events in August 2006. It shows that the estimates of total nutrient input to the surface layer of the Gulf produced by a series of strong upwelling events was not biased remarkably by neglecting the nutrient consumption.

A rapid decrease of total nutrient content as a response to a fast change of the wind regime was an expected result. Due to the transient SW wind, favourable for downwelling along the southern coast, on 18 August (Fig. 2), the intensity of upwelling weakened and a decline

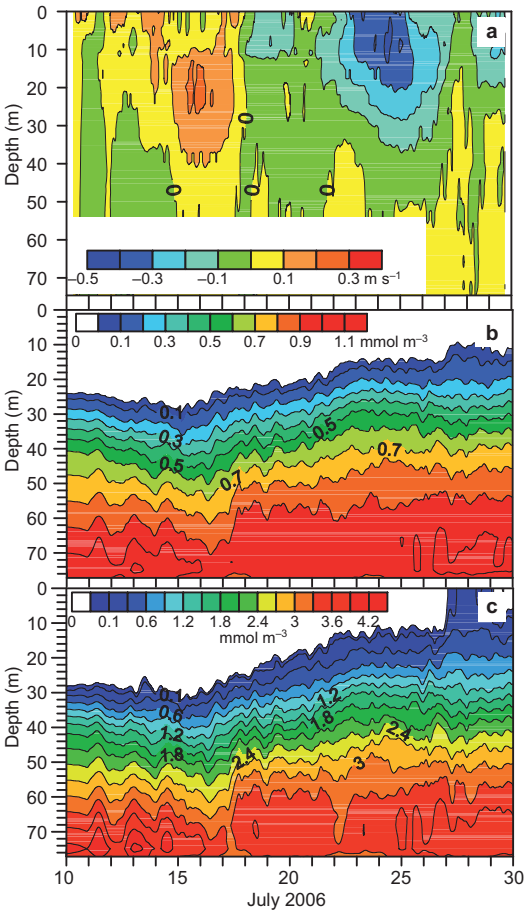

Fig. 9. Temporal course of vertical distribution of (**a**) the *u* component of velocity, (**b**) phosphate, and (**c**) NO_x concentrations at location A (Fig. 1).

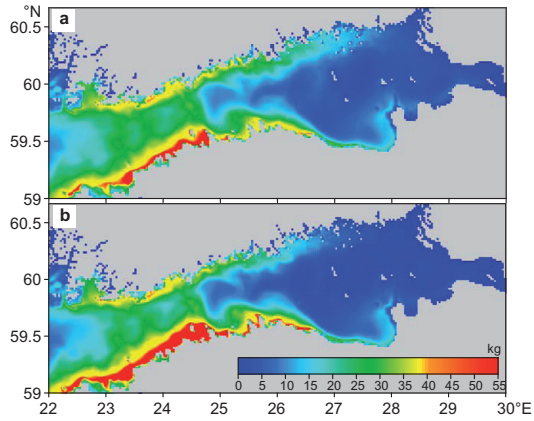

Fig. 10. Maps of mean (**a**) phosphorus and (**b**) nitrogen contents (kg) in the upper 10-m water column with cross section area of 0.5 × 0.5 nautical miles.

of isopycnal surfaces caused a decrease of phosphorus and nitrogen content in the surface layer by 250 and 400 tonnes, respectively. The total amounts of phosphorus and nitrogen transported by upwelling events into the surface layer during July–August was the same (about 1100 tonnes), i.e. with a clear excess of phosphorus (N:P = 1) as compared with the Redfield ratio of 7.2. The clear excess of phosphorus in the upwelled water allows us to suggest that a large part of phosphorus might be utilized by nitrogen-fixing cyanobacteria due to nitrogen limitation of other phytoplankton groups (e.g. Kangro *et al*. 2007). The estimated averaged external bioavailable phosphorus load in the Gulf is about 380 tonnes per month (e.g. Zhurbas *et al*. 2008), which is rather an overestimation due to low river runoff during late summer (Richter and Ebel 2006). Thus, an internal phosphorus load caused by the upwelling events in 2006 likely exceeded the external load during summer months. Combining the current results with those of previous simulations (Zhurbas *et al*. 2008, Laanemets *et al*. 2009) and field measurements (Vahtera *et al*. 2005, Lips *et al*. 2009), one may conclude that summer upwelling events transport phosphorus into the surface layer with a clear excess and the amounts are comparable with the external load.

An important aspect is the identification of areas of the largest nutrient input by upwelling events in the Gulf (Fig. 10). The largest inputs of nutrients occurred in the upwelling zones along both coasts. In the eastern part of the open Gulf, the content of upwelled nutrients was low. One can think of two causes for that. Firstly, the simulation period was characterised by wind patterns more favourable for upwelling events in the western and central parts of the Gulf in comparison to the eastern part. However, an analysis of the seven year (2000–2006) satellite SST data also showed less extensive upwelling events in the eastern part of the Gulf (Uiboupin and Laanemets 2009). Furthermore, the filaments predominantly stretched out from the upwelling front along the Finnish coast and in the western part of the Gulf. Secondly, the sea depth is lower and the bottom slope is less steep in the eastern part of the Gulf than in the central and western parts. The effect of bottom topogra-

phy on upwelling-mediated nutrient input was discussed in Laanemets *et al*. (2009). In the narrow western and central parts of the Gulf, where intensive transverse filaments/squirts and eddies are formed (Fig. 5), the averaged phosphorus and nitrogen content was much higher, because in this area upwelled nutrients are more intensively transported from the coastal zone to the open Gulf area.

Conclusions

Comparisons with satellite SST images and *in situ* measurements showed that upwelling events along both coasts of the Gulf, related mesoscale structures and nutrient distributions were reasonably well reproduced by the model.

The average levels of mean kinetic energy per unit volume of mesoscale/eddy fluctuations (EKE), inertial oscillations (IKE) and mean currents (MKE) in the surface layer of the Gulf were estimated as 0.0072, 0.0021 and 0.0015 $m^2\ s^{-2}$, respectively. The EKE was the highest (up to 0.03 $m^2\ s^{-2}$) in the coastal zones of the Gulf where variable wind forcing produced alternating alongshore baroclinic jet currents due to series of upwelling and downwelling events. Likewise, high values of EKE (0.01–0.02 $m^2\ s^{-2}$) were found in the narrowest western and central part of the Gulf, where intensive transverse squirts and eddies were formed. The distribution of IKE was relatively uniform in open waters (0.004 $m^2\ s^{-2}$) and decreased below 0.002 $m^2\ s^{-2}$ in coastal and shallow zones.

Total inputs of phosphorus and nitrogen caused by upwelling events along the northern and southern coasts were characterised by a clear excess of phosphorus; the input of phosphorus was comparable to or even exceeded the external load. In the eastern part of the Gulf nutrient input was relatively low during the whole simulation period. Spatial distributions of nutrients content in the surface layer caused by a sequence of upwelling events showed that the most intensive coastal offshore exchange occurred in the narrow western and central part of the Gulf.

Acknowledgements: We are thankful to anonymous reviewers for constructive recommendations. The work was supported by the Estonian Science Foundation (grants #7467, #7328 and #6752) and the Russian Foundation for Basic Research (Grant #09-05-00479). Estonian Meteorological and Hydrological Institute kindly provided atmospheric forcing data from HIRLAM and Swedish Meteorological and Hydrological Institute provided initial ocean data in the frame of HIROMB cooperation.

References

Alenius P., Nekrasov A. & Myrberg K. 2003. Variability of the baroclinic Rossby radius in the Gulf of Finland. *Cont. Shelf Res*. 23: 563–573.

Bergström S., Alexandersson H., Carlsson B., Fosefsson W., Karlsson K.G. & Westring G. 2001. Climate and hydrology of the Baltic Sea. In: Wulff F., Rahm L. & Larsson P. (eds.), *A system analysis of the Baltic Sea*, Ecological Studies 148, Springer-Verlag, Berlin Heidelberg New York, pp. 75–112.

Blumberg A.F. & Mellor G.L. 1983. Diagnostic and prognostic numerical calculation studies of the South Atlantic Bight. *J. Geophys. Res*. 88: 4579–4592.

Funkquist L. 2001. HIROMB, an operational eddy-resolving model for the Baltic Sea. *Bulletin of the Maritime Institute in Gdansk* XXVIII: 7–16.

Haapala J. 1994. Upwelling and its influence on nutrient concentration in the coastal area of the Hanko Peninsula, entrance to the Gulf of Finland. *Estuarine Coastal Shelf Sci*. 38: 507–521.

Kahru M., Håkansson B. & Rud O. 1995. Distributions of the sea-surface temperature fronts in the Baltic Sea as derived from satellite imagery. *Cont. Self Res*. 15: 663–679.

Kangro K., Olli K., Tamminen T. & Lignell R. 2007. Species-specific responses of a cyanobacteria-dominated phytoplankton community to artificial nutrient limitation: a Baltic Sea coastal mesocosm study. *Mar. Ecol. Prog. Ser*. 336:15–27.

Kononen K., Huttunen M., Hällfors S., Gentien P., Lunven M., Huttula T., Laanemets J., Lilover M., Pavelson J. & Stips A. 2003. Development of a deep chlorophyll maximum of *Heterocapsa triquetra* Ehrenb. at the entrance to the Gulf of Finland. *Limnol. Oceanogr*. 48: 594–607

Kowalewski M. & Ostrowski M. 2005. Coastal up- and downwelling in the southern Baltic. *Oceanologia* 47: 453–475.

Kuuppo P., Tamminen T., Voss M. & Schulte U. 2006. Nitrogenous discharges to the eastern Gulf of Finland, the Baltic Sea: Elemental flows, stable isotope signatures, and their estuarine modification. *J. Mar. Syst*. 63: 191–208.

Laanemets J., Kononen K., Pavelson J. & Poutanen E.-L. 2004. Vertical location of seasonal nutriclines in the western Gulf of Finland. *J. Mar. Syst*. 52: 1–13.

Laanemets J., Zhurbas V., Elken J. & Vahtera E. 2009. Dependence of upwelling mediated nutrient transport on wind forcing, bottom topography and stratification in the Gulf of Finland: model experiments. *Boreal Env. Res*.

14: 213–225.

Lehmann A., Lorenz P. & Jacob D. 2004. Modelling the exceptional Baltic Sea inflow events in 2002–2003. *Geophys. Res. Lett.* 31: L21308, doi: 10.1029/2004GL020830.

Lehmann A. & Myrberg K. 2008. Upwelling in the Baltic Sea — a review. *J. Mar. Sys.* 74: S3–S12.

Lehtoranta J. 2003. Dynamics of sediment phosphorus in the brackish Gulf of Finland. *Monogr. Boreal Env. Res.* 24: 1–58.

Lips I., Lips U. & Liblik T. 2009. Consequences of coastal upwelling events on physical and chemical patterns in the central Gulf of Finland (Baltic Sea). *Cont. Shelf Res.* 29: 1836–1847.

Lips U., Lips I., Liblik T. & Elken J. 2008. *Estuarine transport versus vertical movement and mixing of water masses in the Gulf of Finland (Baltic Sea)*. US/EU-Baltic International Symposium, 27–29 May 2008, Tallinn. *IEEE/OES*, doi:10.1109/BALTIC.2008.4625535.

Männik A. & Merilain M. 2007. Verification of different precipitation forecasts during extended winter-season in Estonia. *HIRLAM Newsletter* 52: 65–70.

Myrberg K. & Andrejev O. 2003. Main upwelling regions in the Baltic Sea — a statistical analysis based on three-dimensional modeling. *Boreal Env. Res.* 8: 97–112.

Myrberg K., Lehmann A., Raudsepp U., Szymelfenig M., Lips I., Lips U., Matciak M., Kowalewski M., Krężel A., Burska D., Szymanek L., Ameryk A., Bielecka L., Bradtke K., Gałkowska A., Gromisz S., Jędrasik J., Kaluźny M., Kozłowski L., Krajewska-Sołtys A., Ołdakowski B., Ostrowski M., Zalewski M., Andrejev O., Suomi I., Zhurbas V., Kauppinen O.-K., Soosaar E., Laanemets J., Uiboupin R., Talpsepp L., Golenko M., Golenko N. & Vahtera E. 2008. Upwelling events, coastal offshore exchange, links to biogeochemical processes — highlights from the Baltic Sea Science Conference, March 19–22, 2007 at Rostock University. *Oceanologia* 50: 95–113.

Richter K.-G. & Ebel M. 2006. Analysis of runoff for the Baltic Sea basin with an integrated atmosperhic-oceanic-hydrology model. *Advances in Geosciences* 9: 31–37.

Seifert T. & Kayser B. 1995. A high resolution spherical grid topography of the Baltic Sea. *Meereswissenschaftliche Berichte* 9: 72–88.

Soomere T. & Keevallik S. 2003. Directional and extreme wind properties in the Gulf of Finland. *Proc. Estonian Acad. Sci. Eng.* 9: 73–90.

Suursaar Ü. & Aps R. 2007. Spatio-temporal variations in hydrophysical and chemical parameters during a major upwelling event off the southern coast of the Gulf of Finland in summer 2006. *Oceanologia* 49: 209–229.

Tilstone G.H., Míguez B.M., Figueiras F.G. & Fermín E.G. 2000. Diatom dynamics in a coastal ecosystem affected by upwelling: coupling between species succession, circulation and biogeochemical processes. *Mar. Ecol. Prog. Ser.* 205: 23–41.

Vahtera E., Laanemets J., Pavelson J., Huttonen M. & Kononen K. 2005. Effect of upwelling on the pelagic environment and bloom-forming cyanobacteria in the western Gulf of Finland, Baltic Sea. *J. Mar. Sys.* 58: 67–82.

Uiboupin R. & Laanemets J. 2009. Upwelling characteristics derived from satellite sea surface temperature data in the Gulf of Finland, Baltic Sea. *Boreal Env. Res.* 14: 297–304.

Zhurbas V.M., Laanemets J. & Vahtera E. 2008. Modeling of the mesoscale structure of coupled upwelling/downwelling events and the related input of nutrients to the upper mixed layer in the Gulf of Finland, Baltic Sea. *J. Geophys. Res.* 113: C05004, doi: 10.1029/2007JC004280.

Zhurbas V., Oh I. & Park T. 2006. Formation and decay of a longshore baroclinic jet associated with transient coastal upwelling and downwelling: a numerical study with applications to the Baltic Sea. *J. Geophys. Res.* 111: C04014, doi: 10.1029/2005JC003079.

Paper II

Väli, G., Zhurbas, V., Laanemets, J., Elken, J. 2011. Simulation of nutrient transport from different depths during an upwelling event in the Gulf of Finland. Oceanologia, 53(TI), 431–448

Simulation of nutrient transport from different depths during an upwelling event in the Gulf of Finland*

OCEANOLOGIA, 53 (TI), 2011.
pp. 431–448.

KEYWORDS
Princeton Ocean Model
Upwelling
Baltic Sea
Nutrient transport

Germo Väli[1]
Victor Zhurbas[1,2]
Jaan Laanemets[1]
Jüri Elken[1]

[1] Marine Systems Institute,
Tallinn University of Technology,
Akadeemia tee 21, Tallinn 12618, Estonia

[2] P.P. Shirshov Institute of Oceanology,
Russian Academy of Sciences,
36 Nakhimovsky Prospect, Moscow 117851, Russia;

e-mail: germo.vali@phys.sea.ee, zhurbas@ocean.ru, jaan@phys.sea.ee, elken@phys.sea.ee

Received 6 October 2010, revised 22 February 2011, accepted 24 February 2011.

Abstract

Numerical simulation experiments with a high-resolution circulation model were carried out to study nutrient transport from different depths to the surface 10-m layer during an upwelling event along the northern coast of the Gulf of Finland in July 1999. The initial nutrient distribution is based on field measurements performed in the north-western part of the Gulf. Wind forcing covering the period of the upwelling along the northern coast was turned through 180° to simulate an upwelling along the southern coast. The simulation results showed that the main phosphorus transport to the upper 10-m layer occurred from depths shallower than 30 m for the upwelling events along both the northern and the southern

* This work was sponsored by the Estonian Science Foundation (grant No. 7467 & grant No. 7328) and the Russian Foundation for Basic Research (grant No. 09-05-00479).

coasts. Nitrogen transport to the upper 10-m layer was the largest from depths of 40–55 m for the upwelling along the northern and 40–65 m for the upwelling along the southern coast. Simulated cumulative volume transports to the upper 10-m layer from different depths showed that the contribution from deeper layers was larger in the case of the upwelling along the southern coast. The reduction of wind stress had a bigger influence on water transport from the deeper layers.

1. Introduction

Wind-driven coastal upwelling is a typical phenomenon in the Baltic Sea (Gidhagen 1987, Myrberg & Andrejev 2003) with strong upwelling events occurring with an annual average frequency of up to 30% in some parts of the Baltic (Kowalewski & Ostrowski 2005).

In the Gulf of Finland, a sub-basin of the Baltic Sea oriented from west to east, wind-driven coastal upwelling events are caused by either westerly or easterly wind forcing, which must have been operating for at least 60 h to generate an upwelling in the Gulf (Haapala et al. 1994). Upwellings and related mesoscale structures (meanders, filaments and eddies) in the region have been studied with different methods – field observations (e.g. Haapala et al. 1994, Lips et al. 2009, Kuvaldina et al. 2010), remote sensing (Kahru et al. 1995, Uiboupin & Laanemets 2008) and model simulations (Myrberg & Andrejev 2003, Zhurbas et al. 2008, Laanemets et al. 2009). Because the prevailing wind in the region blows from the south-west (e.g. Soomere & Keevallik 2003), upwelling events along the northern coast are more frequent.

Coastal upwelling typically transports nutrient-rich deeper water to the surface euphotic layer. Simulations with the ecohydrodynamic model by Kowalewski (2005) in the Hel region (the Baltic Sea) during an upwelling event showed an elevation of nutrient concentrations and an increase of phytoplankton biomass in the surface layers, especially during the spring bloom. Owing to the difference in vertical locations of the summer nutriclines in the thermocline (the phosphacline is shallower than the nitracline in the Gulf of Finland, as shown by Laanemets et al. (2004)), nutrients may be transported with an excess of phosphorus, compared with nitrogen according to the Redfield ratio. During the nutrient-depleted summer period, an upwelling is probably one of the main phosphorus sources for the formation of nitrogen-fixing cyanobacteria blooms (Vahtera et al. 2005).

Comprehensive reviews of upwelling in the Baltic Sea, its dynamics and effects on the ecosystem have been presented by Lehmann & Myrberg (2008) and Myrberg et al. (2008).

Previous numerical studies showed that the instability of longshore baroclinic jets and related thermohaline fronts caused by coupled upwelling

and downwelling events lead to the development of cold and warm filaments and eddies contributing to a coastal offshore exchange (Zhurbas et al. 2008). During coastal upwelling, nutrients are transported into the upper 10-m layer with a clear excess of phosphorus. In addition, the amount of transported phosphorus by one upwelling event is roughly equal to the monthly external bioavailable phosphorus load to the Gulf (Zhurbas et al. 2008). There is an asymmetry in upwelling response patterns owing to the cross-gulf topography: the southern half of this elongated basin is deeper and has steeper bottom slopes. Thus the amount of nutrients transported into the upper 10-m layer depends on whether upwelling occurs along the northern or the southern coast of the Gulf (Laanemets et al. 2009). Also, in the shallower eastern part of the open Gulf, the content of upwelled nutrients is low. With respect to the geographical distribution of upwelling effects, upwelled nutrients are transported more intensively from the coastal zone to the open sea by filaments and eddies in the narrow western and central part of the Gulf, as can be judged from the maps of mean eddy kinetic energy and phosphorus and nitrogen content in the surface layer (Laanemets et al. 2011).

During upwelling, waters from different layers are both advected and mixed. Lips et al. (2009) showed on the basis of field observations that during a strong upwelling event in summer 2006, the cold intermediate layer water and the upper mixed layer water were mixed in proportions of 85% to 15%. One may assume that the vertical clines separating the water masses and nutrient pools make a major contribution as sources of 'foreign' water upwelled to the surface layer. Nevertheless, the exact contribution of the different layers in the water column to the transport of nutrients is hard to detect from direct measurements, but this is possible from model-based estimates. In topographically asymmetrical regions, like the Gulf of Finland, one may assume a different contribution at different shores under upwelling-favourable wind conditions with the same magnitude.

The objective of this paper was to study and estimate the nutrient transport from different depths to the surface layer during coastal upwelling events along opposite coasts of an elongated basin such as the Gulf of Finland. For this purpose we used a series of numerical experiments in which the initial tracer (simulating short-term nutrient behaviour) source is put at different depths for each experiment. The results of the experiments are summarized as time and depth maps of cumulative nutrient mass transported to the upper layer from a layer of unit thickness at a certain depth in the Gulf of Finland.

2. Material and methods

2.1. Model setup

We applied the Princeton Ocean Model (POM), which is a primitive equation, σ-coordinate, free surface, hydrostatic model with a 2.5 moment turbulence closure sub-model embedded (Mellor & Yamada 1982, Blumberg & Mellor 1983, 1987). The model domain included the whole Baltic Sea closed at the Danish Straits. The digital topography of the sea bottom was taken from Seifert et al. (2001). We used a horizontal resolution of 0.5 nautical miles within the Gulf of Finland and 2 nautical miles in the rest of the Baltic Sea (Figure 1); in the vertical direction we used 41 equally spaced σ-layers, which in the Gulf gave the lowest vertical resolution of $\Delta z = 3$ m at a point of depth 120 m. A model resolution of 0.5 nautical miles allows good resolution of mesoscale phenomena, including upwelling filaments/squirts (Zhurbas et al. 2008) controlled by the internal baroclinic Rossby radius, which in the Gulf of Finland varies within 2–5 km (Alenius et al. 2003).

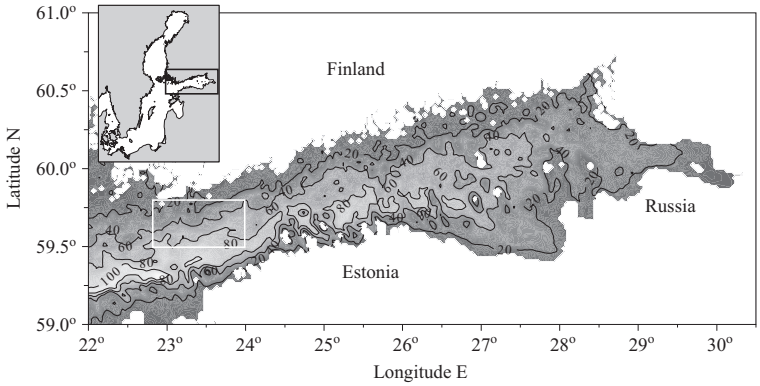

Figure 1. The model domain was the whole Baltic Sea with the model grid refined to 0.5 nautical miles in the Gulf of Finland. The white box indicates the area of the measurements performed on board r/v 'Aranda' in July 1999. The depth contours are given in metres

We chose the simulation period from 20 to 29 July 1999, which represents an intensive upwelling event along the northern coast and is well covered by high-resolution observations including CTD, biological and chemical measurements along with the SST from satellite imagery (Vahtera et al. 2005).

Atmospheric forcing (wind stress and heat flux components) for the simulation period was calculated from a meteorological data set of the Swedish Meteorological and Hydrological Institute (SMHI). The 10 m wind components were calculated from the SMHI geostrophic wind vectors by turning the latter 15° counterclockwise and multiplying by a factor of 0.6. The components and other meteorological parameters obtained were afterwards interpolated in space from the 1° resolution to our 2 and 0.5 nautical mile model grid. Since the winds calculated from the geostrophic gridded winds were lower compared with the wind measurements performed on board r/v 'Aranda' (within the study area of 22°50′–24°00′E, 59°30′–59°48′N, see Figure 1), the gridded wind stress field was multiplied by a correction factor of 2.04. The comparison of the corrected along-gulf wind stress τ_0 (positive eastward) with the wind stress component calculated from the measured wind on board r/v 'Aranda' is presented in Figure 2.

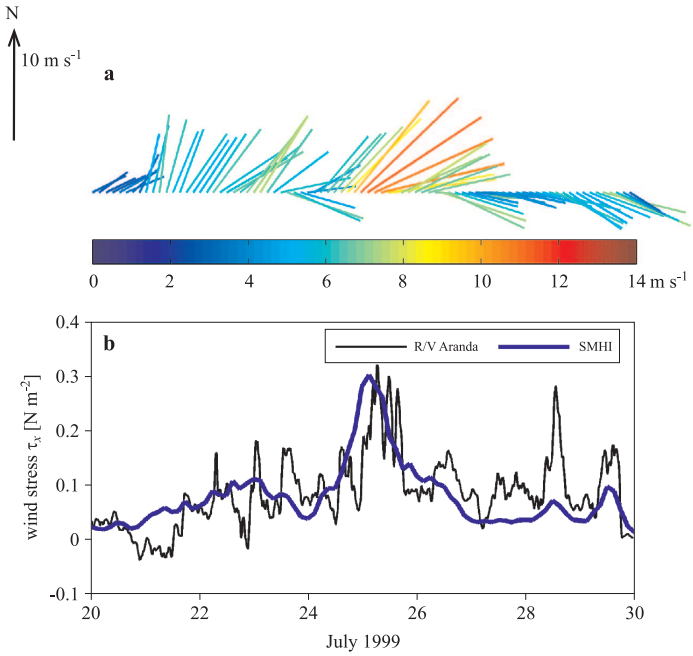

Figure 2. Wind conditions in the western part of the Gulf of Finland during July 1999: (a) representative SMHI wind vectors at 59°36′N, 24°00′E, and (b) the along-gulf wind stress calculated from measurements performed on board r/v 'Aranda' (solid black line) and SMHI gridded meteorological data set (solid blue line)

During the period from 21 to 25 July, westerly winds prevailed (Figure 2a) and the along-gulf wind stress component increased more or less steadily up to about 0.3 N m^{-2} (Figure 2b, SMHI data), causing the development of upwelling along the northern coast of the Gulf. From the peak onwards, the along-gulf wind stress decreased steadily. In order to model the upwelling along the southern coast, the wind vectors were turned through 180° and a wind stress of $\tau = -\tau_0$ was applied.

The initial thermohaline fields were constructed with the help of the Data Assimilation System coupled with the Baltic Environmental Database established and maintained by Alexander Sokolov and Fredrik Wulff at Stockholm University (see http://nest.su.se/das), using the climatological data from July to capture the main large-scale features of temperature and salinity, including the along-gulf salinity gradient. Interpolation of DAS data on 20 July yielded approximately an upper mixed layer temperature of 16°C in the Gulf, which was 3°C less than that measured on board r/v 'Aranda' on 20–21 July 1999 (Vahtera et. al 2005); therefore, the initial temperature field obtained from DAS was increased in the upper 10-m layer of the whole Baltic Sea by the difference. For more details on both factors, see Zhurbas et al. (2008) and Laanemets et al. (2009).

Owing to the smooth climatological density field and weakness of the related geostrophic currents, a windless model adjustment period was not found necessary to study the wind-forced upwelling events. We started the model run from zero currents and sea level and 'switched' the wind forcing on at the beginning of the run as used by Zhurbas et al. (2008). One justification for such an approach is that the Baltic Sea currents respond to changing wind in topographically controlled regions within approximately a day (Krauss & Brügge 1991). However, for seasonal and climatic circulation studies (not the purpose of our investigation), the 'warm-up' period of the model may be much longer than several months. In the present study, we do not present validation against measurements, but refer the reader to the studies by Zhurbas et al. (2008) and Laanemets et al. (2009), who demonstrated very good agreement of their model results with the observations. We note that closing the Danish Straits was of minor importance to the simulated upwelling events, since the mean sea level as observed at Landsort increased only by 10^{-7} m s^{-1}.

Phosphate and nitrate transport were simulated by introducing two equations describing passive tracer balance. During the short upwelling event, nutrients were considered to be conservative passive tracers, although the posterior behaviour of nutrients in the upper layer is not conservative. The equations were solved numerically within the POM code using the central leapfrog advection scheme, as used originally for temperature and

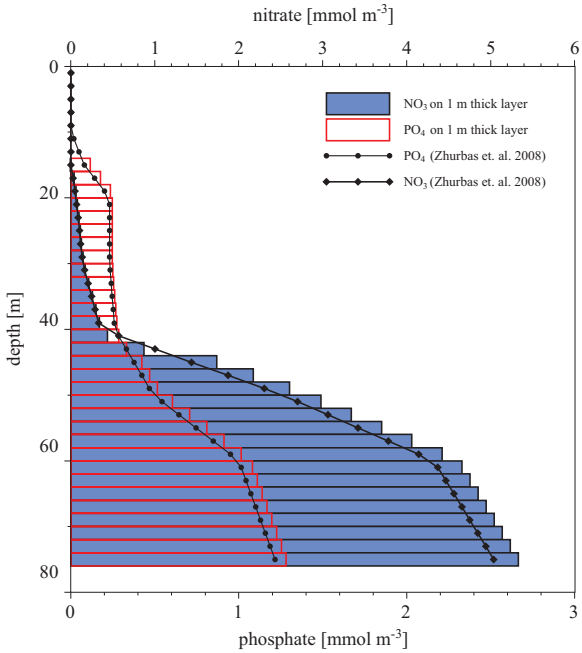

Figure 3. The initial nutrient concentration of different layers at 59°37.5′N, 23°46′E compared with the profiles based on measurements performed onboard r/v 'Aranda' on 20 July 1999 (Zhurbas et al. 2008)

salinity. Initial nutrient fields based on the field measurements on board r/v 'Aranda' in July 1999 and the measured nutrient profiles (see Zhurbas et al. 2008, Figure 3) were extended uniformly to the whole Baltic Sea.

2.2. Experiment setup

We studied the depth-origin vertical transport of nutrients (due to three-dimensional advection and mixing) by a series of numerical experiments in which the tracers had initial non-zero values only in a specific layer $z - \Delta z/2$, $z + \Delta z/2$ of thickness Δz (the values are taken from the initial nutrient profile, see Figure 3) and concentrations were zero elsewhere. Because of the σ-coordinate formulation of the POM, the initial nutrient concentrations were introduced only into one σ-layer closest to a given depth z (i.e. $-\sigma H \approx z$), where H is the sea depth. To leave the total initial nutrient mass unchanged, the nutrient concentration in z-coordinates, $C(z)$ is related to that of σ-coordinates, $C(\sigma)$, as $C(\sigma) = C(z)\,\Delta z/(\Delta\sigma\, H)$ (Figure 3).

Nutrient transport simulations started at 00:00 hrs on 22 July 1999 and lasted for 7 days in every model run, with the tracer source at a different individual depth layer.

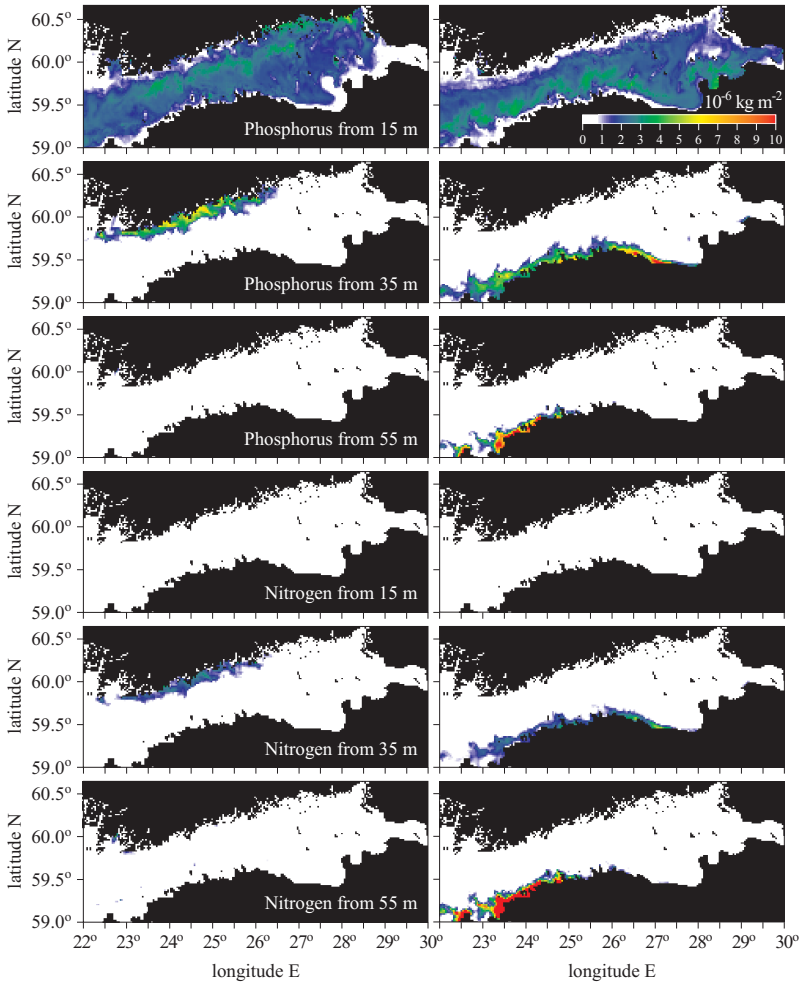

Figure 4. Maps showing the amounts of phosphorus and nitrogen in the upper 10-m water column with unit cross section transported from a layer 2 m thick at depths of 15, 35 and 55 m during the upwelling event along the northern (right panels) and southern coast (right panels) at $t = 6.3$ days

In the further analysis we use plots of nutrient content and water volume, integrated within the upper 10-m layer over the whole Gulf, transported from different depths during the upwelling event. To illustrate the background to the numerical experiments and the spatial distribution of upwelled nutrients along the northern and the southern coasts, the maps of the cumulative amounts of nutrients transported to the upper 10-m water column of unit cross section after 6.3 days simulation, with a source layer of 2 m thickness at 15, 35 and 55 m depth, are shown in Figure 4.

3. Results

3.1. Nutrient transport to the surface from different depths

Within the framework of the experiments, the horizontally integrated cumulative amount of nutrients in the upper 10-m layer over the whole Gulf was calculated as a function of time and initial depth of 2 m thick nutrient layers. Upwelled horizontally integrated cumulative amounts of nutrients

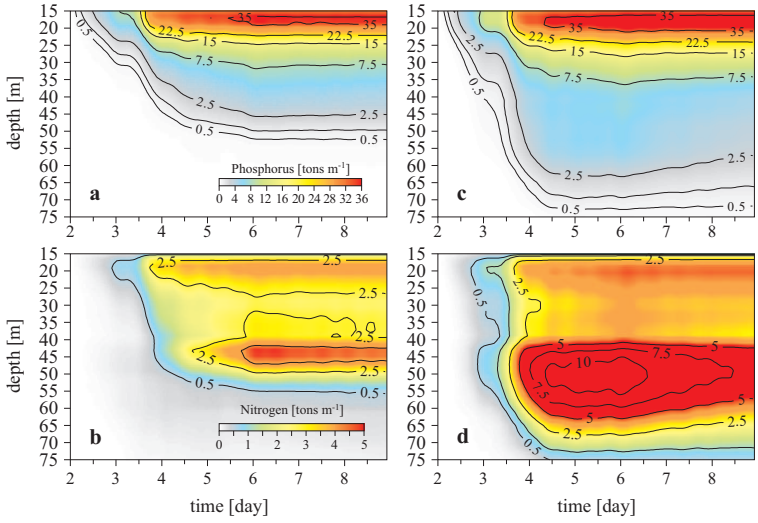

Figure 5. The plots of differential nutrient transport to the upper 10-m layer of the Gulf of Finland (in tons m^{-1}) versus the depth and time obtained from the simulations. The time is from 20 July 1999 onwards and the depth is the one where the nutrients were located in a layer with unit thickness as the initial source and from where they were brought to the surface layer. The results for the upwelling along the northern coast are on the left hand side, those for the upwelling along the southern coast are on the right hand side

in the upper 10-m layer were divided by the nutrient layer thickness Δz, and the plots obtained of the nutrient mass carried up to the top 10-m layer from a layer of unit thickness located at different depths during the upwelling (Figure 5) showed that the main source of phosphorus was between 17–41 m for the upwelling along both coasts of the Gulf – it was slightly deeper, though, along the southern coast. Transport was greatest from 17 m depth during the northern coast upwelling (Figure 5a) and from depths of 17–19 m during the southern coast upwelling (Figure 5c). More than 35 tons m^{-1} of phosphorus were brought to the surface layer from that depth range. With the increase in 'source' depth, the transport of phosphorus was reduced to 2.5 tons m^{-1} at 45 m depth for the upwelling off the northern coast and at 65 m depth off the southern coast. In the case of nitrogen the behaviour was slightly different. The greatest transport was from the depth interval of 40–65 m off the southern coast (Figure 5d) and 43–49 m in the case of the opposite coast (Figure 5b). The regional upwelling response pattern differs more than 2.5 times – during the southern coast upwelling more than 10 tons m^{-1} of nitrogen was brought to the surface layer from depths of 45–55 m, while off the northern coast the highest values were no more than 4 tons m^{-1} from depths of 40–45 m. The deeper layers were quite inefficient as nutrient sources for the euphotic layer during short-term upwelling events. Less than 1 ton m^{-1} of nitrogen was brought to the surface layer from depths

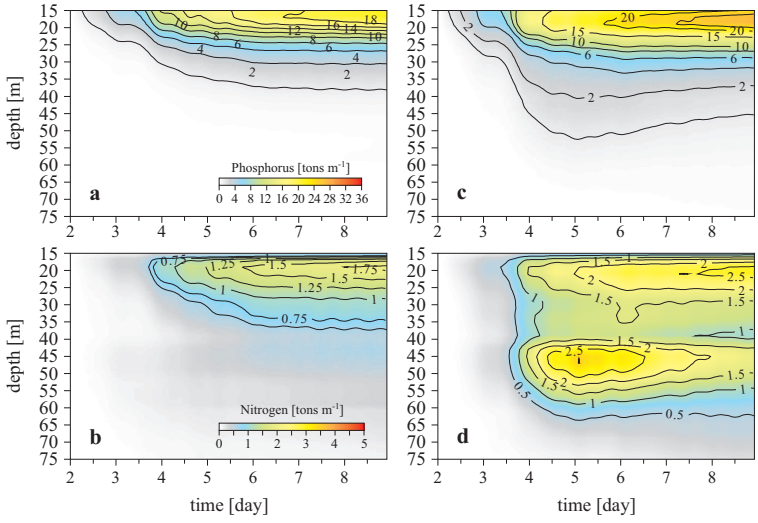

Figure 6. As for Figure 5 but with a 50% smaller wind stress $\tau = 0.5\,\tau_0$

of over 53 m and 73 m during the upwelling events along the northern and the southern coasts respectively.

The results of a similar nutrient transport simulation with a 50% smaller wind stress ($\tau = 0.5\,\tau_0$) are shown in Figure 6. The reduction in wind stress results in the overall decrease of amounts of upwelled nutrients. In particular, the largest transport of phosphorus remained in the upper 15–25 m layer off both coasts, whereas nitrogen transport from deeper layers was vanishingly small for the upwelling along the northern coast (< 0.75 tons m^{-1} from depths greater than 35 m). As regards the southern coast, the largest transport of nitrogen remained in the depth range of 40–55 m with the maximum at 45 m.

3.2. Volume of water transported to the surface

Nutrients are considered to be conservative passive tracers, and it is therefore possible to transform the cumulative amount of nutrients per metre $\Delta \mathrm{m}_{10}/\Delta z$ to a volume of water V_{10}, which is cumulatively transported to the upper 10-m layer from a 1 m thick layer at a certain depth z:

$$V_{10} = \frac{1}{C(z)} \frac{\Delta \mathrm{m}_{10}}{\Delta z}, \tag{1}$$

where $C(z)$ is the initial nutrient concentration at depth z (Figure 3). The cumulative volume transports per unit source layer thickness to the upper 10-m layer during the upwelling along the northern and the southern coasts with different wind stresses are shown in Figure 7, and the snapshot of upwelled volumes during the maxima of nutrient amounts on the 6th simulation day in Figure 8. It is seen in both Figure 7 and Figure 8 that the total volume of water transported to the upper 10-m layer from the top depth interval of 15–19 m was almost the same for the upwelling events off the northern and the southern coasts of the Gulf, with the maximum of 6.7×10^9 m^2 (Figure 8). Such equality of upwelled volumes is achieved as a result of the predominance of vertical turbulent diffusion (vertical mixing) over vertical advection, as the intensity of turbulent mixing in the upper sea is governed by wind force rather than wind direction. The cumulative transport due to vertical mixing is therefore expected to be more or less uniformly distributed within the Gulf area (see Figure 4, the source depth of 15 m for phosphorus), having the same total value for the upwelling events off the northern and the southern coasts. During the upwelling along the southern coast, the volume of water transported to the upper layer was larger than that off the northern coast, and the water mass was brought up from depths greater than 60 m (see Figures 7a, 7b and Figure 8). During the upwelling event along the northern coast, water was

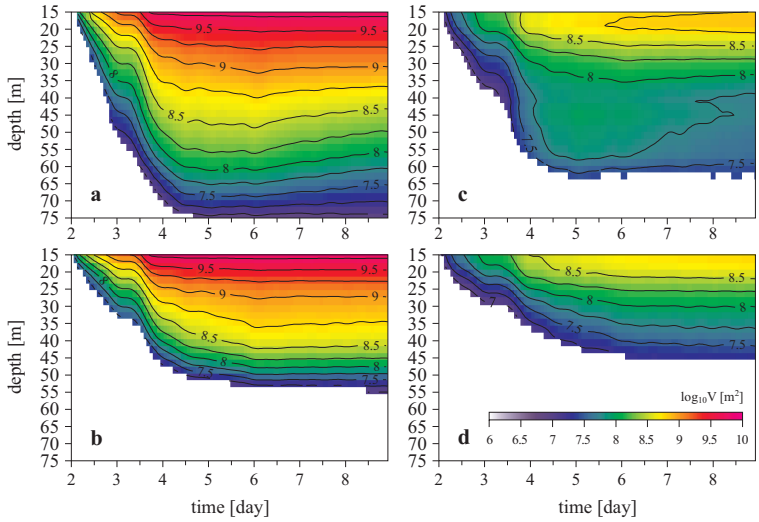

Figure 7. The cumulative volume transports per unit layer thickness to the upper 10-m layer from different depths during the upwelling along the southern (a, c) and the northern (b, d) coast. Cumulative volume transports were calculated for wind stress $\tau = \tau_0$ (a, b) and for wind stress $\tau = 0.5\,\tau_0$ (c, d). Note the logarithmic scale of the volume transports

transported to the surface mainly from the depth range of 21–41 m. There was a remarkable decrease from 3.7×10^8 m^2 to 1.08×10^7 m^2 in the amount of water transported to the surface from the 41–55 m depth range; hence, the maximum depth influenced by the upwelling along the northern coast was about 55 m. In the case of the upwelling along the southern coast, such a depth interval with a rapid decrease of upwelled water volume was not detected; the volume of upwelled water decreased more or less uniformly with depth.

The contribution from deeper layers during the upwelling with reduced wind stress ($\tau = 0.5\,\tau_0$) was lower for the upwelling events along both the northern and the southern coasts (see Figures 7b, 7d and Figure 8). The maximum depth influenced by the upwelling also fell to 45 m for the northern and 65 m for the southern coast. In Figure 8 the shapes of the curves of transported water volume have been transformed into straight lines for both upwelling cases. Comparison of the changes in transported volumes during the upwelling along the northern coast with reduced wind stress from depths of 15–45 m with the results for the upwelling along the southern coast with reduced wind stress shows that transport from intermediate layers was

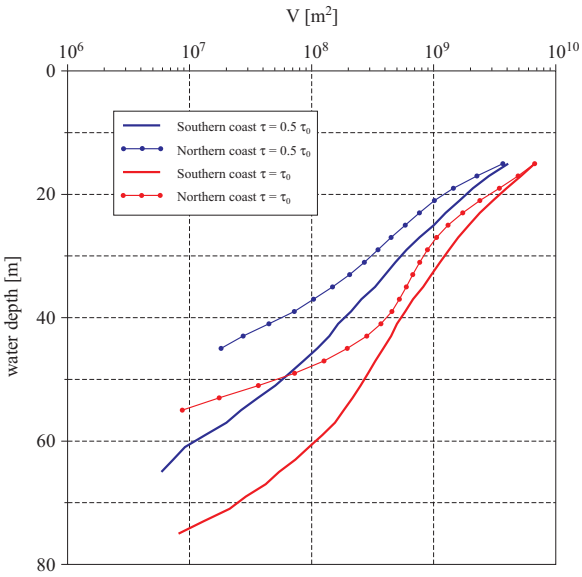

Figure 8. The volumes of water transported to the upper 10-m layer within the Gulf during the upwelling event along either the northern or the southern coast of the Gulf with wind stress $\tau = \tau_0$ and $\tau = 0.5\,\tau_0$ by day 6 of simulation

reduced remarkably: the volume of water transported from 21 m depth was more than 50% smaller, but for the deepest layers, the decrease was 10 times larger.

4. Discussion

According to Lentz & Chapman (2004), the vertical position of the onshore return flow that balances the offshore Ekman transport in an idealized case of stationary 2D upwelling is controlled by the Burger number $S = \alpha N/f$, where α is the bottom slope, N is the buoyancy frequency and f is the Coriolis parameter. For $<< 1$ (weak stratification), bottom stress balances wind stress, and the onshore return flow is primarily in the bottom boundary layer. For $S \approx 1$ or more (strong stratification), the cross-shelf momentum flux divergence balances wind stress and the onshore return flow is in the interior. Despite the fact that real upwelling events in the Gulf of Finland are neither stationary nor two-dimensional, the finding by Lentz & Chapman (2004) may be used for the qualitative interpretation of the results obtained in this study. The estimates of the Burger number

retrieved from the simulations were found to vary within the respective ranges of $S = 0.3$–1.2 and $S = 0.2$–0.9 for the upwellings along the southern and the northern coasts. Both upwelling regimes, $S << 1$ and $S \approx 1$, are therefore likely to be encountered in the Gulf, so there is no rigid restriction for the vertical position of the onshore return flow. As a result, we do not observe an abrupt decease of the volume transport at a certain depth, but a gradual decrease instead (see Figures 7 and 8).

The model results described above showed that the main transport of phosphorus into the upper 10-m layer was from depths less than 30 m for the upwelling along both coasts, whereas for nitrogen transport it was from layers deeper than 40 m. This is explained by the difference of nutricline depths and shape: there is a remarkable increase in nitrate concentration starting from 40 m depth, whereas for phosphate there is no such increase (Laanemets et al. 2004). Along the southern coast, where the depths are greater, nitrogen is more easily transported to the surface than off the northern coast, where the seabed is shallower and the amount of nitrogen in the offshore water column is correspondingly lower.

The total amounts of nutrients transported to the surface are larger during the upwelling along the southern coast. Laanemets et al. (2009) explained these larger amounts by the shorter distance that water particles carrying nutrients have to cover in order to reach the surface.

Lips et al. (2009) showed that during the upwelling event along the southern coast, observed during the summer 2006 measuring campaign, 85% of the upwelled water was from the intermediate layer and the remaining 15% from the surface layer. The plots of the ratios of depth-accumulated amounts of nutrients transported to the upper 10-m layer in the Gulf from a depth range [75 m – given depth z] to the total amount of nutrients transported to the surface (Figure 9) show that for the northern coast the main phosphorus transport is confined within the upper 40-m layer: 95% of nutrients are transported from there (Figure 9a). During the upwelling along the southern coast 95% of phosphorus was transported from the upper 55-m layer and 85% from the upper 40-m layer (Figure 9c). On the other hand, the behaviour of nitrogen was different: 95% of the nitrogen found in the upper 10-m layer by day 6 came from depths shallower than 55 m off the northern (Figure 9b) and 65 m off the southern coast (Figure 9d). 40% of the surface layer nitrogen was from depths shallower than 33 m and 45 m for the northern and the southern coasts respectively. Simulations showed that off the southern coast the upwelled water was transported to the surface mostly from the intermediate layer, as suggested by Lips et al. (2009), whereas off the northern coast transport from the shallower layers has a larger impact.

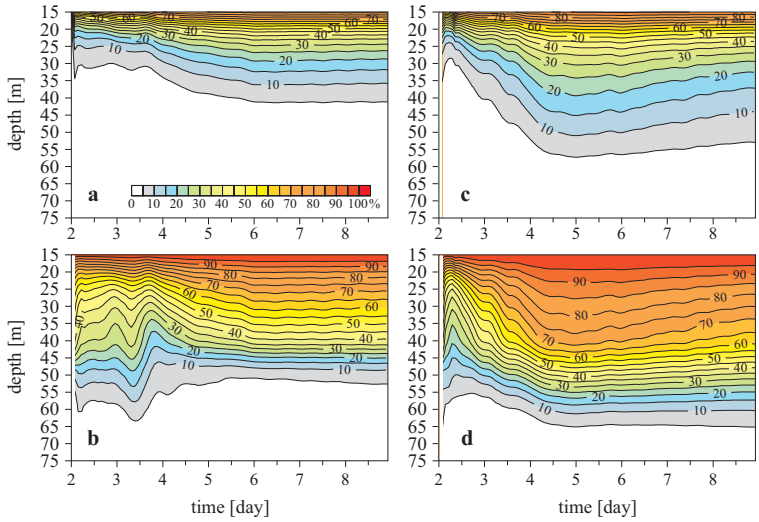

Figure 9. Maps showing the ratios of depth-cumulative nutrient amounts from 75 m to depth z to the total amount of nutrients in the water column as a percentage at a given time for the upwellings off the northern (left) and southern (right) coasts for phosphorus (upper panel) and nitrogen (lower panel)

The intensity of nutrient transport from the middle layers was greater during the upwelling along the southern coast for the same wind forcing magnitude, because the water from the depths of 35–45 m reached the surface layer more quickly, at least in the course of one day (Figure 7, cf. a and b). In addition, as the deeper layers have an earlier impact on the transport of nutrients during the upwelling along the southern coast, the total amounts of nutrients transported to the upper 10-m layer were larger during the upwelling along the southern coast. During the upwelling along the northern coast, water masses from depths of > 50 m reached the upper 10-m layer at least 1.5 days later and the total amount of nutrients transported to the surface layer were therefore lower compared than that off the southern coast.

5. Conclusions

The aim of this paper was to describe nutrient transport from different depths to the surface layer during an upwelling event in the Gulf of Finland. Modelling results showed that during upwelling events off either the northern or the southern coast of the Gulf, the highest phosphorus

transport to the upper 10-m layer was from depths shallower than 35 m. The largest amounts of nitrogen were transported to the surface layer from depths of 40–50 m off the northern and 40–60 m off the southern coast.

The volume of water transported to the upper 10-m layer from the deeper layers is greater during the upwelling along the southern coast – there was a clear decrease in the water volume reaching the surface layer from depths greater than 50 m during the upwelling along the northern coast.

The impact of the upwelling wind impulse was higher on the southern coast; the transport of water from deeper layers started earlier than on the northern coast. Owing to the earlier transport from the bottom layers during the upwelling along the southern coast, the total amount of nutrients transported to the upper 10-m layer at the culmination of the event are larger during the upwelling along the southern coast.

Although the reduction in wind stress lowered the amounts of nutrients transported to the upper 10-m layer during the upwelling event on both coasts, the main transport of phosphorus remained at the depths of 15–25 m. Nitrogen transport from the deeper layers was vanishingly small for the upwelling along the northern coast, whereas for the southern coast, the largest transport remained in the depth range of 40–55 m.

Acknowledgements

The Finnish Meteorological Institute kindly provided wind data. Special thanks go to Oleg Andrejev for supplying the meteorological data. We also thank the anonymous reviewers for their constructive recommendations.

References

Alenius P., Nekrasov A., Myrberg K., 2003, *Variability of the baroclinic Rossby radius in the Gulf of Finland*, Cont. Shelf Res., 23 (6), 563–573.

Blumberg A. F., Mellor G. L., 1983, *Diagnostic and prognostic numerical calculation studies of the South Atlantic Bight*, J. Geophys. Res., 88 (C8), 4579–4592, doi: 1029/JC088iC08p04579.

Blumberg A. F., Mellor G. L., 1987, *A description of the three-dimensional coastal ocean circulation model*, [in:] *Three-dimensional Coastal Ocean Models*, N. S. Heaps (ed.), Am. Geophys. Union, Washington, 1–16.

Gidhagen L., 1987, *Coastal upwelling in the Baltic Sea – Satellite and in situ measurements of sea-surface temperatures indicating coastal upwelling*, Estuar. Coast. Shelf Sci., 24 (4), 449–462.

Haapala J., 1994, *Upwelling and its influence on nutrient concentration in the coastal area of Hanko peninsula, entrance to the Gulf of Finland*, Estuar. Coast. Shelf Sci., 38 (5), 507–521.

Kahru M., Hakansson B., Rud O., 1995, *Distributions of the sea-surface temperature fronts in the Baltic Sea as derived from satellite imagery*, Cont. Shelf. Res., 15 (6), 663–679.

Kowalewski M., 2005, *The influence of the Hel upwelling (in the Baltic Sea) on nutrient concentration and primary production – the results of an ecohydrodynamic model*, Oceanologia, 47 (4), 567–590.

Kowalewski M., Ostrowski M., 2005, *Coastal up- and downwelling in the southern Baltic*, Oceanologia, 47 (4), 453–475.

Krauss W., Brügge B., 1991, *Wind-produced water exchange between the deep basins of the Baltic Sea*, J. Phys. Oceanogr., 21 (3), 373–394, doi: 10.1175/520-0485(1991)021<0373:WPWEBT>2.0.C0;2.

Kuvaldina N., Lips I., Lips U., Liblik T., 2010, *The influence of a coastal upwelling event on chlorophyll a and nutrient dynamics in the surface layer of the Gulf of Finland, Baltic Sea*, Hydrobiologia, 639 (1), 221–230, doi: 10.1007/s10750-009-022-4.

Laanemets J., Kononen K., Pavelson J., Poutanen E.-L., 2004, *Vertical location of seasonal nutriclines in the western Gulf of Finland*, J. Marine Syst., 52 (1–4), 1–13, doi: 10.1016/j.jmsys.2004.03.0030.

Laanemets J., Väli G., Zhurbas V., Elken J., Lips I., Lips U., 2011, *Simulation of mesoscale structures and nutrient transport during summer upwelling events in the Gulf of Finland in 2006*, Boreal Environ. Res., 16 (Suppl. A), 15–21.

Laanemets J., Zhurbas V., Elken J., Vahtera E., 2009, *Dependence of upwelling mediated nutrient transport on wind forcing, bottom topography and stratification in the Gulf of Finland: model experiments*, Boreal Environ. Res., 14 (1), 213–225.

Lehmann A., Myrberg K., 2008, *Upwelling in the Baltic Sea – a review*, J. Marine Syst., 74 (Suppl. 1), S3–S12, doi: 10.1016/j.jmarsys.2008.02.10.

Lentz S. J., Chapman D. C., 2004, *The importance of nonlinear cross-shelf momentum flux during wind-driven coastal upwelling*, J. Phys. Oceanogr., 34 (11), 2444–2457.

Lips I., Lips U., Liblik T., 2009, *Consequences of coastal upwelling events on physical and chemical patterns in the central Gulf of Finland (Baltic Sea)*, Cont. Shelf Res., 29 (15), 1836–1837, doi: 10.101016/j.csr.2009.06.010.

Mellor G. L., Yamada T., 1982, *Development of a turbulence closure model for geophysical fluid problems*, Rev. Geophys., 20 (4), 851–875, doi: 10.1029/RG020i004p00851.

Myrberg K., Andrejev O., 2003, *Main upwelling regions in the Baltic Sea – a statistical analysis based on three-dimensional modeling*, Boreal Environ. Res., 8 (2), 97–112.

Myrberg K., Lehmann A., Raudsepp U., Szymelfenig M., Lips I., Lips U., Matciak M., Kowalewski M., Krężel A., Burska D., Szymanek L., Ameryk A., Bielecka L., Bradtke K., Gałkowska A., Gromisz S., Jędrasik J., Kaluźny M., Kozłowski L., Krajewska-Sołtys A., Ołdakowski B., Ostrowski M., Zalewski M., Andrejev

O., Suomi I., Zhurbas V., Kauppinen O.-K., Soosaar E., Laanemets J., Uiboupin R., Talpsepp L., Golenko M., Golenko N., Vahtera E., 2008, *Upwelling events, coastal offshore exchange, links to biogeochemical processes – Highlights from the Baltic Sea Science Congress at Rostock University, Germany, 19–22 March 2007*, Oceanologia, 50 (1), 95–113.

Seifert T., Tauber F., Kayser B., 2001, *A high resolution spherical grid topography of the Baltic Sea – revised edition*, Baltic Sea Science Congress, Stockholm, 25–29 November 2001, Abstract Vol. 2, Stockholm Mar. Res. Centre, Stockholm Univ., 298.

Soomere T., Keevallik S., 2003, *Directional and extreme wind properties in the Gulf of Finland*, Proc. Estonian Acad. Sci. Eng., 9, 73–90.

Suursaar Ü., Aps R., 2007, *Spatio-temporal variations in hydrophysical and chemical parameters during a major upwelling event off the southern coast of the Gulf of Finland in summer 2006*, Oceanologia, 49 (2), 209–229.

Uiboupin R., Laanemets J., 2009, *Upwelling characteristics derived from satellite sea surface temperature data in the Gulf of Finland, Baltic Sea*, Boreal Environ. Res., 14 (2), 297–304.

Vahtera E., Laanemets J., Pavelson J., Huttonen M., Kononen K., 2005, *Effect of upwelling on the pelagic environment and bloom-forming cyanobacteria in the Western Gulf of Finland, Baltic Sea*, J. Marine Syst., 58 (1–2), 67–82.

Zhurbas V., Laanemets J., Vahtera E., 2008, *Modeling of the mesoscale structure of coupled upwelling/downwelling events and the related input of nutrients to the upper mixed layer in the Gulf of Finland, Baltic Sea*, J. Geophys. Res., 113, C05004, doi: 10.1029/2007JC004280.

Paper III

Zhurbas, V., Elken, J., **Väli, G**., Kuzmina, N., Paka, V. 2010. Pathways of suspended particles transport in the bottom layer of the southern Baltic Sea depending on wind forcing (numerical simulations). Oceanology, 50(6), 841-854

ISSN 0001-4370, Oceanology, 2010, Vol. 50, No. 6, pp. 841–854. © Pleiades Publishing, Inc., 2010.
Original Russian Text © V.M. Zhurbas, Jü. Elken, G. Väli, N.P. Kuzmina, V.T. Paka, 2010, published in Okeanologiya, 2010, Vol. 50, No. 6, pp. 890–903.

MARINE PHYSICS

Pathways of Suspended Particles Transport in the Bottom Layer of the Southern Baltic Sea Depending on the Wind Forcing (Numerical Simulation)

V. M. Zhurbas[a, b], Jü. Elken[b], G. Väli[b], N. P. Kuzmina, and V. T. Paka[c]

[a] *Shirshov Institute of Oceanology, Russian Academy of Sciences, Moscow, Russia*
[b] *Institute of Marine Systems, Tallinn Technology University, Tallinn, Estonia*
[c] *Atlantic Branch of the Shirshov Institute of Oceanology, Russian Academy of Sciences, Kaliningrad, Russia*
E-mail: zhurbas@ocean.ru

Received October 6, 2008; in final form, March 2, 2009

Abstract—A random-walk model for a nonuniform diffusivity media coupled with an ocean circulation model has been applied to describe the pathways of suspended particles transport in the bottom boundary layer (BBL) of the southern Baltic Sea. The circulation model is based on the Princeton Ocean Model, in which the vertical grid size is logarithmically refined towards the bottom in order to resolve the BBL. Fields of the flow velocity and eddy diffusivities simulated by the POM, along with the settling velocity of the suspended particles, are used as an input for the random-walk model. A number of numerical experiments were performed to study the pathways of suspended particles in the southern Baltic BBL depending on the wind conditions. In particular, the suspended particles introduced into the BBL in the center of the Bornholm Basin at westerly and southerly winds are found to be trapped in the basin provided that the particles' settling velocity is equal or greater than 2 m/day. The trapping phenomenon is explained by the combined effect of the Ekman transport convergence in the BBL due to the cyclonic gyre and the gravitational settling of the particles.

DOI: 10.1134/S0001437010060032

INTRODUCTION

The suspended particles originating from river discharges, shore erosion, and biological processes represent a key element of the marine coastal ecosystem. At shallows, the efficient transition of fine-grain sediments into the suspended state (resuspension) takes place thanks to the impact of surface waves, and the further suspension transport is usually directed to the deeper sea areas where the bottom sediment formation occurs [12,28].

The regional object of the present study is the semi-enclosed tide-free Baltic Sea. The latter involves a number of interrelated relatively deep basins. The southern ones are marked with the digits 1–5 in Fig. 1. The deep-water part of these basins with more than 60 m of water covers about 40% of the total area [29]. The effect of the surface waves is insignificant in the deep-water regions, while the currents and other water motions are, in the mean, insufficiently strong to support the excess of bottom friction stress over the threshold level that makes possible the process of resuspension [6, 19]. As a result, about 1–4 mm of sediments accumulate annually in the deep-water southern Baltic Sea [8] with the terrigenous sediment component being dominant in the winter and the organic one being larger in the summer [24].

In spite of the dominance of the sedimentation, the deep-water sediments are not motionless. The analysis of the sediment samples reveals substantial spatial–temporal variations in the sedimentation rates [4, 17]. Being lower against the threshold level, the bottom friction stress exceeds at times the resuspension threshold thanks to the intermittent turbulence due to the instability of internal waves and/or bottom currents that are able to strengthen, for instance, during storms or the North-Sea water flushings.

Understanding of the patterns of the sediments redistribution in the deeper layers of the basins is important for solving applied problems, such as the determination of the natural and man-made changes in the marine ecosystem from sediment samples and forecasting of pollutant dispersion. Specifically, a large amount of chemical weapons (CW) were buried in the Bornholm Basin after World War II [14] and simulation of the suspended particle transport in the bottom boundary layer (BBL) can help to reveal the migration pathways of the CW components and their decay products from the initial burial place.

Based on information on the composition and thickness of the bottom sediments and the rate of the sedimentation, a chart of the bottom currents in the Bornholm Basin was proposed in [1]. According to the chart, the bottom current forks after entering the Basin

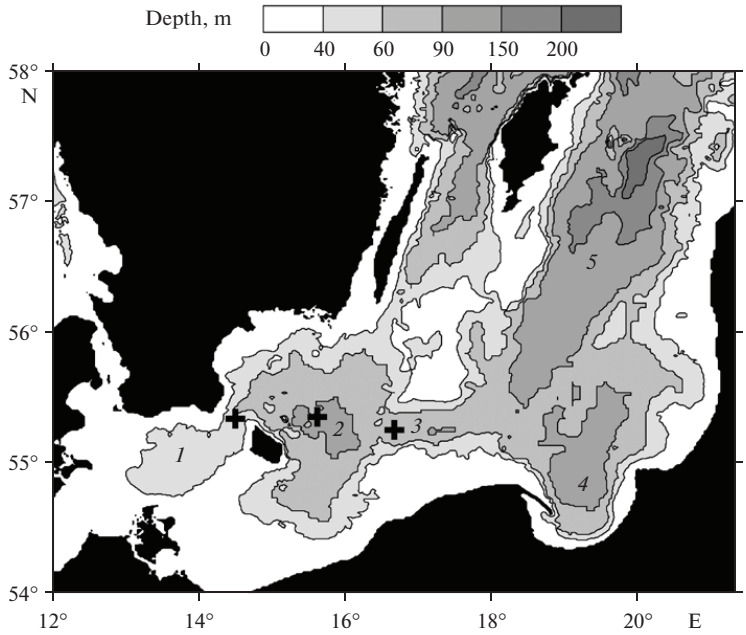

Fig. 1. Bathymetric map of the South Baltic Sea. The digits mark the sea basins: (*1*) Arkona Basin; (*2*) Bornholm Basin; (*3*) Slupsk Trench; (*4*) Gulf of Gdansk; (*5*) eastern Gotland Basin. The crosses mark the sites of suspended particles released into the BBL in the course of the numerical experiments.

from the west via the Bornholm strait. Two current branches emerging as a result of the forking (bifurcation) go north and south round the Basin, respectively, and then they join before the Slupsk Sill and, finally, enter the Slupsk Trench transporting the salty bottom water further east within the trench. Note that the pattern of the bottom circulation developed in [10] involves the northern branch of the current in the Bornholm Basin only.

The patterns of the sediment transport in the deep-water parts of the Baltic basins derived from geological evidence [1, 13] agree in general with the cyclonic mode of circulation in the numerical models [20, 22], including those that involve elements of the Lagrangian approach [7, 15]. Another hypothetical point of bifurcation of the bottom transport is the outflow site in the east of the Slupsk Trench, where salty waters can turn both in the southeastward direction to make a cyclonic loop around the Gdansk Basin and northeastwardly immediately streaming to the Gotland Basin [9]. As follows from the recent simulation results [22], the outflow from the Slupsk Trench streamed directly to the northeast after the large Baltic flushing in January 2003 (according to [21]), whereas the deep waters flowed along the southern loop after the baroclinic summer flushing in August–September of 2002.

As is known [18, 11], the pattern of the deep circulation in the Baltic Sea radically changes depending on the wind conditions. The goal of the present work is the simulation of the idealized pathways of transport of the sediment material in the deep-water parts of the southern Baltic Sea basins as a function of the wind direction. In addition, we would like to reveal the ability of simplified model experiments based on launching settling Lagrangian particles to reproduce the bifurcations of the pathways of the sediment transport in the Bornholm Basin and east of the Slupsk Trench noted in [1, 22].

2. DESCRIPTION AND VALIDATION OF THE MODEL

The mean currents, turbulence, and gravitational sedimentation determine the transport of suspended material in the sea. Therefore, our model system involves a circulation model and a model of the material transport. It is assumed that the circulation model yields three-dimensional fields of the mean current velocity and effective diffusion coefficients that serve as input parameters for the model of the material

transport. Since we are primarily interested in the pathways of the transport of suspended material, it is reasonable to apply the Lagrangian approach based on the consideration of the motion of individual particles exposed to currents, gravitational sedimentation, and turbulence with the turbulence effect being simulated by the process of the random walk of a particle.

2.1. The circulation model. The Princeton Ocean Model (POM) [3] was used as a circulation model. The POM is a free surface model and based on primitive equations of motion in a hydrostatic approximation. Instead of the ordinary vertical coordinate (the depth), the model involves the so-called sigma-coordinate (the vertical coordinate normalized to the full thickness of the water column). A turbulence model of Kolmogorov-type closure at the level of second order statistical moments [23] has been built into the POM to calculate the vertical exchange coefficients. The lateral exchange is parameterized by means of Smagorinsky's formula [27] with the proportionality constant $C = 0.1$.

The work region of the model comprised the entire Baltic Sea closed by an artificial shore line in the Denmark straits. As the trend calculation was confined to a quite short period of three days, it is unlikely that the results of the calculations of the currents in the deep-water areas of the Baltic Sea could be substantially changed by accounting for the water exchange across the straits because of the remoteness of the latter. The bottom topography was taken from [26]. The finite-difference grid pitch in longitude and latitude was (1/30)° and (1/60)°, respectively, i.e., about 2 km. In total, there were 30 sigma layers in the vertical with their thickness being logarithmically refined towards the bottom making up 20 cm in the bottom-closest layer at the depth of 100 m. Such a refinement facilitated the adequate resolution of the vertical structure of the currents and the diffusion coefficients in the BBL, which is of primary importance in the context of the present study. The vertical grid pitch made up 4.5 m in the main water body, but it logarithmically reduced to 40 cm in the surface layer at the sea depth of 100 m. The initial thermohaline fields were specified as horizontally-homogeneous ones within the main basins of the Baltic Sea using the vertical profiles of the temperature and salinity actually measured during the summer season. The comprehensive description of the procedure of specifying the initial thermohaline fields is given in [2, 32]. The zero fluxes of heat and salt were specified on the surface. The prognostic calculations of the circulation started from the state of immobility (zero initial current velocities).

2.2. The model of the particle transport. Let us assume that a particle occurs at a point (x_i, y_i, z_i) at the instant t_i where the current velocity components and effective diffusion coefficients (diffusivities) in the horizontal and the vertical are equal to (U_i, V_i, W_i), Kh_i, and Kv_i, respectively. One finds the values of (U_i, V_i, W_i), Kh_i, and Kv_i by means of the trilinear interpolation of the components of the velocity and the effective diffusion coefficients from the POM grid to the point (x_i, y_i, z_i, t_i). The coordinates of the same particle $(x_{i+1}, y_{i+1}, z_{i+1})$ at the next instant $t_{i+1} = t_i + \tau$, where τ is a small time increment, can be expressed as

$$\begin{aligned} x_{i+1} &= x_i + U_i\tau + x_i', \\ y_{i+1} &= y_i + V_i\tau + y_i', \\ z_{i+1} &= z_i + (W_i - w_S)\tau + z_i', \end{aligned} \tag{1}$$

where (x_i', y_i', z_i') are the components of the random particle displacements due to the turbulent velocity fluctuations, and w_S is the rate of the sedimentation.

The random displacement (x_i', y_i', z_i') can be expressed in terms of the diffusivity Kh or Kv and the time increment. In the simplest case of a homogenous field of diffusivity, these expressions look like

$$(x_i', y_i') = (2Kh_i\tau)^{1/2}A, \tag{2}$$

$$z_i' = (2Kv_i\tau)^{1/2}A, \tag{3}$$

where A is the random variate having the Gaussian distribution with zero mean value and unit dispersion. It was shown in [16, 30, 31] that the random walk approximation (3) (for the sake of simplicity, we confine ourselves to the consideration of the vertical walk of a particle) is equivalent to the continuous equation

$$\frac{\partial q}{\partial t} = \frac{\partial^2}{\partial z^2}[Kv \times q], \tag{4}$$

where $q(z, t)$ is the probability of the particle's occurrence in the vicinity of the point z (or the particle concentration is proportional to the probability). (Note that equivalence is considered here to mean that the vertical concentration profiles obtained from the problem of a random walk (3) unrestrictedly approach the solution of the respective initial boundary value problem (4) with the increase in the number of degrees of freedom.). Equation (4) is a simplified case of the Fokker–Plank equation [25], which has to be distinguished from Fick's diffusion equation

$$\frac{\partial q}{\partial t} = \frac{\partial}{\partial z}\left[Kv\frac{\partial q}{\partial z}\right]. \tag{5}$$

In the case of the inhomogeneous diffusivity $0 < Kv(z) \neq \text{const}$, equation (4) and its stochastic equivalent (3) describe a process whose features differ from classical diffusion. As an example, a numerical experiment was described in [31] concerning the random walk of particles that were homogeneously distributed at the zero time in a layer of inhomogeneous diffusivity and reflecting boundaries. When describing the random walk with equation (3), the initially homogeneous particle distribution has been violated in the

short run, and particles accumulated at sites of the minimum diffusivity. Hence, the use of a "naive" model of random walking (3) in the case of inhomogeneous diffusivity results in the transformation of the initially homogeneous distribution of the particles into a inhomogeneous one, which is inconsistent with the traditional concept of diffusion.

The use of equation (3) under the conditions of the deep basins of the Baltic Sea is fraught with the risk of the unrealistic wash-out of suspended particles from the BBL, where Kv has a maximum, and of their accumulation in the upper layers. To avoid this outcome, advantage has been taken of the random walk equation adapted to the case of inhomogeneous diffusivity [16, 31]:

$$z_i' = \left.\frac{\partial Kv}{\partial z}\right|_{z=z_i} \tau + \left\{ 2Kv\left[z_i + 0.5\left.\frac{\partial Kv}{\partial z}\right|_{z=z_i} \tau \right]\tau \right\}^{1/2} A. \quad (6)$$

Equation (6) is equivalent to diffusion equation (5). In principle, the analog of equation (6) can be applied instead of (2) to the horizontal random displacements x_i' and y_i'. However, this is not urgent because there is no physical justification for the occurrence of quasi-stationary domains with the Kh level substantially exceeding the background one (the BBL too, where the Kv level is always much higher than in the upper layer). In addition, the horizontal dispersion of particles in the sea is determined by the combined effect of diffusion (both horizontal and vertical) and the mean current shear [5] rather than by the Kh variate proper. As for the order of the Kh value, the POM calculations have given 10^{-1}–10^{0} m^2/s for the BBL and 10^{0}–10^{1} m^2/s for the upper layers of the Baltic Sea.

Thus, the equation system (1), (2), and (6) was used for describing the transport of suspended particles in the deep layers of the Baltic Sea. As for the boundary conditions, it was accepted that the sea surface reflects the particles while they are absorbed at the shore line. The sea bottom condition is usually specified so that it enables one to allow for the resuspension of sediment particles at high near-bottom friction stress τ and for sedimentation at low τ (see, for instance, [19]). Three modes of the exchange between the suspension and bottom sediments are usually distinguished:

(1) The sedimentation mode. If the BBL turbulence is weak ($\tau < \tau_S$, where τ_S is the threshold of the sedimentation), then particles sinking to the bottom remain there and the production of new particles (resuspension) is lacking. As a result, the number of suspended particles diminishes with time.

(2) The equilibrium mode. If $\tau_S < \tau < \tau_R$, where τ_R is the resuspension threshold, the particles sinking to the bottom are reflected and remain in suspension but there is no production of new particles or resuspension. As a result, the number of suspended particles remain unchanged.

(3) The resuspension mode. If $\tau_R > \tau_S$, the particles sink to the bottom and are reflected, but new particles are produced too, passing from the sediments into the suspended state. This results in the growth of the number of particles.

The main goal of the present work is the examination of the pathways of the transport of the suspended particles rather than their redistribution along the path. Therefore, a simple condition of reflection maintaining the total number of particles in the water thickness has been used for the bottom boundary.

2.3. The Verification of the Model. So far as our study is dedicated to the processes of the suspended particles transport within the BBL, the analytical treatment of the simulation results has to be preceded by convincing evidence that (a) the circulation model is really able to resolve the layer of higher Kv near the Baltic Sea bottom and (b) the random walk model is free of the unrealistic wash-out of particles from the BBL and of their accumulation in the upper layer of low vertical diffusivity.

Figure 2 shows the vertical profiles of Kv at the Slupsk Sill and in the Bornholm Basin computed from the circulation model at a northerly wind. Both cases characterize extreme conditions in the southern Baltic Sea at the maximum and minimum turbulence levels in the BBL, respectively. Both profiles exhibit the bottom layer of increased estimates of Kv about 2–4 m thick with the Kv values for the Slupsk Sill being one and a half order of magnitude higher than those in the Bornholm Basin BBL (0.01 m^2/s against 0.00025 m^2/s). This allows us to infer that the circulation model resolves the turbulent BBL. Although it is impossible to directly compare the model and the real BBL due to the lack of adequate observational information, the obtained model estimates of the BBL thickness and of coefficient Kv within the BBL are quite consistent with the present day physical concepts. As for the main water thickness outside the bottom and surface turbulent layer, the model gives $Kv < 1 \times 10^{-7}$ m^2/s, which is lower than the molecular thermal-conductivity coefficient. This is caused by the fact that the POM does not resolve the short-period internal waves, which are the main source of intermittent turbulence in the pycnocline, while the turbulence model built into the POM involves no parameterization of the effect of internal waves breaking. In order to correct this deficiency, the use has been made of the empirical formula proposed in [29] for the Baltic halocline for computing Kv in the random walk model outside the near-bottom and near-surface turbulent boundary layers:

$$Kv = \min\left(\frac{\alpha}{N}, K_0\right), \quad (7)$$

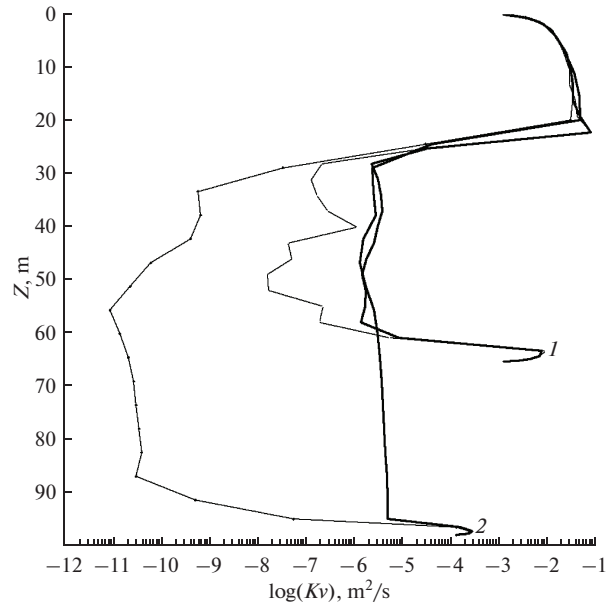

Fig. 2. The depth profiles of the vertical turbulent diffusion coefficient *Kv* at the Slupsk Sill (*1*) and in the Bornholm Basin (*2*) obtained from the model calculations under the northerly winds (thin lines). The thick lines designate the same profiles of *Kv* corrected with the help of parameterization (7) [29].

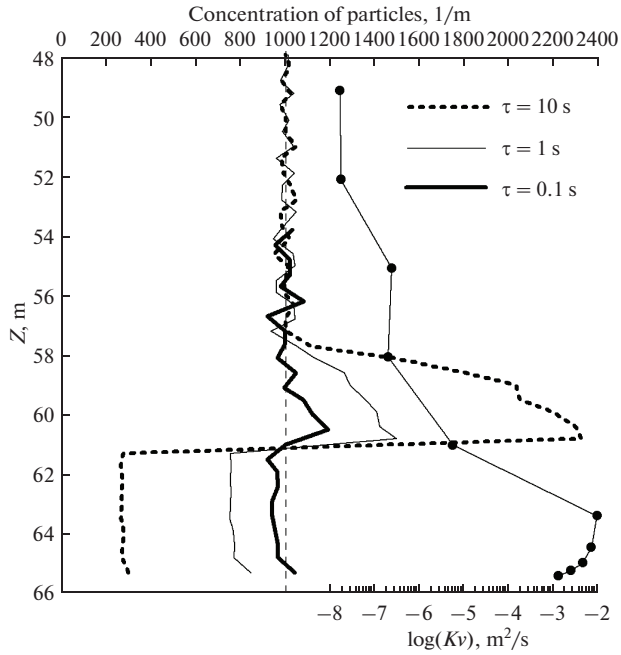

Fig. 3. The depth profiles of the particle concentration at the instant $t = 10$ days obtained from the walking model (6) in the course of testing experiments with the vertically homogenous initial distribution of the particles at different values of the time increment τ. The right-hand part of the picture shows the bottom sector of the depth profile of *Kv* at the Slupsk Sill used in the testing experiments.

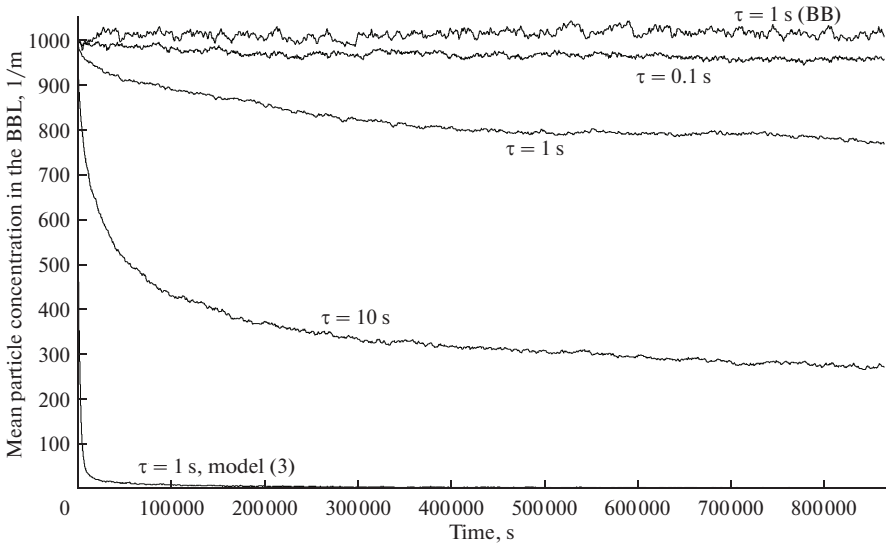

Fig. 4. The time-dependence of the mean particle concentration in the BBL found from testing experiments at different time increments τ. The upper curve was obtained for the depth profiles of *Kv* at the Bornholm Basin (marked with the letters BB); the rest of the curves were found for the depth profiles of *Kv* at the Slupsk Sill. The lowest curve was computed from the walk model (3), while model (6) was used to calculate the other ones.

where $\alpha = 0.87 \times 10^{-7}$ m^2/s^2 and $K_0 = 0.5 \times 10^{-5}$ m^2/s, where N is the Brunt–Väisälä frequency [22].

To ascertain that the random walk model (6) is able to adequately describe the particle transport in the Baltic BBL, numerical testing experiments were fulfilled using a vertically homogeneous initial particle distribution in the layer with the reflecting boundaries and "real" *Kv* profiles taken from Fig. 2. The diffusion equation (5) has a trivial solution $q(z, t) = q_0$= const under such initial and boundary conditions, and the results of testing the numerical model experiments has to be consistent with this solution.

Every testing experiment involved 20000 simulated particles evenly distributed in a layer 20 m thick (the starting concentration was 1000 per meter), where the *Kv*(*z*) profile was identical to the diffusivity profiles in the Baltic BBL (Fig. 2). The perfect reflection condition was set at the layer boundaries. To calculate the particle profile, the whole layer was subdivided into 40 equal intervals, and the number of particles was found for each of them.

Figure 3 demonstrates the vertical profiles of the particles' concentration obtained from the testing experiments with the random walk model (6) at $t = 10$ days; $\tau = 10$, 1, and 0.1 s (i.e., after 8640, 86400, and 864000 random steps, respectively); and the diffusivity profile typical of BBL at the Slupsk Sill. Considerable particle migration from the strongly turbulent BBL into the upper layer occurs at $\tau = 10$ s, so the particle concentration in the BBL decreases from 1000 to 260 particles/m (i.e., by 74%). At $\tau = 1$ s, the artificial particle migration from the BBL falls to 23%, and it becomes virtually insignificant (less than 4%) at $\tau = 0.1$ s.

The time dependences of the mean particle concentration in the BBL obtained from the testing experiments at various time increments τ, different *Kv* profiles, and random walk models ((3) or (6)) are given in Fig. 4. Judging by the behavior of the solution in Fig. 4, it may be assumed that the nonzero asymptotic value of the particles concentration in the BBL, as dependent on τ, will be reached at $t \longrightarrow \infty$. As it follows from the displayed dependences, the application of the random walk model (3) is absolutely inconsistent under the Baltic Sea BBL conditions: 95% of the particles artificially leave the BBL limits during the first two hours at $\tau = 1$ s and the *Kv* profile typical of the Slupsk Sill. The effect of the artificial particle migration from the BBL becomes virtually negligible even at $\tau = 1$s if one takes the vertical *Kv* profile typical of the Bornholm Basin, where the maximum value of *Kv* in the BBL is one and a half orders of magnitude lower than at the Slupsk Sill, and applies the random walk model (6).

Note that the particle concentration in Fig. 3 (the mean particle concentration in the BBL in Fig. 4) was estimated as the ratio of the number of particles occurring within the specified depth interval $\Delta z = 0.45$ m

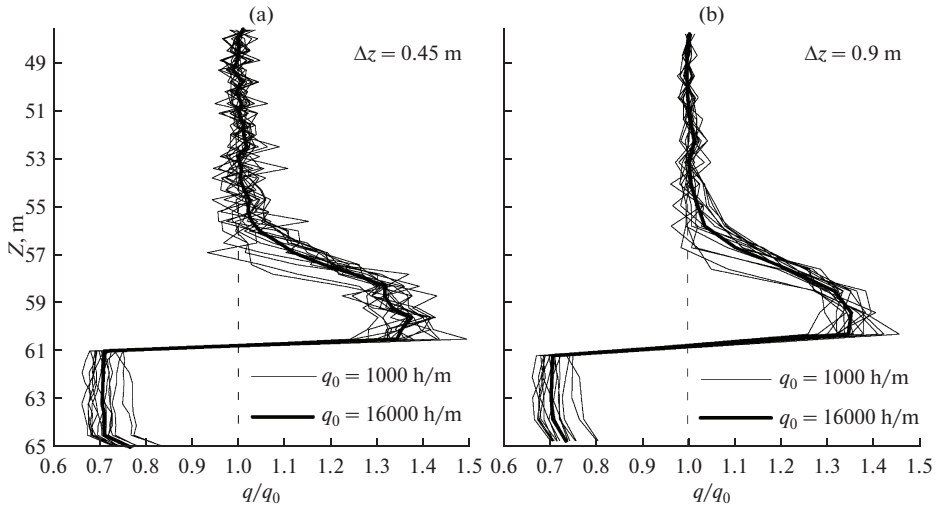

Fig. 5. The depth profiles of the particle concentration $q(z)$ normalized to the initial value of the concentration q_0 at the instant $t = 10$ days with the profiles being found from the random walk model (6) in testing experiments with the vertically homogenous initial distribution of the particles at the time increment $\tau = 1$ s and at different values of $q_0 = 1000$ particles/m (thin line, 16 realizations) and 16 000 particles/m (thick lines). The calculations were performed for the depth profile of the diffusivity Kv at the Slupsk Sill (see Fig. 2). The concentration was assessed by means of counting the particles in the layers of thickness $\Delta z = 0.45$ m (a) and 0.9 m (b).

(within the BBL) at this point in time to the thickness of the interval Δz (the BBL thickness). Since the particle quantity within the interval of Δz in the BBL fluctuates thanks to the random walk process, the estimates of the concentration (the mean concentration in the BBL) are subjected to fluctuations too. Let us show that the fluctuations in Figs. 3 and 4 relate to the statistical errors of the concentration estimates but are unrelated to numerical unsteadiness which, in principle, may be expected in the process of the numerical solution of equation (6). To do this, we undertake additional numerical calculations whose idea is in the following. If the concentration fluctuations in the vertical profile (Fig. 3) are related to the statistical errors of the assessment of the average value of a random quantity (i.e., the concentration of particles), then the root-mean-square fluctuation amplitude has to diminish in proportion to $N^{-1/2}$ with the growth of the number of degrees of freedom N (in our case, N is the particle quantity used for estimating the concentration). At that rate, the amplitude of the concentration fluctuations can be reduced to a level as small as one likes by means of increasing the number of particles per unit of length or/and by increasing the length interval by which the concentration is estimated.

Based on the foregoing considerations, we performed 16 independent testing experiments similar to that shown in Fig. 3 at $\tau = 1$ and different realizations of the random quantity A in equation (6). Averaging the results of 16 experiments allowed us to obtain the estimates of the concentration featuring the number of degrees of freedom N 16 times greater than similar estimates from the "initial" testing experiment. The additional two-fold increase in the depth interval Δz (from 0.45 to 0.9 m) resulted in an extra two-fold increase in N, which must reduce the root-mean-square fluctuation of the concentration amplitude by a factor of 4 and $4\sqrt{2}$, respectively.

The outcomes of the additional testing experiments are shown in Fig. 5. As indicated in the latter, the averaging of the 16 independent concentration estimates and the two-fold increase in Δz resulted in about a five-fold decrease in the fluctuation amplitude. So, it is reasonable to believe that the concentration fluctuations in Figs. 3–5 are statistical in nature.

The testing experiments (Figs. 3 and 4) demonstrate that, under the Baltic Sea conditions, the adequate description of the vertical turbulent transport of particles in the near-bottom layer with inhomogeneous diffusivity can be achieved through the application of the random walk model (6) at a time increment of $\tau \le 1$ s.

2.4. Performing Numerical Experiments. The following idealized numerical experiments were scheduled using the models of the circulation and particle transport. In order to find the current velocity field

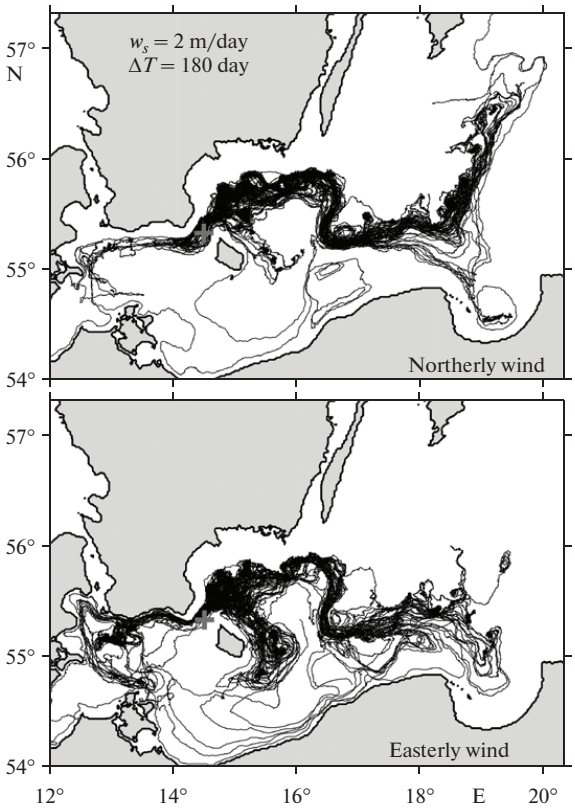

Fig. 6. The pathways of particles with the settling velocity w_S = 2 m/day released in the bottom layer of the Bornholm strait at northerly and southerly winds. Here and in what follows, the grey crosses mark the site of the particle release and ΔT designates the period of the particle walking.

and the effective diffusion coefficients typical of the wind of a specified direction, the prognostic calculation for a three day period has to be fulfilled based on the circulation model at a steady and homogeneous wind of such direction (in our case, we set the sea surface friction stress at 0.2 N/m^2, which corresponds a 10 m/s wind velocity). It is expected that three days suffice for achieving the steady state of the current velocity fields under the specified wind direction, since a one day period is estimated as the typical time of the restructuring of the Baltic Sea circulation after changes in the wind conditions [18]. The fields of the current velocity and diffusion coefficients after shaping for three days are used in a "frozen" state in the random walk model defined by equations (1), (2), and (6) to calculate the pathways of 100 particles released from a single point in the BBL and having a specified settling velocity. The random walk of a particle was calculated at the time increment $\tau = 0.01$ s. The settling velocity varied over the range of $w_S \le 0.4$ m/day corresponding to the fine-grain component of the silt sediments [19]. The choice of such a settling velocity range was determined by the fact that this range is the most convenient for revealing certain physical effects related to the specific features of the propagation of the suspended matter in the BBL in the southern Baltic Sea (see Section 3). The particles were released 1 cm apart from the sea floor at one of three points in the BBL, namely, in the Bornholm strait, the Bornholm Basin, and the Slupsk Trench (Fig. 1). It should be mentioned that one of the release points coincides with site of the chemical weapons burial [14]. The experiments must be performed with winds of 16 directions (W, SWW, SW, SSW, S, SSE, SE, SEE, E, NEE, NE, NNE, N, NNW, NW, and NWW).

The predicted pathways of the particles will differ from those produced by "real" alternating wind, since the fields of the velocity and diffusion coefficients are specified as changeless ("frozen") ones during the whole period of the particle walking ranging from 90 to

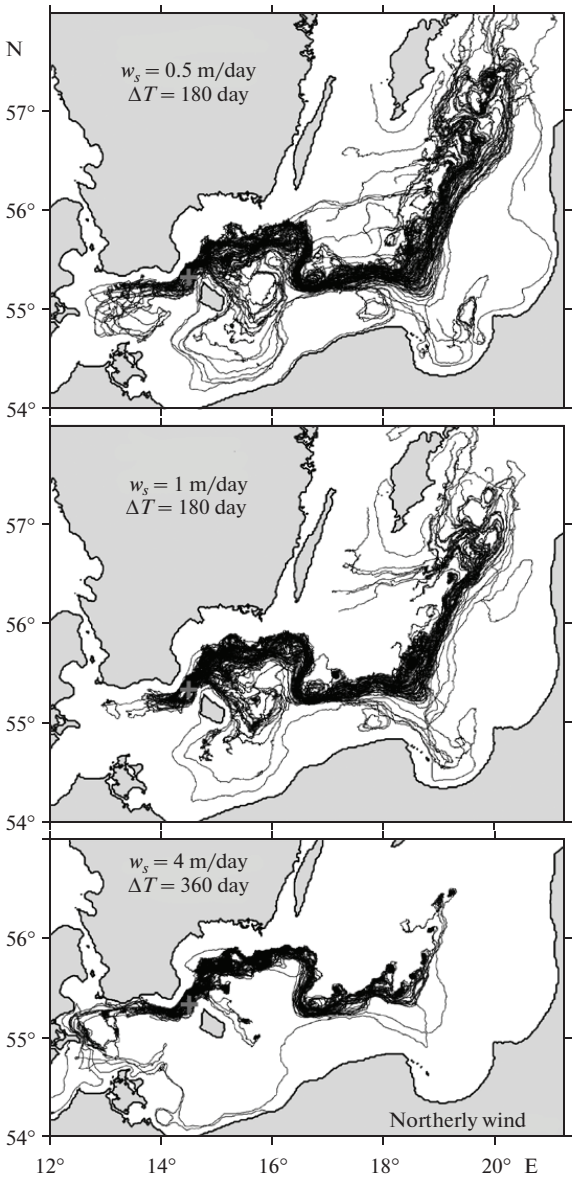

Fig. 7. Pathways of particles characterized by different settling velocities w_S and released in the bottom layer of the Bornholm Basin under a northerly wind.

180 days. But it is exactly the particle pathways computed from the "frozen" fields of the velocity and diffusion coefficients that are consistent with the goal of the present work aimed at the examination of the dependence of the pathways of the particle transport in the BBL upon the wind direction.

3. RESULTS OF THE NUMERICAL EXPERIMENTS

3.1. The release of particles in the bottom layer of the Bornholm Strait. The propagation pathway of the suspended particles released in the BBL of the Bornholm strait under northerly and easterly winds imme-

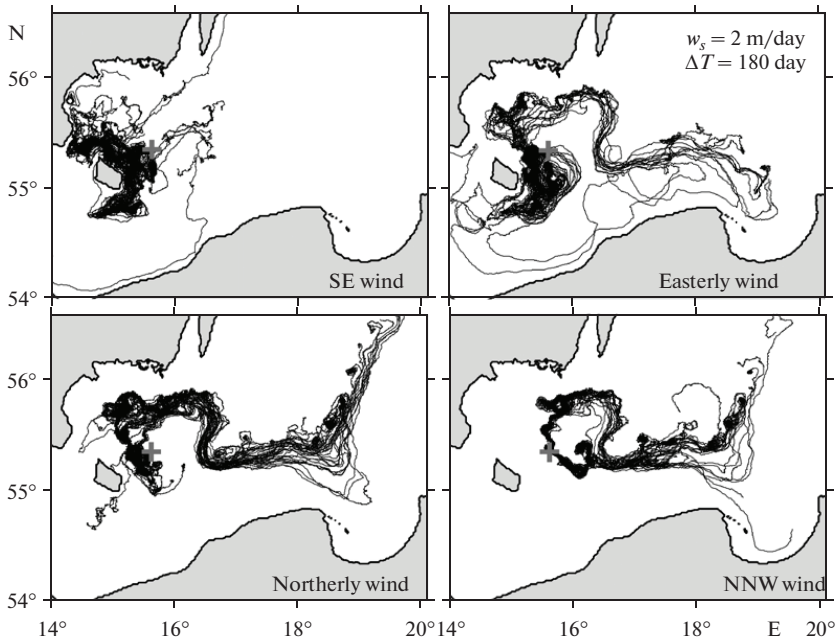

Fig. 8. Pathways of particles characterized by the settling velocity $w_S = 2$ m/day and released in the bottom layer of the Bornholm Basin under the southeasterly, easterly, northerly, and north-northwesterly winds.

diately forks: some particles move westwards along the Swedish coast and enter the Arkona Basin, while the others travel eastwards and enter the Bornholm Basin (Fig. 6). The forking of the particle transport pathways occurs thanks to the oppositely directed currents in the deep layer of the strait. The westward transport takes place at the northern slope of the strait close to the Swedish coast, while the eastward one occurs at the southern slope of the strait near Bornholm Island.

After entering the Bornholm Basin, the particle pathway forks again. A portion of the particles passes around the north of the Bornholm Basin clockwise, while the second portion moves counterclockwise around the southern periphery of the Basin. After completing the semicircle, the particles of the northern pathway are intaken into the Slupsk Trench and move further eastwards in the trench. The particles from the southern pathway don't enter the Slupsk Trench but continue to follow the cyclonic gyre in the Bornholm Basin. The occurrence of the northern and southern round-about ways of the suspended particles in the Bornholm Basin is consistent with the pattern of the near-bottom circulation by Emelyanov [1] with the only difference being that, according to the latter, both branches of the bottom current enter the Slupsk Trench.

Interestingly enough, when the northerly winds change for the easterly ones, the southern pathway of the particle transport becomes more preferable, and larger quantity of particles that entered the Bornholm Basin through the same strait from the west are turned southwards (Fig. 6). Intuitively, it appears explicable by the Eckman dynamics. The easterly wind causes the Eckman northward water transport in the surface layer. Because of the side boundaries of the basin, such transport has to be somehow compensated for by a southward water transport in the deeper layers. Similar physical reasoning can be applied to the fact that, under northerly (easterly) winds and after passing the Slupsk Trench from the west to east, the suspended particles turn northwards (southwards) to the Gotland Basin (to the Gulf of Gdansk).

Figure 7 illustrates the dependence of the particle pathways on the settling velocity w_S. The increase in w_S makes the northern go-round of the Bornholm Basin more preferable than the southern one. This trend may be related to the Eckman dynamics too. Namely, the greater w_S is, the closer to the bottom the particles travel and, consequently, the stronger they deviate to the left from the main current due to the near-bottom Eckman friction. The shortening of the particle pathways with w_S is also easy to explain: the higher the settling velocity, the closer to the bottom they are and, therefore, the slower the particles move (Fig. 7).

3.2. Release of particles in the Bornholm Basin bottom layer. Under northerly and easterly winds, the par-

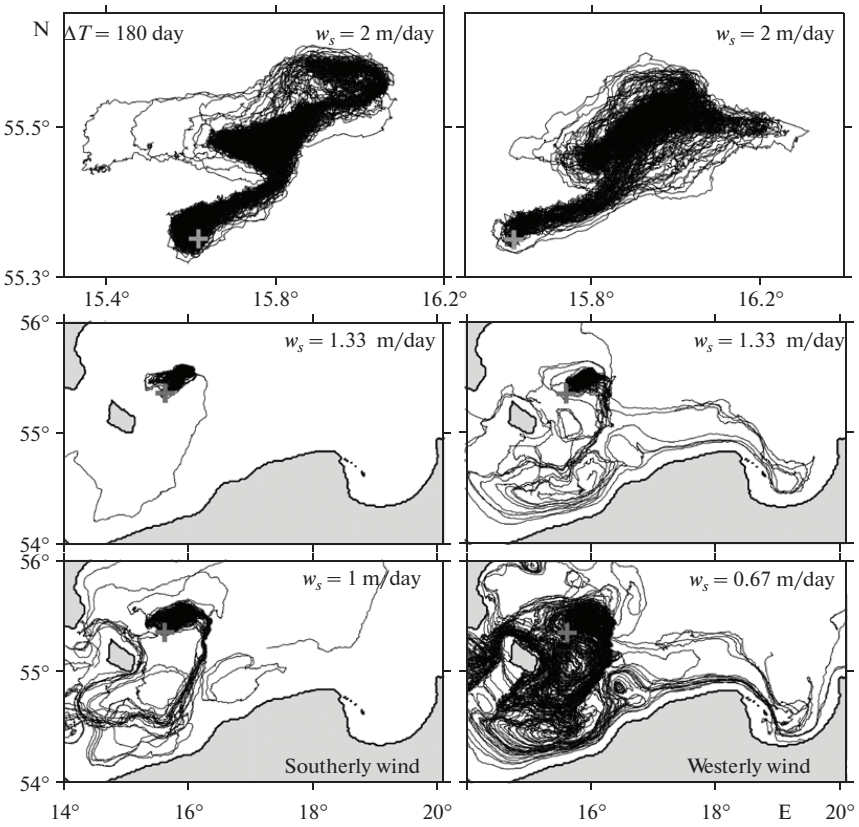

Fig. 9. Pathways of particles characterized by different settling velocities w_S and released in the bottom layer of the Bornholm Basin under the southerly (on the left) and westerly (on the right) winds. The scale in upper panel is increased in the proportion 20 : 3.

ticles initially move westwards to Bornholm Island and, after that, they are entrained into either the northern or the southern go-round the Bornholm Basin (Fig. 8). Subsequently, the particles' trajectories behave as in the case of particles released in the Bornholm Strait (Fig. 6).

Under the southeasterly wind (Fig. 8), the particles travel within the sector of directions from the SSW to NWW, and the pathways span Bornholm Island as semirings in the north, east, and south. Finally, under the SSW wind, the particles are immediately entrained into either the northern or the southern go-round of the Bornholm Basin. Under these conditions, all of the particles involved in the northern go round are subsequently drawn into the Slupsk Trench, while one fraction of the particles of the southern go-round is also drawn into the Slupsk Trench and the other one contributes to the circle around the Basin. Notice that the SSW is the only wind direction under which a substantial fraction of the southern go-round branch leaves the Bornholm Basin and enters the Slupsk Trench.

The numerical experiments demonstrated that the particles released in the BBL of the central Bornholm Basin actively leave the Basin under the SE, SEE, E, NEE, NE, NNE, N, and NNW winds when the settling velocity w_S = 2 m/day. Under the winds of the other eight directions (i.e., NW, NWW, W, SWW, SW, SSW, S, and SSE), the particles continue to be trapped within the Basin limits. For instance, under the southerly and westerly winds, the particles with a settling velocity of w_S = 2 m/day initially move to the NE by a distance of 20 km, but next they are entrained into the cyclonic gyre and remain within a ring 40 km in diameter (Fig. 9, upper plates).

If w_S decreases by 1.3 m/day and 1.6 m/day under southerly and westerly winds, respectively, the trapping of the particles ends and they begin to leave the Bornholm Basin. At that, the lower w_S is, the faster this occurs with the greater fraction of particles (see the medium and lower plates in Fig. 8).

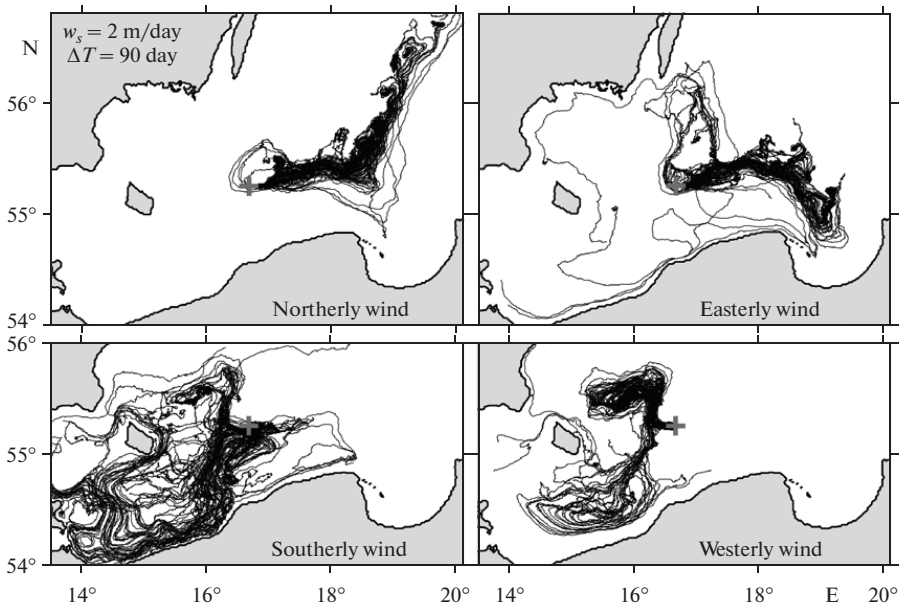

Fig. 10. Pathways of particles characterized by the settling velocity $w_S = 2$ m/day and released in the bottom layer of the Slupsk Trench under winds of different directions.

It is simple to understand the physics of the effect of the suspended particle trapping revealed in the Bornholm Basin. Under the easterly and southerly winds, the cyclonic circulation reaches a steady state in the deep layer of the Bornholm Basin, which is characterized by the convergence of the Eckman transport in the BBL (because the bottom Eckman transport is directed to the left of the main current in the upper layer). In turn, thanks to the continuity, the convergence of the currents in the BBL generates the water upwelling. If one releases the particles in the BBL, their horizontal dispersion is obstructed by the convergence, and the particles remain trapped under the condition that their settling velocity w_S exceeds the upwelling velocity.

The trapping effect can be a dominant factor of the contaminant spreading from the sites of the chemical weapon burial because the westerlies and southerlies are the climatically prevailing winds in the Bornholm Basin.

3.3. The Release of Particles in the Near-Bottom Layer of the Slupsk Trench. The numerical experiments revealed that the suspended particles released in the BBL of the Slupsk Trench are eastwards transported according to the wind either eastwards into the eastern Gotland/Gdansk Basin (NNW, N, NNE, NE, NEE, and E winds) or westwards into the Bornholm Basin (SE, SSE, S, SSW, SW, SWW, W, and NWW winds); an intermediate pattern occurs at the SEE and NW winds characterized by an ambiguous pattern of the particle transport direction. As an example, Fig. 10 demonstrates the pathways of the particles released into the BBL of the Slupsk Trench under northerly, easterly, southerly, and westerly winds.

Interestingly enough, the forking of the trajectories into the south and north branches occurs in the cases of the suspended particles entering the Bornholm Basin both from the east through the Slupsk Trench (Fig. 10) and from the west through the Bornholm Strait (Fig. 6). In contrast, similar forking does not occur when the suspended particles enter the eastern Gotland/Gdansk Basin from the Slupsk Trench. Depending upon the wind direction, the particles mainly either turn to the north towards the Gotland Basin (under a northerly wind) or to the south towards the Gulf of Gdansk (under an easterly wind). So, it is reasonable to suppose that the direction of the wind controls the direction of the transport of the suspended particles leaving the Slupsk Trench in the east.

4. CONCLUSIONS

1. The numerical experiments provided evidence that the pathways of the suspended particles that enter the Bornholm Basin from the Bornholm Strait in the west fork into the north and south branches. The particles involved in the northern go-round of the Bornholm Basin are sucked into the Slupsk Trench, while the most of those in the southern pathway avoid the

latter and continue to cyclonically circle within the Bornholm Basin. In total, the outcomes of the numerical computations of the pathways of the suspended particle transport are consistent with the geological pattern of the bottom currents by Emelyanov [1] with the exception of his inference that the north and south branches of the bottom currents in the Bornholm Basin enter the Slupsk Trench.

2. The northern go-round of the Bornholm Basin becomes more preferable with the greater settling velocity of the particles, which is attributable to the bottom Ekman transport.

3. The particles whose settling velocity is w_S = 2 m/day remain trapped and do not leave the basin's boundaries if released in the bottom layer of the Bornholm Basin under westerly and southerly winds. According to the additional calculations, the phenomenon of trapping of the suspended particles can be explained by the combined effects of the gravitational particle settling and the convergence of the Ekman transport in the BBL, which induces the water upwelling in the middle of a cyclonic gyre. The particle trapping effect vanishes with the decrease in w_S, because the vertical velocity in the BBL exceeds the particle settling velocity under the upwelling conditions.

4. The wind direction is a factor that shapes the transport pathway of the suspended particles as they enter the eastern Baltic Sea from the Slupsk Trench: the particles go round to the north towards the Gotland Basin under the northerly wind but they turn to the south towards the Gulf of Gdansk under the easterly wind. Unlike the case of the suspended particles arrival into the Bornholm Basin, there is no bifurcation (forking) of the pathway of the particle transport into the north and south branches when the suspended particles enter the Eastern Gotland Basin from the Slupsk Trench.

ACKNOWLEDGMENTS

The authors are grateful to V.B. Zalesny for discussing the paper and helpful comments.

This work was supported by the 6th Frame EC Program (project MERCW no. 013408), the Russian Foundation for Basic Research (project no. 09-05-00479a), and the Scientific Foundation of Estonia (project no. 7467).

REFERENCES

1. E. M. Emel'yanov, V. A. Gritsenko, and V. D. Egorikhin, "Near-Bottom Circulation in the Gdansk Deep of the Baltic Sea: Bottom Sediments and Dynamics of Inflows of the North Sea Waters," Okeanologiya **44** (2), 261–271 (2004) [Oceanology **44** (2), 262–274 (2004)].
2. V. M. Zhurbas, T. Stipa, P. Malkki, et al., "Mesoscale Variability of the Upwelling in the Southeastern Baltic Sea: IR Images and Numerical Modeling," Okeanologiya **44** (5), 495–504 (2004) [Oceanology **44** (5), 620–627 (2004)].
3. A. F. Blumberg and G. L. Mellor, "Diagnostic and Prognostic Numerical Calculation Studies of the South Atlantic Bight," J. Geophys. Res. **88** (1983).
4. C. Christiansen, H. Kunzendorf, K.-C. Emeis, et al., "Temporal and Spatial Sedimentation Rate Variabilities in the Eastern Gotland Basin, the Baltic Sea," Boreas **31** (1), 65–74 (2002).
5. G. T. Csanady, *Turbulent Diffusion in the Environment.*, D. Reidel Publishing Company, Holland/Boston-U, Dordrecht., (1973).
6. Danielsson, A. Jönsson, and L. Rahm, "Resuspension Patterns in the Baltic Proper," J. Sea Res. **57** (4) 257–269 (2007).
7. K. Döös, H. E. M. Meier, and R. Döscher, "The Baltic Haline Conveyor Belt or the Overturning Circulation and Mixing in the Baltic," Ambio **33** (4), 261–266 (2004).
8. J. Eckhéll, P. Jonsson, M. Meili, et al., "Storm Influence on the Accumulation and Lamination of Sediments in Deep Areas of the Northwestern Baltic Proper," Ambio **29** (4–5), 238–245 (2000).
9. J. Elken, Deep Water Overflow, Circulation and Vertical Exchange in the Baltic Proper, Report Series No. 6, Estonian Marine Institute, Tallinn, Estonia (1996).
10. J. Elken and W. Matthäus, *Sea Oceanography. BALTEX Assessment of Climate Change for the Baltic Sea Basin (BACC)*, Ed. by H. Storch, Annex A.1.1 (Springer, Berlin, 2008), pp. 379–386.
11. J. Elken, U. Raudsepp, and U. Lips, "On the Estuarine Transport Reversal in Deep Layers of the Gulf of Finland," J. Sea Res. **49** (4), 267–274 (2003).
12. K. Emeis, C. Christiansen, K. Edelvang, et al., "Material Transport from the Near Shore to the Basinal Environment in the Southern Baltic Sea II: Synthesis of Data on Origin and Properties of Material," J. Mar. Syst. **35** (3–4), 151–168 (2002).
13. E. M. Emelyanov, "Biogenic Components and Elements in Sediments of the Central Baltic and Their Redistribution," Mar. Geol. **172** (1–2), 23–41 (2001).
14. *Helcom. Report on Chemical Munitions Dumped in the Baltic Sea. Report to the 15th Meeting of the Helsinki Commission from the Ad-Hoc Working Group on Dumped Chemical Munition, January 1994. Helcom, 1994* (Commission from the Ad-Hoc Working Group on Dumped Chemical Munition, January, Helsinki, 1994).
15. H.-H. Hinrichsen, G. Kraus, R. Voss, et al., "The General Distribution Pattern and Mixing Probability of Baltic Sprat Juvenile Populations," J. Mar. Syst. **58** (1–2), 52– 66 (2005).
16. J. R. Hunter, P. D. Craig, and H. E. Phillips, "On the Use of Random Walk Models with Spatially Variable Diffusivity," J. Comput. Phys. **106** (2), 366–376 (1993).
17. A. T. Kotilainen, J. M. S. Hämälainen, and B. Winterhalter, "Reconstructing a Continuous Holocene Composite Sedimentary Record for the Eastern Gotland Deep, Baltic Sea," Boreal Environment Research **7** (1), 1–12 (2002).

18. W. Krauss and B. Brügge, "Wind-Produced Water Exchange between the Deep Basins of the Baltic Sea," J. Phys. Oceanogr. **21** (3), 373–384 (1992).
19. C. Kuhrts, W. Fennel, and T. Seifert, "Model Studies of Transport of Sedimentary Material in the Western Baltic," J. Mar. Sys. **52** (1–4), 167–190 (2004).
20. A. Lehmann, W. Krauss, and H.-H. Hinrichsen, "Effects of Remote and Local Atmospheric Forcing on Circulation and Upwelling in the Baltic Sea," Tellus **54A** (3), 299–316 (2002).
21. W. Matthäus and H. Franck, "Characteristics of Major Baltic Inflows—A Statistical Analysis," Cont. Shelf. Res. **12** (12), 1375–1400 (1992).
22. H. E. M. Meier, "Modelling of the Pathways and Ages of Inflowing Salt- and Freshwater in the Baltic Sea," Estuarine, Coastal and Shelf Science **74** (4), 610–627 (2007).
23. G. L. Mellor and T. Yamada, "Development of a Turbulence Closure Model for Geophysical Fluid Problems," Rev. Geophys. Space Phys. **20** (4), 851–875 (1982).
24. C. Pohl, A. Löffler, and U. Hennings, "A Sediment Trap Flux Study for Trace Metals under Seasonal Aspects in the Stratified Baltic Sea (Gotland Basin; 57°19.20′N; 20°03.00′E)," Mar. Chem. **84** (3–4), 143–160 (2004).
25. H. Risken, *The Fokker-Plank Equation: Methods of Solution and Application* (Springer-Verlag, Heidelberg, 1984).
26. T. Seifert and B. Kayser, "A High Resolution Spherical Grid Topography of the Baltic Sea, Meereswissenschaftliche Berichte," Marine Science Reports, Institut fur Ostseeforschung Warnemnde (1995).
27. J. Smagorinsky, "General Circulation Experiment with the Primitive Equations. I. The Basic Experiment," Mon. Weather Rev. **91** (3), 99–164 (1963).
28. C. K. Sommerfield and H. J. Lee, "Magnitude and Variability of Holocene Sediment Accumulation in Santa Monica Bay, California," Marine Environmental Research **56** (1–2), 151–176 (2003).
29. A. Stigebrandt, "A Model of the Vertical Circulation of the Baltic Deep Water," J. Phys. Oceanogr. **17** (10), 1772–1785 (1987).
30. D. J. Thomson, "Random Walk Modelling of Diffusion in Inhomogeneous Turbulence," Q. J. R. Meteorol. Soc. **110** (466), 1107–1120 (1984).
31. A. W. Visser, "Using Random Walk Models to Simulate the Vertical Distribution of Particles in a Turbulent Water Column," Mar. Ecol.: Proc. Ser. **158**, 275–281 (1997).
32. V. Zhurbas, T. Stipa, P. Mälkki, et al., "Generation of Subsurface Cyclonic Eddies in the Southeast Baltic Sea: Observations and Numerical Experiments," J. Geophys. Res. **109** (C5), doi: 10.1029/2003JC002074 (2004).

APPENDIX B: ELULOOKIRJELDUS

1. Isikuandmed

Ees- ja perekonnanimi	Germo Väli
Sünniaeg ja –koht	21. mai 1984, Viljandi, Eesti
Kodakondsus	Eesti

2. Kontaktandmed

Aadress	Akadeemia tee 15b, Tallinn, 12618
Telefon	+372 620 4321
E-posti aadress	germo.vali@phys.sea.ee

3. Hariduskäik

Õppeasutus (nimetus lõpetamise ajal)	Lõpetamise aeg	Haridus (eriala/kraad)
Carl Robert Jakobsoni nim. gümnaasium	2002	Keskharidus
Tallinna Tehnikaülikool	2007	Tehniline füüsika/M.Sc.

4. Keelteoskus (alg-, kesk- või kõrgtase)

Keel	Tase
Eesti keel	Emakeel
Inglise keel	Kõrgtase
Vene keel	Algtase

5. Teenistuskäik

Töötamise aeg	Tööandja nimetus	Ametikoht
2005-2007	TTÜ Meresüsteemide Instituut	Tehnik
2007- tänaseni	TTÜ Meresüsteemide Instituut	Insener

6. Teadustegevus

Väli, Germo; Zhurbas, Victor; Laanemets, Jaan; Elken, Jüri (2011). Simulation of nutrient transport from different depths during an upwelling event in the Gulf of Finland. Oceanologia, 53(TI), 431–448

Laanemets, Jaan; Väli, Germo; Zhurbas, Victor; Elken, Jüri; Lips, Inga; Lips, Urmas (2011). Simulation of mesoscale structures and nutrient transport during summer upwelling events in the Gulf of Finland in 2006. Boreal Environment Research, 16A, 15–26

Zhurbas, Victor; Elken, Jüri; Väli, Germo; Kuzmina, Natalia; Paka, Vadim (2010). Pathways of suspended particles transport in the bottom layer of the southern Baltic Sea depending on wind forcing (numerical simulations). Oceanology, 50(6), 841–854

Zhurbas, Victor; Elken, Jüri; Väli, Germo (2008). Pathways of suspended particles released in the bottom boundary layer of the Bornholm Deep, Baltic Sea (numerical simulations). In: US/EU-Baltic International Symposium, 2008 IEEE/OES: US/EU-Baltic Symposium "Ocean Observations, Ecosystem-Based Management & Forecasting", Tallinn, 27–29 May, 2008. IEEE, 2008, (IEEE Conference Proceedings), 1–5

Elken, Jüri; Kõuts, Tarmo; Lagemaa, Priidik; Lips, Urmas; Raudsepp, Urmas; Väli, Germo (2008). Sub-regional observing and forecast system for the NE Baltic: Needs and first results . In: US/EU-Baltic International Symposium, 2008 IEEE/OES: US/EU-Baltic Symposium "Ocean Observations, Ecosystem-Based Management & Forecasting", Tallinn, 27–29 May, 2008. IEEE, 2008, (IEEE Conference Proceedings), 1–9.

Alari, Victor; Erm, Ants; Väli, Germo; Lips, Inga; Lips, Urmas (2008). Optical properties of north-eastern Baltic Sea in spring and summer 2007. US/EU-Baltic International Symposium, 27–29 May, Tallinn, Estonia. IEEE, 2008, 1–7.

Raudsepp, U.; Pavelson, J.; Alari, V.; Väli, G.; Kõuts, T. (2006). Loode Eesti õlireostuse lokaliseerimine ja selle edasise käitumise prognoos.

7. Kaitstud lõputööd

Magistritöö, 2007, Vee läbipaistvuse muutlikkus Läänemere avaosas, Tallinna Tehnikaülikool, TTÜ Meresüsteemide Instituut

8. Teadustöö põhisuunad

Numbriline modelleerimine, tsirkulatsioon, apvelling, ainelevi

CURRICULUM VITAE

1. Personal data

Name	Germo Väli
Date and place of birth	21. May 1984, Viljandi, Estonia

2. Contact information

Address	Akadeemia tee 15a, Tallinn, Estonia
Phone	+372 620 4321
E-mail	germo.vali@phys.sea.ee

3. Education

Educational institution	Graduation year	Education (field of study/degree)
CRJG	2002	Secondary
Tallinn University of Technology	2007	Engineering physics/M.Sc

4. Language competence/skills (fluent; average, basic skills)

Language	Level
Estonian	Native language
English	Fluent
Russian	Basic skills

5. Professional Employment

Period	Organisation	Position
2005–2007	Marine Systems Institute	Technician
2007–present	Marine Systems Institute	Engineer

6. Scientific work

Väli, Germo; Zhurbas, Victor; Laanemets, Jaan; Elken, Jüri (2011). Simulation of nutrient transport from different depths during an upwelling event in the Gulf of Finland. Oceanologia, 53(TI), 431–448

Laanemets, Jaan; Väli, Germo; Zhurbas, Victor; Elken, Jüri; Lips, Inga; Lips, Urmas (2011). Simulation of mesoscale structures and nutrient transport during summer upwelling events in the Gulf of Finland in 2006. Boreal Environment Research, 16A, 15–26.

Zhurbas, Victor; Elken, Jüri; Väli, Germo; Kuzmina, Natalia; Paka, Vadim (2010). Pathways of suspended particles transport in the bottom layer of the southern Baltic Sea depending on wind forcing (numerical simulations). Oceanology, 50(6), 841–854.

Zhurbas, Victor; Elken, Jüri; Väli, Germo (2008). Pathways of suspended particles released in the bottom boundary layer of the Bornholm Deep, Baltic Sea (numerical simulations). In: US/EU-Baltic International Symposium, 2008 IEEE/OES: US/EU-Baltic Symposium "Ocean Observations, Ecosystem-Based Management & Forecasting", Tallinn, 27–29 May, 2008. IEEE, 2008, (IEEE Conference Proceedings), 1–5.

Elken, Jüri; Kõuts, Tarmo; Lagemaa, Priidik; Lips, Urmas; Raudsepp, Urmas; Väli, Germo (2008). Sub-regional observing and forecast system for the NE Baltic: Needs and first results . In: US/EU-Baltic International Symposium, 2008 IEEE/OES: US/EU-Baltic Symposium "Ocean Observations, Ecosystem-Based Management & Forecasting", Tallinn, 27–29 May, 2008. IEEE, 2008, (IEEE Conference Proceedings), 1–9.

Alari, Victor; Erm, Ants; Väli, Germo; Lips, Inga; Lips, Urmas (2008). Optical properties of north-eastern Baltic Sea in spring and summer 2007. US/EU-Baltic International Symposium, 27–29 May, Tallinn, Estonia. IEEE, 2008, 1–7.

Raudsepp, Urmas; Pavelson, Juss; Alari, Victor; Väli, Germo; Kõuts, Tarmo (2006). Loode Eesti õlireostuse lokaliseerimine ja selle edasise käitumise prognoos.

7. Defended theses

Master's thesis, 2007, Annual changes of water transparency in the Baltic Proper, Tallinn University of Technology, Institute of Marine Systems at TUT

8. Main areas of scientific work/Current research topics

Numerical modeling, circulation, upwelling, transport

DISSERTATIONS DEFENDED AT TALLINN UNIVERSITY OF TECHNOLOGY ON *NATURAL AND EXACT SCIENCES*

1. **Olav Kongas**. Nonlinear dynamics in modeling cardiac arrhytmias. 1998.
2. **Kalju Vanatalu**. Optimization of processes of microbial biosynthesis of isotopically labeled biomolecules and their complexes. 1999.
3. **Ahto Buldas**. An algebraic approach to the structure of graphs. 1999.
4. **Monika Drews**. A metabolic study of insect cells in batch and continuous culture: application of chemostat and turbidostat to the production of recombinant proteins. 1999.
5. **Eola Valdre**. Endothelial-specific regulation of vessel formation: role of receptor tyrosine kinases. 2000.
6. **Kalju Lott**. Doping and defect thermodynamic equilibrium in ZnS. 2000.
7. **Reet Koljak**. Novel fatty acid dioxygenases from the corals *Plexaura homomalla* and *Gersemia fruticosa.* 2001.
8. **Anne Paju**. Asymmetric oxidation of prochiral and racemic ketones by using sharpless catalyst. 2001.
9. **Marko Vendelin**. Cardiac mechanoenergetics *in silico*. 2001.
10. **Pearu Peterson**. Multi-soliton interactions and the inverse problem of wave crest. 2001.
11. **Anne Menert**. Microcalorimetry of anaerobic digestion. 2001.
12. **Toomas Tiivel**. The role of the mitochondrial outer membrane in *in vivo* regulation of respiration in normal heart and skeletal muscle cell. 2002.
13. **Olle Hints**. Ordovician scolecodonts of Estonia and neighbouring areas: taxonomy, distribution, palaeoecology, and application. 2002.
14. **Jaak Nõlvak**. Chitinozoan biostratigrapy in the Ordovician of Baltoscandia. 2002.
15. **Liivi Kluge**. On algebraic structure of pre-operad. 2002.
16. **Jaanus Lass**. Biosignal interpretation: Study of cardiac arrhytmias and electromagnetic field effects on human nervous system. 2002.
17. **Janek Peterson**. Synthesis, structural characterization and modification of PAMAM dendrimers. 2002.
18. **Merike Vaher**. Room temperature ionic liquids as background electrolyte additives in capillary electrophoresis. 2002.
19. **Valdek Mikli**. Electron microscopy and image analysis study of powdered hardmetal materials and optoelectronic thin films. 2003.

20. **Mart Viljus**. The microstructure and properties of fine-grained cermets. 2003.
21. **Signe Kask**. Identification and characterization of dairy-related *Lactobacillus.* 2003.
22. **Tiiu-Mai Laht**. Influence of microstructure of the curd on enzymatic and microbiological processes in Swiss-type cheese. 2003.
23. **Anne Kuusksalu**. 2–5A synthetase in the marine sponge *Geodia cydonium*. 2003.
24. **Sergei Bereznev**. Solar cells based on polycristalline copper-indium chalcogenides and conductive polymers. 2003.
25. **Kadri Kriis**. Asymmetric synthesis of C_2-symmetric bimorpholines and their application as chiral ligands in the transfer hydrogenation of aromatic ketones. 2004.
26. **Jekaterina Reut**. Polypyrrole coatings on conducting and insulating substracts. 2004.
27. **Sven Nõmm**. Realization and identification of discrete-time nonlinear systems. 2004.
28. **Olga Kijatkina**. Deposition of copper indium disulphide films by chemical spray pyrolysis. 2004.
29. **Gert Tamberg**. On sampling operators defined by Rogosinski, Hann and Blackman windows. 2004.
30. **Monika Übner**. Interaction of humic substances with metal cations. 2004.
31. **Kaarel Adamberg**. Growth characteristics of non-starter lactic acid bacteria from cheese. 2004.
32. **Imre Vallikivi**. Lipase-catalysed reactions of prostaglandins. 2004.
33. **Merike Peld**. Substituted apatites as sorbents for heavy metals. 2005.
34. **Vitali Syritski**. Study of synthesis and redox switching of polypyrrole and poly(3,4-ethylenedioxythiophene) by using *in-situ* techniques. 2004.
35. **Lee Põllumaa**. Evaluation of ecotoxicological effects related to oil shale industry. 2004.
36. **Riina Aav**. Synthesis of 9,11-secosterols intermediates. 2005.
37. **Andres Braunbrück**. Wave interaction in weakly inhomogeneous materials. 2005.
38. **Robert Kitt**. Generalised scale-invariance in financial time series. 2005.
39. **Juss Pavelson**. Mesoscale physical processes and the related impact on the summer nutrient fields and phytoplankton blooms in the western Gulf of Finland. 2005.
40. **Olari Ilison**. Solitons and solitary waves in media with higher order dispersive and nonlinear effects. 2005.
41. **Maksim Säkki**. Intermittency and long-range structurization of heart rate. 2005.

42. **Enli Kiipli**. Modelling seawater chemistry of the East Baltic Basin in the late Ordovician–Early Silurian. 2005.
43. **Igor Golovtsov**. Modification of conductive properties and processability of polyparaphenylene, polypyrrole and polyaniline. 2005.
44. **Katrin Laos**. Interaction between furcellaran and the globular proteins (bovine serum albumin β-lactoglobulin). 2005.
45. **Arvo Mere**. Structural and electrical properties of spray deposited copper indium disulphide films for solar cells. 2006.
46. **Sille Ehala**. Development and application of various on- and off-line analytical methods for the analysis of bioactive compounds. 2006.
47. **Maria Kulp**. Capillary electrophoretic monitoring of biochemical reaction kinetics. 2006.
48. **Anu Aaspõllu.** Proteinases from *Vipera lebetina* snake venom affecting hemostasis. 2006.
49. **Lyudmila Chekulayeva**. Photosensitized inactivation of tumor cells by porphyrins and chlorins. 2006.
50. **Merle Uudsemaa**. Quantum-chemical modeling of solvated first row transition metal ions. 2006.
51. **Tagli Pitsi**. Nutrition situation of pre-school children in Estonia from 1995 to 2004. 2006.
52. **Angela Ivask**. Luminescent recombinant sensor bacteria for the analysis of bioavailable heavy metals. 2006.
53. **Tiina Lõugas**. Study on physico-chemical properties and some bioactive compounds of sea buckthorn (*Hippophae rhamnoides* L.). 2006.
54. **Kaja Kasemets**. Effect of changing environmental conditions on the fermentative growth of Saccharomyces cerevisae S288C: auxo-accelerostat study. 2006.
55. **Ildar Nisamedtinov**. Application of ^{13}C and fluorescence labeling in metabolic studies of Saccharomyces spp. 2006.
56. **Alar Leibak**. On additive generalisation of Voronoï's theory of perfect forms over algebraic number fields. 2006.
57. **Andri Jagomägi**. Photoluminescence of chalcopyrite tellurides. 2006.
58. **Tõnu Martma**. Application of carbon isotopes to the study of the Ordovician and Silurian of the Baltic. 2006.
59. **Marit Kauk**. Chemical composition of $CuInSe_2$ monograin powders for solar cell application. 2006.
60. **Julia Kois**. Electrochemical deposition of $CuInSe_2$ thin films for photovoltaic applications. 2006.
61. **Ilona Oja Açik**. Sol-gel deposition of titanium dioxide films. 2007.

62. **Tiia Anmann**. Integrated and organized cellular bioenergetic systems in heart and brain. 2007.
63. **Katrin Trummal**. Purification, characterization and specificity studies of metalloproteinases from *Vipera lebetina* snake venom. 2007.
64. **Gennadi Lessin**. Biochemical definition of coastal zone using numerical modeling and measurement data. 2007.
65. **Enno Pais**. Inverse problems to determine non-homogeneous degenerate memory kernels in heat flow. 2007.
66. **Maria Borissova**. Capillary electrophoresis on alkylimidazolium salts. 2007.
67. **Karin Valmsen**. Prostaglandin synthesis in the coral *Plexaura homomalla*: control of prostaglandin stereochemistry at carbon 15 by cyclooxygenases. 2007.
68. **Kristjan Piirimäe**. Long-term changes of nutrient fluxes in the drainage basin of the gulf of Finland – application of the PolFlow model. 2007.
69. **Tatjana Dedova**. Chemical spray pyrolysis deposition of zinc sulfide thin films and zinc oxide nanostructured layers. 2007.
70. **Katrin Tomson**. Production of labelled recombinant proteins in fed-batch systems in *Escherichia coli*. 2007.
71. **Cecilia Sarmiento**. Suppressors of RNA silencing in plants. 2008.
72. **Vilja Mardla**. Inhibition of platelet aggregation with combination of antiplatelet agents. 2008.
73. **Maie Bachmann**. Effect of Modulated microwave radiation on human resting electroencephalographic signal. 2008.
74. **Dan Hüvonen**. Terahertz spectroscopy of low-dimensional spin systems. 2008.
75. **Ly Villo**. Stereoselective chemoenzymatic synthesis of deoxy sugar esters involving *Candida antarctica* lipase B. 2008.
76. **Johan Anton**. Technology of integrated photoelasticity for residual stress measurement in glass articles of axisymmetric shape. 2008.
77. **Olga Volobujeva**. SEM study of selenization of different thin metallic films. 2008.
78. **Artur Jõgi**. Synthesis of 4'-substituted 2,3'-dideoxynucleoside analogues. 2008.
79. **Mario Kadastik**. Doubly charged Higgs boson decays and implications on neutrino physics. 2008.
80. **Fernando Pérez-Caballero**. Carbon aerogels from 5-methylresorcinol-formaldehyde gels. 2008.
81. **Sirje Vaask**. The comparability, reproducibility and validity of Estonian food consumption surveys. 2008.
82. **Anna Menaker**. Electrosynthesized conducting polymers, polypyrrole and poly(3,4-ethylenedioxythiophene), for molecular imprinting. 2009.

83. **Lauri Ilison**. Solitons and solitary waves in hierarchical Korteweg-de Vries type systems. 2009.
84. **Kaia Ernits**. Study of In_2S_3 and ZnS thin films deposited by ultrasonic spray pyrolysis and chemical deposition. 2009.
85. **Veljo Sinivee**. Portable spectrometer for ionizing radiation "Gammamapper". 2009.
86. **Jüri Virkepu**. On Lagrange formalism for Lie theory and operadic harmonic oscillator in low dimensions. 2009.
87. **Marko Piirsoo**. Deciphering molecular basis of Schwann cell development. 2009.
88. **Kati Helmja**. Determination of phenolic compounds and their antioxidative capability in plant extracts. 2010.
89. **Merike Sõmera**. Sobemoviruses: genomic organization, potential for recombination and necessity of P1 in systemic infection. 2010.
90. **Kristjan Laes**. Preparation and impedance spectroscopy of hybrid structures based on $CuIn_3Se_5$ photoabsorber. 2010.
91. **Kristin Lippur**. Asymmetric synthesis of 2,2'-bimorpholine and its 5,5'-substituted derivatives. 2010.
92. **Merike Luman**. Dialysis dose and nutrition assessment by an optical method. 2010.
93. **Mihhail Berezovski**. Numerical simulation of wave propagation in heterogeneous and microstructured materials. 2010.
94. **Tamara Aid-Pavlidis**. Structure and regulation of BDNF gene. 2010.
95. **Olga Bragina**. The role of Sonic Hedgehog pathway in neuro- and tumorigenesis. 2010.
96. **Merle Randrüüt**. Wave propagation in microstructured solids: solitary and periodic waves. 2010.
97. **Marju Laars**. Asymmetric organocatalytic Michael and aldol reactions mediated by cyclic amines. 2010.
98. **Maarja Grossberg**. Optical properties of multinary semiconductor compounds for photovoltaic applications. 2010.
99. **Alla Maloverjan**. Vertebrate homologues of Drosophila fused kinase and their role in Sonic Hedgehog signalling pathway. 2010.
100. **Priit Pruunsild**. Neuronal Activity-Dependent Transcription Factors and Regulation of Human *BDNF* Gene. 2010.
101. **Tatjana Knazeva**. New Approaches in Capillary Electrophoresis for Separation and Study of Proteins. 2011.
102. **Atanas Katerski**. Chemical Composition of Sprayed Copper Indium Disulfide Films for Nanostructured Solar Cells. 2011.

103. **Kristi Timmo.** Formation of Properties of $CuInSe_2$ and $Cu_2ZnSn(S,Se)_4$ Monograin Powders Synthesized in Molten KI. 2011.
104. **Kert Tamm**. Wave Propagation and Interaction in Mindlin-Type Microstructured Solids: Numerical Simulation. 2011.
105. **Adrian Popp**. Ordovician Proetid Trilobites in Baltoscandia and Germany. 2011.
106. **Ove Pärn**. Sea Ice Deformation Events in the Gulf of Finland and This Impact on Shipping. 2011.